

Marquette University

e-Publications@Marquette

Master's Theses (2009 -)

Dissertations, Theses, and Professional
Projects

X-Ray Tube Anode Balance Analysis and Vacuum Balancer Parameter Optimization

Matthew Malak
Marquette University

Follow this and additional works at: https://epublications.marquette.edu/theses_open



Part of the [Mechanical Engineering Commons](#)

Recommended Citation

Malak, Matthew, "X-Ray Tube Anode Balance Analysis and Vacuum Balancer Parameter Optimization" (2017). *Master's Theses (2009 -)*. 421.

https://epublications.marquette.edu/theses_open/421

X-RAY TUBE ANODE BALANCE ANALAYSIS AND VACUUM BALANCER
PARAMETER OPTIMIZATION

by

Matthew Malak, B.S.

A Thesis submitted to the Faculty of the Graduate School,
Marquette University,
in Partial Fulfillment of the Requirements for
the Degree of Master of Science

Milwaukee, WI

August 2017

ABSTRACT
X-RAY TUBE ANODE BALANCE ANALYSIS AND VACUUM BALANCER
PARAMETER OPTIMIZATION

Matthew Malak, B.S.

Marquette University, 2017

A manufacturing facility is introducing the company's first straddle mount liquid metal spiral groove bearing (SGB) on a rotating anode x-ray tube. In a manufacturing environment, it is critical that processes are robust and timely to drive down costs while also responding to market demand for improvement. There is currently a lot of variation in the anode balance process. Furthermore, there are repeatability questions surrounding the new balancing system that is used in this anode balance process. To better understand the characteristics of the new liquid metal SGB anode and the effects of measurement system variation, the measurement system will be isolated to determine the critical variables. It is hypothesized that the characteristics of the spiral groove liquid metal bearing are the cause of measurement system uncertainty below 1.0 g*cm. Data has been collected using two rotating anode platforms: i) liquid metal SGB; and ii) a ball bearing rotating anode system. The data will be used to compare measurement system repeatability of the SGB anode against the ball bearing anode for the same balance and correction process. After each unbalance measurement, a correction process is initiated where by material is removed from the correction planes as determined by the balance machine. Cutter depth, operator interaction, and machine repeatability play a vital role in the balance quality of the rotating anode system. The success of this thesis is to determine the critical variables and factors driving the measurement uncertainty in order to reduce cycle time.

ACKNOWLEDGEMENTS

Matthew Malak, B.S.

I would like to thank Dr. Rice and Dr. Bowman for their help and accommodation. Thank you for all the effort proof reading and for taking the time to meet with me. I would also like to thank my company for their support and use of resources. They have given me the tools and freedom to test and explore new ideas. I want to extend a special thanks to Will Schaefer, Kevin Kruse, Chris Schultz, and Andy Triscari. I want to especially thank Mike Danyluk for his coaching, mentoring, and guidance. Mike, thank you for always taking the time to teach me; you have helped me grow as an engineer and as a person – I am ever so grateful. I would like to thank my family for their inspiration and motivation. Finally, I would like to thank my wife Alicia for her never-ending love and encouragement.

TABLE OF CONTENTS

| | |
|---|-----|
| ACKNOWLEDGEMENTS..... | i |
| LIST OF TABLES..... | v |
| LIST OF FIGURES..... | vii |
| 1 INTRODUCTION | 1 |
| 1.0 Overview | 1 |
| 1.1 Problem Statement | 2 |
| 1.2 Objective of the Work | 4 |
| 1.3 Focus of Work | 4 |
| 2 LITERATURE REVIEW | 11 |
| 2.1 X-ray Basics | 11 |
| 2.2 Overview of X-ray Production..... | 12 |
| 2.2.1 X-ray Production: Class II medical device..... | 13 |
| 2.2.2 X-ray Production Line Overview | 15 |
| 2.2.3 Process Oriented vs Assembly Oriented Production..... | 16 |
| 2.3 X-ray Tube and Bearing Environment..... | 16 |
| 2.3.1 Mechanical Load | 17 |

| | | |
|-------|--|----|
| 2.3.2 | Heat..... | 18 |
| 2.3.3 | Vacuum..... | 19 |
| 2.3.4 | High Voltage | 20 |
| 2.3.5 | Focal Spot Impact..... | 20 |
| 2.4 | Spiral Groove Bearings | 21 |
| 2.5 | Fundamentals of Balancing..... | 24 |
| 2.5.1 | History of Balancing..... | 24 |
| 2.5.2 | Present Status of the Balancing | 27 |
| 3 | DATA COLLECTION | 41 |
| 3.1 | Statement of Procedure and Methodology..... | 41 |
| 3.2 | Overview of Manufacturing Facility’s Balance Machine | 41 |
| 3.2.1 | Detailed Process of Balancing..... | 42 |
| 3.3 | Data Collection Overview | 53 |
| 3.3.1 | Measurement Repeatability | 59 |
| 3.3.2 | Collet Rigidity | 69 |
| 3.3.3 | SGB Repeatability Study..... | 72 |
| 3.3.4 | Balance Equipment..... | 76 |
| 3.3.5 | SGB Multiple Run Repeatability Issues..... | 80 |

| | | |
|-------|---|-----|
| 3.4 | Gallium Movement | 84 |
| 3.4.1 | Gallium Migration Theory | 84 |
| 3.4.2 | Ga Movement Proved in Bearing Autopsy | 87 |
| 3.4.3 | Smoking Gun bearing..... | 90 |
| 4 | CONCLUSIONS, OBSERVATIONS, and RECOMMENDATIONS..... | 97 |
| 4.1 | Conclusions:..... | 97 |
| 4.2 | Observations:..... | 99 |
| 4.3 | Recommendations:..... | 100 |
| 4.4 | Explicit Contributions:..... | 103 |
| 5 | BIBLIOGRAPHY..... | 105 |
| 6 | APPENDIX..... | 108 |
| 6.1 | Future Work: Ga High Speed Wear Tests and Theory Behind Higher Balance Speed | 110 |
| 6.1.2 | High Speed Consecutive Run Study based on Chamber Venting | 112 |
| 6.1.3 | More High Speed Trials | 115 |

List of Tables

| | |
|---|-----|
| Table 1: Displacement or eccentricity of rotor CG in mm and microns..... | 36 |
| Table 2: Machine designation..... | 46 |
| Table 3: Bias Check Requirements..... | 57 |
| Table 4: Bias Check Results for Target Plane | 58 |
| Table 5: Bias Check Results for the Rotor Plane..... | 58 |
| Table 6: The unbalance range for the target and rotor, along with the tolerance allocation..... | 60 |
| Table 7: Mean and Standard Deviation for the 6 runs with each 'part'..... | 62 |
| Table 8: Investigation to determine the variation by keeping the collets on, shown as Part 6. | 70 |
| Table 9: The average of the runs for Target Unbalance for Part 1, 5, 6. Collets were removed between each run for Parts 1 and 5. The collets were kept on during Part 6..... | 70 |
| Table 10: Every 5 runs, the chamber was vented. | 73 |
| Table 11: The average and standard deviation of the 5 separate runs from Table 9. Runs 2-11 had a 0.3798g weight attached while runs 12-16 had a 0.7638g weight attached..... | 73 |
| Table 12: Data from the ball bearing testing. Highlighted sections are graphed in Figure 51. Each 'Run' represents the average of 5 consecutive runs under vacuum. | 78 |
| Table 13: Total Error and Error Squared | 95 |
| Table 14: Data from Gage R&R Trials with SGB..... | 108 |
| Table 15: Schenck System Limitations..... | 110 |
| Table 16: Vented chamber after 5 consecutive runs for two different rotor specific calibration programs..... | 113 |

List of Figures

| | |
|---|----|
| Figure 1: The anode or RoSS (Rotating Sub Assembly) which will be balanced. The anode is comprised of the rotor, target and SGB (Spiral Groove Bearing)..... | 5 |
| Figure 2: Fishbone diagram of the many sources contributing to the high balance cycles, with the focus area highlighted. | 6 |
| Figure 3: The balance machine which performs the balancing operation. | 6 |
| Figure 4: Balance Process Map showing what constitutes a balance cycle..... | 7 |
| Figure 5: Testing will encompass all of the variables highlighted above. Green area are known fixes to get rid of external variation. Numbers coorespond with the testing performed shown in Figure 6. | 8 |
| Figure 6: The studies and tests highlighted in blue all have explicit purposes..... | 9 |
| Figure 7: Typical x-ray tube insert cross section [11] | 12 |
| Figure 8: Example of a track melt on an x-ray tube anode..... | 17 |
| Figure 9: Diagram of the location of the x-ray tube on a CT scanner. [18]..... | 18 |
| Figure 10: Approximate temperatures of a glass insert x-ray tube. [11] | 19 |
| Figure 11: Hydrodynamic Journal Bearing [29]..... | 22 |
| Figure 12: Configuration differences between ball bearing and SGB anode. [18]..... | 23 |
| Figure 13: Example of Philips iMRC x-ray tube insert with SGB [11]..... | 23 |
| Figure 14: Example of cut away from a SGB insert showing two radial bearings of a liquid metal lubricated SGB [11]. | 24 |
| Figure 15: Unbalance causes centrifugal force [6]. | 28 |
| Figure 16: Side view of rotor with 10 g*cm unbalance..... | 29 |
| Figure 17: Rotating Sub Assembly also known as a ROSS or anode..... | 30 |
| Figure 18: Balance quality grades for various groups of representative rigid rotors [8][9] | 35 |

| | |
|---|----|
| Figure 19: Disk shaped rotor with displaced CG due to unbalance..... | 36 |
| Figure 20: Maximum permissible residual unbalance [8] [9]. The red lines show where the anode balance would lie on this chart using the 0.23 micron center of gravity displacement along with the 8400rpm max service speed..... | 38 |
| Figure 21: Comparison of API, ISO & MIL-STD-167-1 balance tolerances. Calculations show that the current balance spec is off the chart using the ISO 1940 Standard calculation of 0.0034 oz*in (which is 0.25g*cm) and 8400rpm. [19]..... | 39 |
| Figure 22: Balancer system comprised of Schenck Cabinet, HMI or Human Machine Interface, and balancer table. | 42 |
| Figure 23: An anode which has the collets attached and is ready for placement into the machine. | 43 |
| Figure 24: An anode that is ready for balance. | 43 |
| Figure 25: The balance table before and after anode installation. | 43 |
| Figure 26: Balance machine with vacuum chamber closed with the anode inside..... | 44 |
| Figure 27: Schenck set up screen where the diameters and distances of the rotor and target planes are configured. | 45 |
| Figure 28: Two sets of pickup coils which measure the unbalance..... | 46 |
| Figure 29: SF-14/SF-15 Vibration Pickup Installation [20]. | 48 |
| Figure 30: Example of the Schenck output that tells where and what the unbalance is after a balance measurement run. | 48 |
| Figure 31: This screen outputs where and how the correction will take place based on the unbalance. This information is sent to the HMI, Figure 32, so that the operator can begin the material removal process. | 49 |
| Figure 32: HMI screen showing the depths and degree of the cuts to be made for the rotor and target planes. | 50 |
| Figure 33: Run chart of the Target Unbalance vs the number of cycles for 15 different balance runs. | 51 |
| Figure 34: Zoomed in view of Figure 33 run chart showing the 0.25g*cm specification shown in red..... | 52 |

| | |
|---|----|
| Figure 35: Initial Target Unbalance..... | 52 |
| Figure 36: Example of a specific bearing being spun multiple times producing different unbalance results. The target unbalance is plotted on the y axis and the run number is plotted on the x axis. | 54 |
| Figure 37: Overview of Data Collection and Results | 56 |
| Figure 38: Set screw, which is a calibrated weight, placement in the modified target and the rotor. | 60 |
| Figure 39: RoSS attached to collets..... | 61 |
| Figure 40: Unbalance average vs the unbalance standard deviation | 63 |
| Figure 41: Gage R&R report for rotor unbalance showing part to part variation can be detected..... | 64 |
| Figure 42: Gage R&R for target unbalance. | 65 |
| Figure 43: Run chart of Target 'parts' 1 and 5 which were balanced near the specification limit..... | 66 |
| Figure 44: Run chart of Rotor 'parts' 1 and 5 which were balanced near the specification limit..... | 67 |
| Figure 45: Gage R&R report for Target which shows very high percent contribution. The gage R&R as a percent of tolerance is over 300%..... | 68 |
| Figure 46: Gage R&R report for the Rotor shows very high percent contribution. The Gage R&R as a percent of tolerance is 86%..... | 69 |
| Figure 47: Plot of Table 9 showing the Avg Unbalance vs Avg STDEV of Parts 1 and 5 (removal of collets between each run) and Part 6 (consecutive runs without collet removal). The standard deviation was similar. | 71 |
| Figure 48: The rotor and target unbalance are graphed as the standard deviation vs the average. Each dot represents the 5 run average and standard deviation from the Table 11..... | 74 |
| Figure 49: Each dot represents the 5 run average and standard deviation from the table above. The rotor and target angle are graphed. | 75 |
| Figure 50: Ball Bearing ROSS in balancer. | 77 |

| | |
|---|----|
| Figure 51: The results of performing similar repeatability tests on a ball bearing anode. | 79 |
| Figure 52: Ball Bearing Testing (BB1 and BB2) from Figure 51 combined with the SGB results from Figure 48, appearing in the legend as Rotor NK and Target NK. The specification limit is highlighted in red at 0.25g*cm. | 79 |
| Figure 53: A balance was performed on bearing MAN280 to specification. Before venting the chamber the anode was spun 4 more times. The target unbalance increased on subsequent runs. | 81 |
| Figure 54: Plot showing Figure 53's data. The target unbalance trended upward after the ROSS MAN280 was balanced to specification. | 82 |
| Figure 55: ROSS MAN304 was balanced to specification and then spun 4 more times while it remained under vacuum. The target unbalance lowered on subsequent runs. | 83 |
| Figure 56: Plot showing Figure 55's data. The target unbalance lowered on subsequent runs after ROSS MAN280 was balanced to specification. | 83 |
| Figure 57: Cross section of a ROSS. | 85 |
| Figure 58: Cross section of the liquid metal SGB. | 86 |
| Figure 59: Sleeve seal was removed and weighed on the scale to determine the amount of Ga in the traps. | 88 |
| Figure 60: Consecutive runs under vacuum. The chamber was vented in-between runs, denoted by the color change. Rotor average shifted drastically. | 89 |
| Figure 61: Run chart of Figure 60. | 90 |
| Figure 62: Chart laying out the test parameters showing no Gallium in the traps on the repeatable runs, while there was 1.0g of Gallium in the traps during the less repeatable runs for the Target unbalance. | 92 |
| Figure 63: Plot showing where on the run chart the Gallium shifted into the first trap. | 93 |
| Figure 64: Cross section of the anode showing the target to sleeve fit and the shaft to sleeve gap. | 94 |
| Figure 65: Investigation of balance variables reduced the average number of balance cycles by two. | 99 |

| | |
|---|-----|
| Figure 66: Air Balance setup. | 101 |
| Figure 67: A bearing which leaked in the balancer resulting in a pool of Gallium. | 102 |
| Figure 68: PowerFlex Drive showing the parameter changes to increase the speed | 111 |
| Figure 69: Changing the measurement speed to 1500rpm | 112 |
| Figure 70: MAN245 Target Unbalance run chart showing the high speed "Janus- BB-Vac Program" and the normal "Nessus-BB-Vac"Program | 114 |
| Figure 71: High and Low speed comparisons of the same ROSS. The best run was highlighted in green for each vertical column/category. Note that there some tied. The avg is of 5 back to back runs. | 115 |
| Figure 72: Target Unbalance comparison at high and low speeds. | 116 |
| Figure 73: Rotor Unbalance comparison at high and low speeds..... | 116 |

CHAPTER 1

INTRODUCTION

1.0 Overview

This work specifically focuses on balance in vacuum of spiral groove liquid metal bearings (SGB) in rotating anode x-ray tubes for CT scanners. However, this work can be transferred to any process involving the balance of rotating systems in a vacuum environment.

The balancing of liquid metal bearings for x-ray systems is unique because of its tight balance specification. The balance measurement is performed in a vacuum chamber environment below operating speed. Tight balance specification is required to produce: i) a stable x-ray focal spot, ii) a long lasting x-ray tube, iii) an accurate diagnostic image. Spiral groove liquid metal bearings must be operated under vacuum conditions or else the ambient gases at atmospheric pressure will oxidize and seize the bearing. The vacuum chamber in the balance machine keeps the SGB at an acceptable pressure below 10^{-3} Torr. Most of the world's industrial bearings are ball bearings that operate with grease or oil at atmospheric pressure and relatively low temperatures. However, x-ray tube liquid metal bearings operate in a vacuum at temperatures reaching 500°C [2] [3].

The motivation for this work is to help a manufacturer of x-ray tubes to set up a new balancing system for its novel spiral groove bearing design. Challenges have risen from the newly installed vacuum balance machine which removes material from the rotating x-ray tube anode to correct the unbalance. There are key variables in this new

process including equipment, bearing design, and operator interaction. Analysis of the entire balance system needs to be performed. This work will provide the tools and foundation to improve reliability and decrease cycle time of the x-ray anode SGB balance process.

Balancing of ball bearing anodes that use solid lubrication such as lead or silver is well established [1] [4]. The balancing of ball bearing anodes has significant advantages as compared to the balancing of liquid metal SGB's due to the fact that ball bearing balance is determined by the tolerance run out and part stack up of the anode assembly. Liquid metal anode bearings must address liquid gallium movement with this new anode bearing platform. The following thesis is an analytical technique that demonstrates equipment set up and machine reliability for a specific product. The work is concluded by finding the variables that affect the repeatability and uncertainty in this particular balance machine for SGB x-ray tube anodes [4] [5]. The success of this thesis is to determine the critical variables and factors driving the measurement uncertainty to reduce cycle time.

1.1 Problem Statement

In x-ray machines and Computerized Tomography (CT) scanners, x-ray photons are produced by directing a focused electron beam from a cathode to the target of the rotating anode. The x-ray focal spot used to produce a diagnostic image is defined by the rotating target's focal track. The track is the area where the electron beam impacts the anode [1].

To produce images free of artifacts and unwanted motion, a stable focal spot is critical. Stability of the spot is largely dependent on how well the anode is balanced about its rotational axis. If the anode is unbalanced, centrifugal force may cause the hot anode

to deform during rotation, tilting the anode target about the plane perpendicular to the anode's rotational axis and causing the focal spot and image to jitter. Because the centrifugal force of the unbalance varies with the square of the speed, this jitter is worse at higher speeds [1].

Anode balance is also critical to the longevity of the x-ray tube assembly, as it will affect the wear on the bearings supporting the rotating anode assembly. Bearing wear causes numerous problems, such as excess heating leading to thermal creep of the anode. Thermal creep causes focal spot drift leading to inaccurate images. Bearing and rotor fretting can drift particles toward the cathode resulting in arcing [1]. In fact, the operating environment is so specialized there are less than a handful of manufactures in the world that can even produce spiral groove liquid metal bearings of sufficient quality, cleanliness, and precision required to operate in a high vacuum (10^{-7} Torr), high voltage (140kV), and high heat environment (500°C). The increased specialization severely limits the amount of knowledge available to take on credible design work and manufacturing.

Thus, with new product introduction x-ray tube anodes, it is very challenging and laborious to set up new equipment. The motivation of this work is to better understand the reliability of a new vacuum balance machine which balances the liquid metal SGB anode platform. The balance measurement repeatability plays a vital role in producing a quality product. It is hypothesized that the uncertainty in the balance measurement repeatability is due to the gallium shifting and moving in the spiral groove liquid metal bearing. The success of this thesis is to determine the critical variables and factors driving the measurement uncertainty in order to reduce cycle time. Determining these

critical variables will enable future work to focus on areas that will optimize the balance machine parameters to further reduce cycle time, improve balance quality, and drive down costs.

1.2 Objective of the Work

The objective is to determine the critical variables and factors driving the measurement uncertainty in order to reduce cycle time. Independent studies have been performed to isolate features. Isolating the measurement system from the liquid metal bearing will determine the critical variables within the balance machine that cause repeatability issues. To better understand the characteristics of the new liquid metal bearing and the effects that the measurement system has on its perceived unbalance, a similar configuration ball bearing anode platform has been created to test the repeatability of the balance machine without the influence of liquid gallium. Isolating the measurement system with a known ball bearing configuration will help identify critical variables and confirm the measurement system capability as defined by the calibration bias checks. This work develops the logic to describe the repeatability of a liquid metal SGB during the vacuum balance process by proving or disproving the hypothesis that the uncertainty in the balance measurement repeatability is due to the gallium shifting in the SGB.

1.3 Focus of Work

There are many factors that contribute to the difficult balance process of the new liquid metal bearing, which is shown in Figure 1. However, the main variables that contribute to a better anode balance operation are target pre-balance, material volume removal accuracy, and measurement repeatability seen in Figure 2. Specifically, the focus of this work surrounds the balance measurement repeatability of the SGB anode. Variables will be isolated to find the critical x's of the anode balance problem. Bearing design will not be studied or questioned in detail, as it has proven to be reliable over years of HALT testing, engineering analysis, and thousands of x-ray exams measuring focal spots and image quality. Yet, the impact this design has on the balance process will be considered.

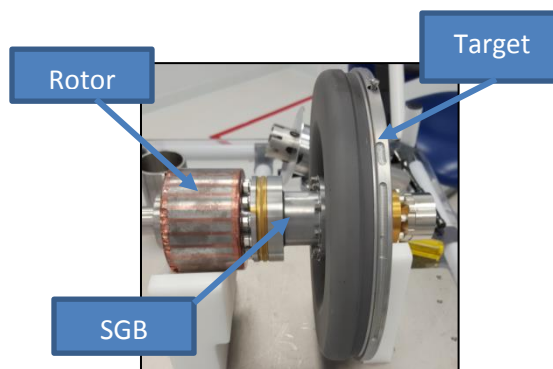


Figure 1: The anode or RoSS (Rotating Sub Assembly) which will be balanced. The anode is comprised of the rotor, target and SGB (Spiral Groove Bearing).

The driving variable causing the uncertainty in the measurement repeatability is hypothesized to be the shifting gallium inside the liquid metal bearing. To prove this,

testing will be performed covering all the areas highlighted in Figure 2 on the balance machine which shown in Figure 3.

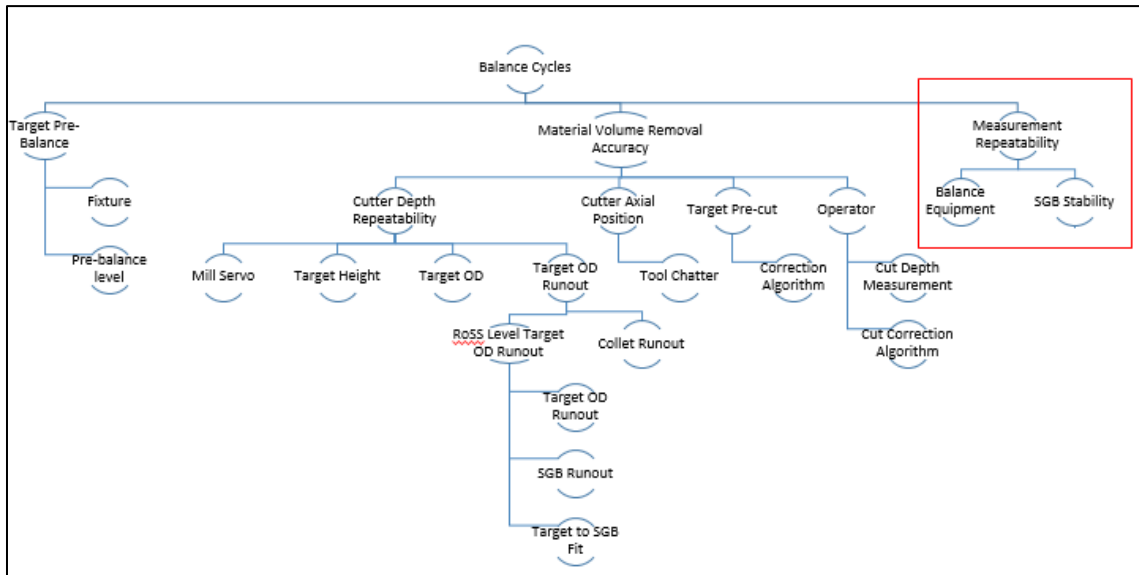


Figure 2: Fishbone diagram of the many sources contributing to the high balance cycles, with the focus area highlighted.



Figure 3: The balance machine which performs the balancing operation.

An overview of the balance process shown in Figure 4 is comprised of many cycles. Each “cycle” takes roughly 15 to 20 minutes. The cycle begins by taking a balance measurement of the anode under vacuum. The chamber then vents to atmosphere so that material can be removed by drilling the rotor or milling the target in the area of unbalance. The chamber then closes again to pull vacuum and another measurement is taken to see how well the correction was performed. Section 3.2 goes into detail explaining many of the intricacies of the balance process.

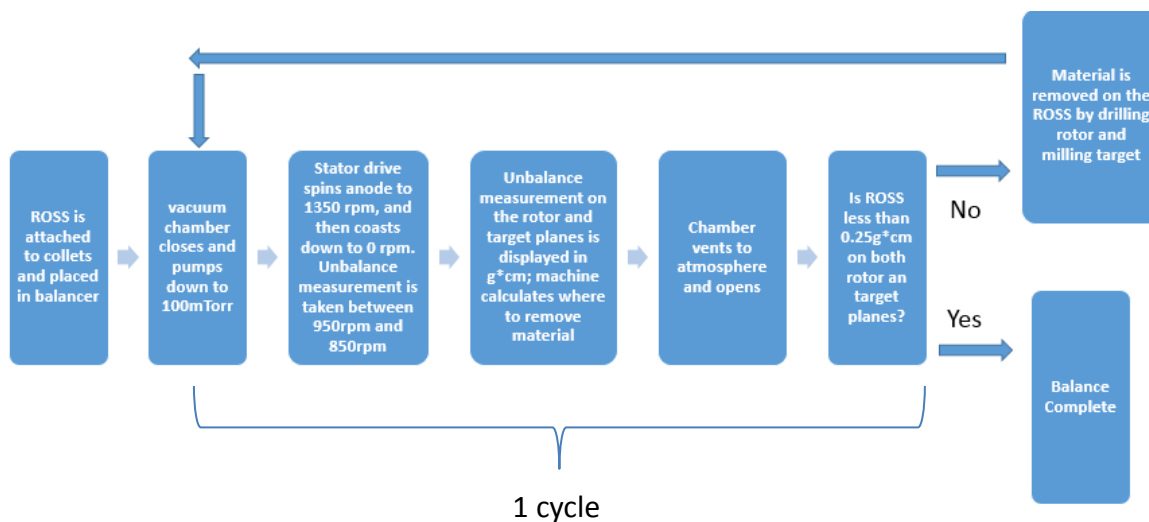


Figure 4: Balance Process Map showing what constitutes a balance cycle.

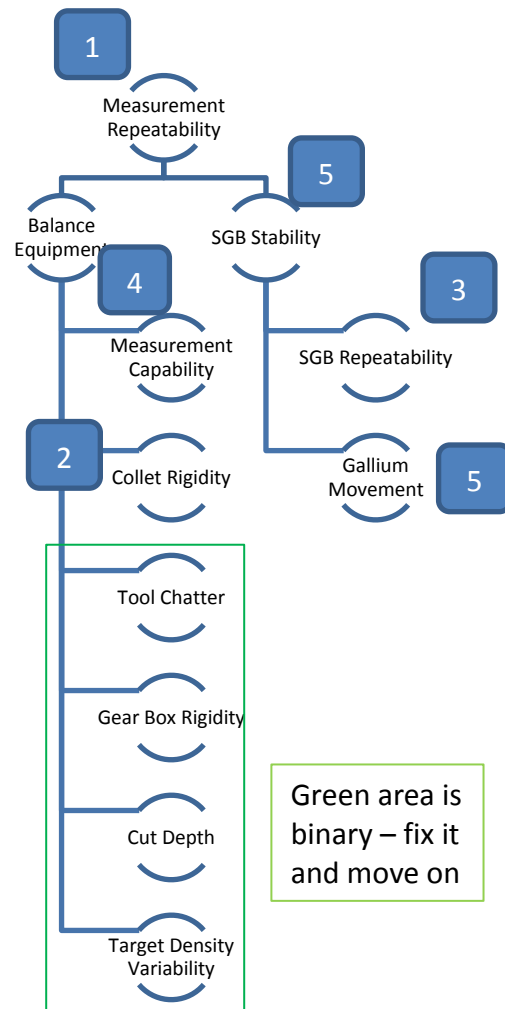


Figure 5: Testing will encompass all of the variables highlighted above. Green area are known fixes to get rid of external variation. Numbers correspond with the testing performed shown in Figure 6.

Tool chatter, gear box rigidity, cut depth, and target density variability all play a role in the equipment's effect on the unbalance. However, these have all been isolated in testing, proving that their effect is negligible on the unbalance if they are controlled

properly. The other variables such as measurement capability, collet rigidity, SGB repeatability, and Gallium movement will all be studied in detail.

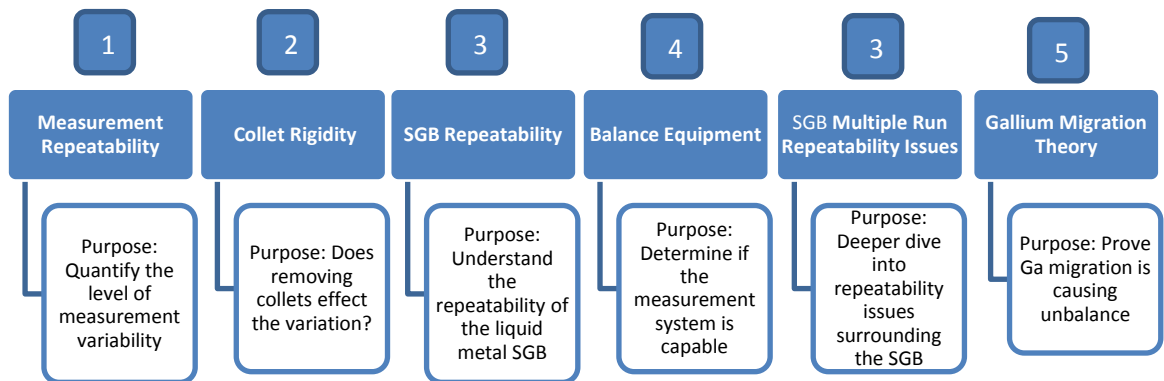


Figure 6: The studies and tests highlighted in blue all have explicit purposes. Later, Figure 37 combines these variables and tests with their outcome, closing the loop.

Finally, this work concludes with the determination of the critical variables causing the measurement uncertainty. The identification of these variables and the response they have on the system will enable future work to focus on areas that will optimize the balance machine parameters to reduce cycle time, improve balance quality, and drive down costs. A current baseline for the SGB repeatability has been established. A known quantity ball bearing platform has been created to isolate the measurement system from the SGB and prove measurement system capability and resolution. By using a model such as the ball bearing to replicate the process of a spiral groove bearing balance, and subsequent repeatability testing to determine which factors are critical, the

manufacturability and operation of the x-ray tube balance equipment will be analyzed. The metric for measuring the repeatability is the average unbalance over consecutive runs and its standard deviation.

The work is performed under vacuum with a liquid metal SGB for x-ray tube production, conditions not readily documented or accomplished in industry. The literature review section describes the operation of an x-ray tube and the rationale behind the tight balance specification limit. Additionally, a portion of this paper focuses on balancing fundamentals to develop a sufficiently well understood knowledge base of the physics under test. The words “ROSS” and “anode” will be used interchangeably in this document, both referring the bearing assembly comprised of the rotor and target. Most of the repeatability testing will surround the target unbalance. The target has proven to be less repeatable due to its large size, weight, fit up, and variable density which all contribute to a large starting unbalance.

CHAPTER 2

LITERATURE REVIEW

2.1 X-ray Basics

X-ray tubes provide an x-ray beam with a specified size, shape, location, intensity and energy spectrum to enable diagnostic imaging of the body. X-rays are generated through the interaction of high-speed electrons with the atomic structure of a target material. By electrically heating a tungsten alloy filament in the cathode to very high temperatures, an electron cloud is created. Electrons are accelerated toward the anode by applying a high potential between the cathode and anode. For example, 150kV causes electrons to travel at $2/3$ the speed of light. The X-ray tube is designed to produce electrons at the cathode, accelerate them via a high potential difference toward the anode where they are suddenly stopped by the target. To avoid electrons interacting with gas molecules, a high vacuum of about 10^{-6} Torr is required. The efficiency of creating X-rays is only 1%, the remaining is converted to heat. X-rays are generated in all directions and with energies up to that of the incident electron [11].

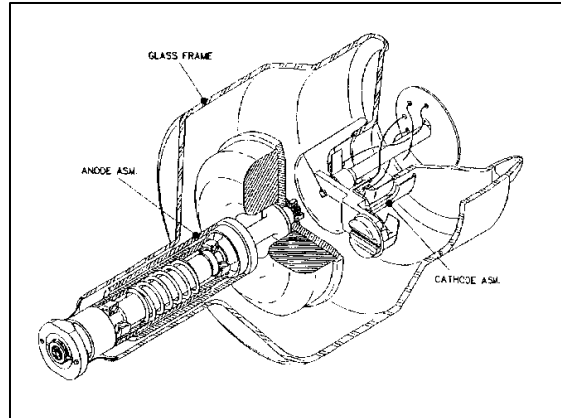


Figure 7: Typical x-ray tube insert cross section [11]

2.2 Overview of X-ray Production

The number of quality manufacturers of medical imaging equipment is limited due to high entrance barriers into this market. National laws by the US Food and Drug Administration regulate minimal performance, constancy testing, risk management, good manufacturing practice, and quality assurance. International standards provide performance metrics while various nations all have their own unique requirements. Hence, the manufacturing of x-ray sources demands a broad set of skills and an experienced and well trained staff.

Fueled by increasing public attention to patient dosing of ionizing radiation, incidents in medical practice, progress of failure prevention, legal enforcement of obligation, and quality control of manufacturing have gained unprecedented importance since the turn of the millennium. Measures to ensure compliance and efforts to verify and validate products and production processes have increased tremendously during the past

two decades. The effort consumes a significant share of time in development. Only a limited number of vendors of medical x-ray sources are able to comply with these strict rules. Technical challenges add to the complexity, notably because vacuum electronics has departed from being part of mainstream industrial technology development. [10]

2.2.1 X-ray Production: Class II medical device

Class II medical devices fall under Special Controls, which sets performance standards or other requirements for particular devices to assure safety and effectiveness. They are intended for devices for which general controls alone would not assure safety and effectiveness or for which sufficient knowledge exists to develop such standards. Performance standards may relate to the construction, components, ingredients, and properties of the device. A standard may also provide for devices to be tested to assure that lots or individual products conform to regulatory requirements. Special controls also can include special labeling requirements, patient registries, or post market surveillance [12].

The major impact on the federal Food, Drug, and Cosmetic Act on medical device manufacturers began with the enactment of the Medical Device Amendments of 1976. However, medical device legislation officially began in 1938 when the Food and Drug Act of 1906 was amended to cover devices. Classification is one key difference between regulating drugs and devices. The law recognizes the enormous diversity among devices on the market and provides a system where all devices are regulated in proportion to their degree of significance to public health. As declared in this act, all devices intended for human use marketed in the United States must be classified by panels of nongovernment

experts into one of three regulatory classes according to the difficulty in assuring their safety and effectiveness. [12] Since x-ray systems for CT scanners are considered a Class II medical device, much care is taken during the manufacturing of the product.

Meticulous cleaning of components is a prerequisite for acceptable high voltage stability, long bearing life, stable electron emission, and high overall production yield. A single fingerprint may ruin the x-ray tube. Human dander may leave marks of carbon after high temperature processes, which could cause field emission of electrons and electrically destabilize electrode surfaces under high electric fields. Particulate material may end up in the raceways of a ball bearing, causing dents or fretting of the metal coating. Therefore, quality manufacturers have invested in environmentally controlled dust free assembly rooms. Production associates must wear hair nets, clear room gowns, booties, and rubber gloves before entering the room through an air shower which removes any particulate from the outside manufacturing environment. Transfer locks, through which cleaned subcomponents are channeled, decouple polluted and clean areas [10].

Before final assembly, piece parts of x-ray tubes are subject to multiple mechanical, chemical, galvanic, and thermal treatments. Compatibility of all these processes is a key ingredient to quality. Each vendor pursues a proprietary set of recipes that mirror years of good and bad experience and scientific analysis. The suppliers for x-ray tube components often receive unique and challenging requirement specifications. The supply chain for important parts typically consists of a few trusted suppliers rather than an abundance of different vendors [10].

2.2.2 X-ray Production Line Overview

After assembly, x-ray tubes are evacuated to a residual gas pressure of about $10E-7$ Torr by baking the entire tube, thermal degassing individual sub components such as the cathode and anode, and intense heating beyond the service temperature of the assembled tube. After pinch off, the vacuum tubes are placed into the lead shielded casing which is filled with degassed and dried mineral oil. The assemblies are still not yet electrically stable at this point. Vacuum discharges may occur for tube voltages above about half of the nominal value, or 70kV. Therefore, a high voltage conditioning process to about 20% overvoltage is applied to destroy troublesome electrode microstructures and to further reduce the residual gas inside. Maximal high voltage and temperature of the focal spot and other parts of the tube are driven beyond the limits for clinical use to make sure that the tube operates as promised for the customer [10].

Usually, all parameters critical to quality are measured under worst case conditions during final testing, including focal spot size and position, focal spot deflection characteristics, grid switch functionality, emission characteristics, and bearing noise. In addition, look up tables for generator and system adaptation may be filled. Leakage of radiation requires particular attention and is measured by a spherical radiation monitoring system. Ion chambers inside the machine detect any unwanted radiation that is leaking through the x-ray tube casing. Quality manufacturers perform a 100% test and measure across the entire space angle about the tube assembly [10].

2.2.3 Process Oriented vs Assembly Oriented Production

Vacuum electrical discharges are still regarded as ‘stochastic’ and are unpredictable. Due to the complex physics of the various subcomponents of an x-ray tube, their interdependency is not yet understood fully. In this field of knowledge, the theory of electron field emission is still incomplete, as is knowledge about the atomic microstructure of all relevant surfaces, despite major advancements in recent years. Similar assessments hold for bearing systems. Inevitable fluctuations of the quality of the raw material add to this uncertainty. Under these conditions, acceptable x-ray tube quality can only be ensured through: (i) accurate repetition of well documented processes by skilled personnel, (ii) vigilant tracking of key performance indicators, and (iii) immediate correction of deviations. Manufacturers use various methods of quality maintenance and improvement, such as LEAN, statistical engineering, six sigma methodology, and other company specific manufacturing strategies. Excellent motivation of personnel, engaged and open communication, and pride in craftsmanship are essential, as well as efficiency. This holds true for assemblers and suppliers. Tube production is thus process oriented [10].

2.3 X-ray Tube and Bearing Environment

The focal spot rises to about 2450°C during x-ray production with a heat flux up to 8300 W/mm^2 . The thermal energy from the electron beam can easily melt a hole through a stationary target tungsten material as shown in Figure 8 [16, 40].



Figure 8: Example of a track melt on an x-ray tube anode.

Therefore, the x-ray tube typically rotates the target to deliver fresh material for purposes of distributing heat generated at the focal spot [28]. Catastrophic material failure is avoided because rotation keeps the heat generation per unit area per unit time at a permissible level during x-ray production. As such, the anode must be composed of an integral bearing assembly to rotate the target assembly [16, 40], generally from 6k-10k RPM.

2.3.1 Mechanical Load

Figure 9 depicts an x-ray tube on a CT gantry. The target, or anode, of the x-ray tube rotates around its bearing while the CT gantry that it is attached to also rotates 360 degrees. The anode is spinning to cool the target and the gantry is spinning to get and

image of the entire body. At faster gantry speeds, the mechanical loads on the structural components increase dramatically. For example, a gantry speed of 0.2s per revolution (300rpm) will produce a load of 65g on the anode. This requires the use of strong materials & appropriate section thicknesses to avoid catastrophic failures. Anodes rotate at greater than or equal to 140Hz, which can cause burst of anode materials as well [11].

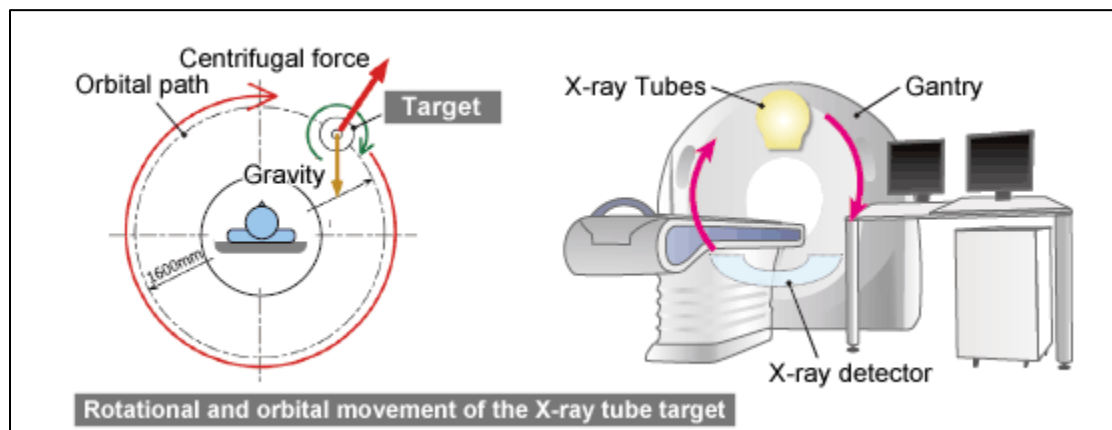


Figure 9: Diagram of the location of the x-ray tube on a CT scanner. [18]

2.3.2 Heat

To provide high patient throughput and good image quality, a tremendous heat flow in the anode must be dealt with. The temperature of the focal spot can reach 2450C, and if the anode is not rotating at the required speed, it can melt Tungsten, which has a melting point of 3400C. Temperatures are so high in portions of the tube that sublimation of metal films on insulating surfaces can lead to high voltage breakdowns. Strength of materials at elevated temperatures and expansion coefficients of dissimilar materials in joined assemblies are key to modeling thermal and mechanical stresses in an x-ray tube as shown in

Figure 10. Bearings run at temperatures up to 500C, including frictional and stator heat. Therefore, grease or oil cannot be used due to outgassing. The bearing requires solid metal film lubricant. [11]

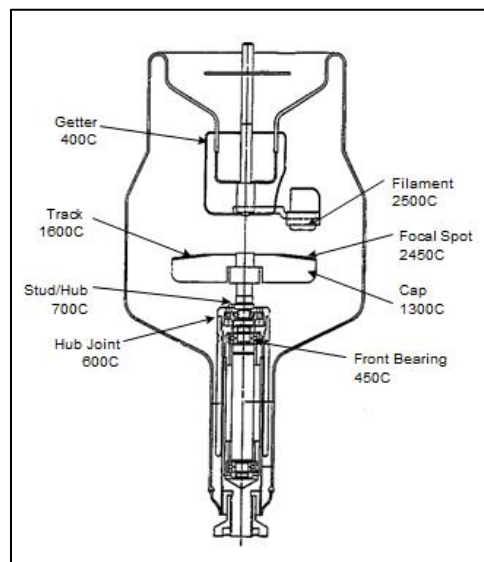


Figure 10: Approximate temperatures of a glass insert x-ray tube. [11]

2.3.3 Vacuum

Even at a pressure of 5×10^{-7} torr, there are still 10^{10} gas molecules per cm^3 to contend with in tube operation. These gas molecules can lead to high voltage discharges and image artifacts depending on severity [11].

2.3.4 High Voltage

X-ray tube operation over a range of 80-160kV can precipitate breakdown due to: i) poor vacuum quality, leaks, virtual leaks, and hydrocarbon outgassing; ii) particle contamination such as metal burrs, ceramic particles; iii) sharp edges and rough surfaces in high voltage field regions; and iv) incorrect spacing between surfaces at different potential. [11]

2.3.5 Focal Spot Impact

The National Electrical Manufacturers Association (NEMA) , in the United States, established standards for measuring focal spot size. Focal spot size is dependent on filament size, voltage bias, and the target angle. If a tube is said to have a 0.6mm focal spot one assumes 0.6mm x0.6mm (width and length). NEMA allows 50% variance on one measurement and 100% variance on the other. For example, a 0.6mm focal spot could measure out at 9mm x 1.2mm and it would be within NEMA's acceptable standard [11].

Focal Spot Size impacts the maximum resolution of the device. Typical focal spot sizes range from 0.3 mm sq. to 1.2 mm sq. In general, the smaller the spot size the better the resolution, and as noted as magnification goes to zero, spot size has no impact. Ultimately it is a balancing act to obtain good resolution, with intermediate spot sizes, anode angles, and coverage [11].

2.4 Spiral Groove Bearings

Fluid Film Bearings are machine elements which should be studied within the broader context of tribology, “the science and technology of interactive surfaces in relative motion and of the practices related thereto.” The three subfields of tribology – friction, lubrication, and wear – are strongly interrelated. If a bearing is not well designed, or is operated under other than the design conditions, other modes of lubrication, such as boundary lubrication, might result, and frictional heating and wear would also have to be considered.

The Spiral Groove Bearing (SGB) is a hydrodynamic journal bearing recently used in X-ray tubes. Hydrodynamic lubrication is a fluid dynamic mechanism that maintains a fluid film between two surfaces sliding relative to each other preventing contact between them. When applied to a journal bearing where a bearing sleeve rotates around a stationary journal shaft, a pressure wave is generated within the fluid on the leading edge of the journal resulting in a pressure wave sufficiently large enough to carry a load on the rotating member. This pressure wave is generated through both squeeze film action and a viscous wedge of fluid generated by the two converging surfaces of the journal bearing shown in Figure 11 [23] [29].

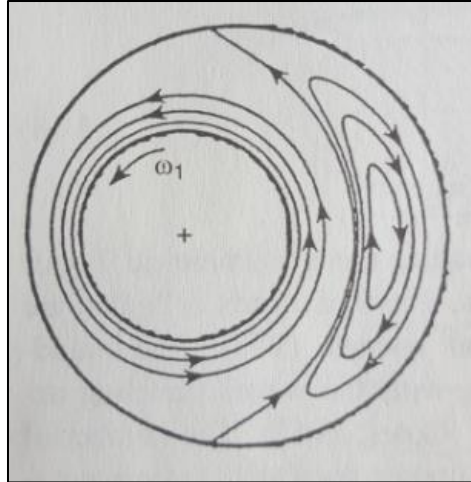


Figure 11: Hydrodynamic Journal Bearing [29].

Bearing type is key for tube life and practical experience such as tube prep and cooling. Ball bearings of hardened steel that are coated with silver and lead have been common in x-ray tubes of the past. However, they have limited life and deteriorate more rapidly with high speed, load, and temperature. In 1989, Philips came out with the first SGB. The gap between the sleeve and shaft is around 10 to 50 μm and is filled with liquid metal GaInSn. If made properly with the anti-wetting seals, these bearings have almost infinite rotation life with the only wear coming from starts and landings. The continuous rotation meant zero prep time for emergency CT scans. The bearings are virtually noiseless as well and very stable [11] [17]. Figure 12 Shows the cross-section difference between a ball bearing x-ray tube and a SGB x-ray tube.

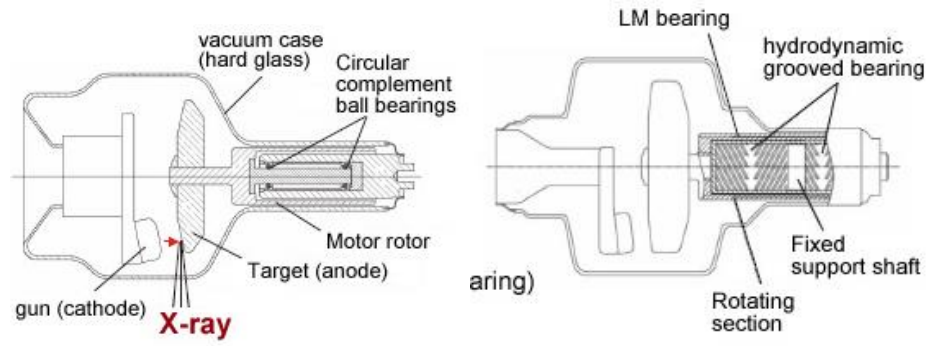


Figure 12: Configuration differences between ball bearing and SGB anode. [18]



Figure 13: Example of Philips iMRC x-ray tube insert with SGB [11]



Figure 14: Example of cut away from a SGB insert showing two radial bearings of a liquid metal lubricated SGB [11].

The tight tolerances on the bearing shaft and sleeve means manufacturing processes are tightly controlled. Piece part processing of bearings with micron level tolerance is a challenge not only to assemble, but also to inspect incoming parts from diverse suppliers.

2.5 Fundamentals of Balancing

A working knowledge of fundamentals of balancing allows one to understand why the balancing of the rotating parts of an x-ray tube are such an integral and important aspect of tube performance. The section to follow highlights the history of balancing as well as the essential characteristics of balancing. The knowledge gained through this rudimentary review establishes the foundation of the methodology to optimize the balancing machine and determine its repeatability.

2.5.1 History of Balancing

It was a primary requirement for rotors of the earliest steam engines to run smoothly that made balancing a point of interest. It is hard to believe the balancing of a steam turbine rotor took three to four weeks of hard manual labor – the technology available then was still comparatively simple and the results of the balancing process very inaccurate. Boilers exploding and flywheels disintegrating at high speeds contributed to hazardous work environments and inadequate balance quality also caused bearings to wear down quicker. Experienced engineers recognized these dangers and began looking for solutions [16].

Canadian engineer H. Martinson was one of the first to consider the subject of balancing from a theoretical point of view. In 1870, he was granted what was likely the first patent for a balancing machine. The rotor was mounted isotropically on soft coil springs, and driven by a universal-joint shaft. By gradually moving a piece of chalk towards the rotating rotor, he was able to determine the position of the unbalance with some degree of accuracy. No records were ever found as to whether this machine worked, or if it was ever built in major quantities [16].

In 1908 Carl Schenck, who had also started looking into "roll-off" balancing at that time concluded a license agreement with Lawaczeck. The "Lawaczeck principle" remained valid right up to the 1940's. The Lawaczeck consisted of a pendulum-mounted fixed bearing on the one side of the rotor and a radially flexible bearing on the other side. After initial correction in one plane, the rotor was re-installed. In 1915, Schenck took over the sole worldwide license for this machine [16].

During this period, a number of new optical and mechanical measuring methods were developed, whose measuring accuracy was quite remarkable. The "Lawaczeck

model" was capable of achieving a balance quality equivalent to a center of gravity displacement of 0.001 mm (.00003937 inches) - a balance quality which would even today be perfectly adequate for many applications [16].

2.5.1.1 From Mechanical to “Electrical Machines”

In 1935 a machine patented in the USA, featuring electrodynamic vibration sensors and stroboscopic determination of the unbalance angle pioneered a change over to a new design.

In 1942 Schenck was granted a patent for a "Method and facility for dynamic balancing by determination of the angular position of unbalance by means of a periodic curve displayed on the screen of an oscilloscope". This was the first balancing system suitable for large-volume production. Due to its high accuracy, the system was used through World War II for balancing gyroscopic stabilizers for naval vessels [16].

The rapid economic and technical development in post World War II period also left its marks on balancing technology. Until the present time, the automotive industry, aeronautical and aerospace technology, energy generating and electrical industries, and mechanical engineering with their constant increase in standards and requirements were the driving forces in balancer technology continuous development [16].

In the 1970s, the mechanical foundations for balancing machines established themselves and electronics made their first appearance in balancing and diagnostic technology. In 1971, the electronic wattmeter measuring principle was introduced, the first computer-controlled balancing systems followed in 1974. The next major change

came with the emergence of digital technology. In the early 1980s, microprocessors started appearing in balancer measuring systems [16].

2.5.2 Present Status of the Balancing

Balancing is performed in many different industries and on many different types of rotating products. Rotating components experience significant quality and performance improvements when balanced. Balancing is the process of aligning a principal inertia axis with the geometric axis of rotation through the addition or removal of material. By doing so, the centrifugal forces are reduced, minimizing vibration, noise and associated wear. Virtually all rotating components experience significant improvements when balanced. Consumers throughout the global market continue to demand value in the products they purchase. They demand performance along with smaller, lighter, more efficient, more powerful, quieter, smoother running and longer lasting rotating systems. Balancing can contribute to each of these and is one of the most cost effective means of providing value to the consumer [3].

The purpose of balancing a rotor is to help ensure that the machinery is safe and reliable. This is achieved when the rotor mass and rotational centerlines are as close to equal as possible. Excessive unbalance can cause vibration and stress in the shaft or attached pieces. As the rotor spins, centrifugal forces act upon it. The surface around the periphery is stressed as particles are pulled outward from the axis of rotation. If all of these radial forces are equal, the rotor is said to be in balance and should not vibrate. However, if the rotor contains a heavy spot to one side, the radial forces will not cancel and the unbalanced force will try to force a new center of rotation [2]. As seen in Figure

15, the entire rotor is being pulled in the direction of the arrow F due to centrifugal force exerted by the mass during rotation.

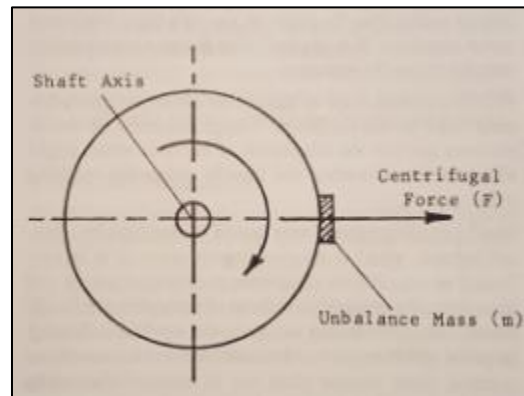


Figure 15: Unbalance causes centrifugal force [6].

A rotating element having an uneven mass distribution will vibrate due to excess centrifugal force exerted during rotation by the heavier side of the rotor. Unbalance causes centrifugal force, which in turn causes vibration. When at rest, the excess mass exerts no centrifugal force and, therefore, causes no vibration. Yet, the actual unbalance is still present. Unbalance, therefore, is independent of rotational speed and remains the same whether the part is at rest or is rotating – assuming the part does not deform during rotation. Centrifugal force, however, varies with speed. When rotation begins, the unbalance will exert centrifugal force tending to vibrate the rotor. The higher the speed, the greater the centrifugal force exerted by the unbalance and the more violent the vibration. Centrifugal force increases proportionately with the square of the increase in

speed. If the speed is doubled, the centrifugal force quadruples; if the speed is tripled, the centrifugal force is multiplied by nine [6].

Unbalance is measured in mass times distance, or gram-centimeters, which is the mass multiplied by its distance from the axis of rotation or its radius. An unbalance of 10 g*cm for example indicates that one side of the rotor has an excess mass equivalent to 5 grams at 2 cm radius or 10 grams at 1 cm radius.

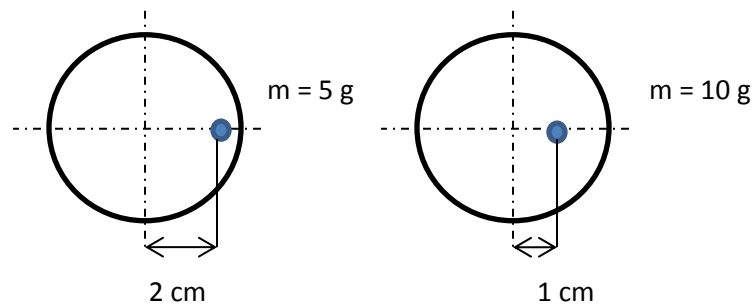


Figure 16: Side view of rotor with 10 g*cm unbalance.

In each case, the mass multiplied by its distance from the shaft axis amounts to the same unbalance value of 10 g*cm as shown in Figure 16. A given mass will create different unbalances depending on its distance from the shaft axis. To determine the unbalance, simply multiply the mass by its radius. The term “unbalance” is sometimes used as a synonym for “amount of unbalance” or “unbalance vector”. There are many different causes of unbalance including the following:

- a) Tolerances in fabrication including casting, machining and assembly

- b) Variation within materials such as voids, porosity, inclusions, grain, density and finishes
- c) Non-symmetry of the design including drive motor windings and part shapes
- d) Non-symmetry in use, including distortion, dimensional changes, and shifting of parts due to rotational stresses, aerodynamic forces and temperature changes

X-ray tubes with a rotary anode are used in different x-ray systems such as a CT-system. For this generation of x-rays, the anode is rotated inside the tube. Unbalance correction methods include mass addition, mass removal or mass centering. Prior to the assembly of the tube, balancing is achieved by cutting away materials from rotatable components. Although balanced, during operation thermo-mechanical and material ageing effects may cause a change of the state of balance of an x-ray tube's anode and, for example, the x-ray tube's rotor as well. The balance performed in this thesis will be a 2-plane balance on the rotor plane and target plane as shown in Figure 17.

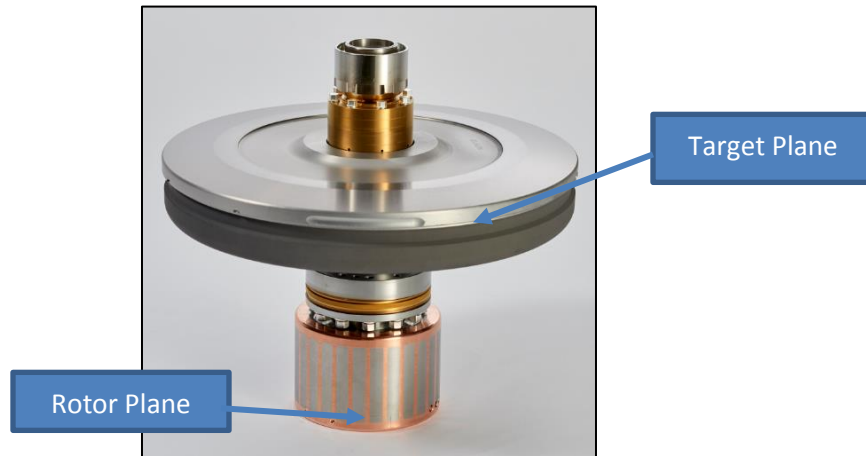


Figure 17: Rotating Sub Assembly also known as a ROSS or anode.

In some cases, this might go beyond acceptable levels so that the tube has to be replaced. Furthermore, as an example, in a CT-system, an x-ray tube is rotating about the patient and generates a fan beam of x-rays. Opposite and with it on a gantry rotates a detector system which converts the attenuated x-rays to electrical signals. Then, a computer system reconstructs an image of the patient's body in the region of interest. The unbalance of the anode may cause severe vibration of the tube housing assembly and thus malfunction of the detectors resulting in low image data quality. The unbalance may further cause reduction of bearing life and also an increase of acoustic noise leading to patient discomfort. Usually, prior to mounting them into x-ray tubes, anode rotors will be assembled, then tested for vibration and balanced by drilling or cutting away material at the required locations. After insert assembly, no further balancing is possible, as the rotors are enclosed in vacuum-tight tube frames [4] [5].

Dynamic balancers rely on the effects of centrifugal force to detect unbalance. They can detect all forms of unbalance – static, couple, dynamic or quasi-static. The distinction between so called soft and hard bearing balance is made based on the natural frequency of the parts to be balance and the relative speed of operation. Balance operations at speeds below the natural frequency of the rotating parts (usually less than half) are classified as hard and those operating at speeds above the natural frequency are classified as soft (usually more than double) [3]

Patent 5689543 describes how x-ray tubes are balanced. This method is currently followed at the x-ray tube manufacturing facility and is entitled “Method for balancing rotatable anodes for x-ray tubes”. The patent is a method of balancing x-ray anodes wherein the anode rotor is dynamically balanced separately from the anode target. The

anode target is then attached to the anode rotor to provide the assembled anode, and the assembled anode is then dynamically balanced. This sequential balancing method has the advantage that it results in an anode which remains balanced during operation at speeds up to and exceeding the anode's critical speeds, even though the dynamic balancing steps may be performed at speeds substantially below the anode's critical speeds. This is also convenient because at such low balancing speeds, the dynamic balancing steps can be performed in air rather than vacuum without concern for damage of the rotor bearings, excessive vibration, and potential safety concerns [1].

2.5.2.1 Balance Quality Grades

International Standard ISO 1940/1 is a widely accepted reference for selecting rigid rotor balance quality. ISO 21940-11:2016 replaces ISO 1940-1:2003, which has been technically revised. The main changes are deletion of the terms and definitions which were transferred to ISO 21940-2 and a more pronounced explanation of the application of permissible residual unbalances for the processes of balancing a rotor and verifying its residual unbalance. Figure 18 shows the balance quality grades for a variety of rotor types. The "G" number as defined in Equation 2.5.2.1 is the product of specific unbalance and the angular velocity of the rotor at maximum operating speed and is a constant for rotors of the same type. This is because geometrically similar rotors running at the same speed will have similar stresses in the rotor and its bearings. The quality grade number represents the maximum permissible orbital velocity of the center of gravity in mm per second around the rotational axis.

$$G = e \times \omega = \text{constant} \quad 2.5.2.1$$

Balance quality grades are separated by a factor of 2.5. However, G numbers of intermediate value may be used to satisfy special requirements. For example, a standard pump impeller or a fan has a suggested balance quality grade of G 6.3. Yet, special conditions may require better balance quality of G 4.0 to satisfy installation requirements. A grade of less than G2.5 is usually only achievable on very special equipment [7] [9].

2.5.2.2 Determining Permissible Residual Unbalance - U_{per}

The term "unbalance" is referred to two quantities. First is the balancing acceptance limit of a rotor and is usually called permissible or allowable unbalance. Second is the existing or residual unbalance in a rotor.

$$U_{per} = e_{per} \times W \quad 2.5.2.2$$

Permissible residual unbalance (U_{per}) is a function of G number, rotor weight (W) and maximum service speed of rotation. U_{per} is the maximum permissible residual unbalance or the so called balance tolerance. e_{per} is the maximum permissible residual specific unbalance or balance tolerance in terms of displacement of rotor CG. U_{per} and e_{per} are related as shown in Equation 2.5.2.2. Instead of using the graph to look up the "specific unbalance" value for a given G number and service RPM and then multiplying by rotor weight, U_{per} can be calculated by using the following formulae also presented in Equation 2.5.2.3 [9]:

$$U_{per} \text{ (g-mm)} = 9549 \times G \times W/N \quad 2.5.2.3$$

G = Balance quality grade

W = Rotor weight (Kg)

N = Maximum service RPM

Assuming the balance quality grade for the rotating part is G0.4, which is the highest quality graded of balance, the balance tolerance can be calculated. Applying the known conditions for a rotating anode target x-ray tube such as the ROSS in Figure 17 and plugging these values into Equation 2.5.2.3 the results are:

$$G = 0.4$$

$$W = 11\text{kg}$$

$$N = 8400\text{rpm}$$

$$U_{\text{per}} (\text{g}\cdot\text{mm}) = 9549 \times 0.4 \times 11\text{kg}/8400\text{rpm} = 5.0 \text{ g}\cdot\text{mm} \quad 2.5.2.4$$

The calculation in Equation 2.5.2.4 lines up very closely to the company's specification. The company specification for the anode balance is 2.5 g*mm, or 0.25g*cm, confirming that this balance operation is considered high quality. Figure 20 indicates the maximum permissible residual imbalance for certain balance quality grades, and the company's specification limit will be plotted. This required balance specification is beyond the requirements of most other industrial applications. This high quality balance specification is a continuous challenge at the x-ray tube manufacturing facility. Furthermore, the anode's focal spot operating temperature is around 2500°C, while spinning at close to 65 G's during gantry rotation. There is ongoing work to determine the critical x's that impact this very precise manufacturing balance process.

| Balance Quality Grade | Product of the Relationship ($e_{per} \times \omega$) ^{(1) (2)} mm/s | Rotor Types - General Examples |
|-----------------------|---|--|
| G 4 000 | 4 000 | Crankshafts/drives ^(a) of rigidly mounted slow marine diesel engines with uneven number of cylinders ^(a) |
| G 1 600 | 1 600 | Crankshafts/drives of rigidly mounted large two-cycle engines |
| G 630 | 630 | Crankshafts/drives of rigidly mounted large four-cycle engines Crankshafts/drives of elastically mounted marine diesel engines |
| G 250 | 250 | Crankshafts/drives of rigidly mounted fast four-cylinder diesel engines ^(a) |
| G 100 | 100 | Crankshafts/drives of fast diesel engines with six or more cylinders ^(a) Complete engines (gasoline or diesel) for cars, trucks and locomotives ^(a) |
| G 40 | 40 | Car wheels, wheel rims, wheel sets, drive shafts Crankshafts/drives of elastically mounted fast four-cycle engines with six or more cylinders ^(a) Crankshafts/drives of engines of cars, trucks and locomotives |
| G 16 | 16 | Drive shafts (propeller shafts, cardan shafts) with special requirements Parts of crushing machines Parts of agricultural machinery Individual components of engines (gasoline or diesel) for cars, trucks and locomotives Crankshafts/drives of engines with six or more cylinders under special requirements |
| G 6.3 | 6.3 | Parts of process plant machines Marine main turbine gears (merchant service) Centrifuge drums Paper machinery rolls; print rolls Fans Assembled aircraft gas turbine rotors Flywheels Pump impellers Machine-tool and general machinery parts Medium and large electric armatures (of electric motors having at least 80 mm shaft height) without special requirements Small electric armatures, often mass produced, in vibration insensitive applications and/or with vibration-isolating mountings Individual components of engines under special requirements |
| G 2.5 | 2.5 | Gas and steam turbines, including marine main turbines (merchant service) Rigid turbo-generator rotors Computer memory drums and discs Turbo-compressors Machine-tool drives Medium and large electric armatures with special requirements Small electric armatures not qualifying for one or both of the conditions specified for small electric armatures of balance quality grade G 6.3 Turbine-driven pumps |
| G 1 | 1 | Tape recorder and phonograph (gramophone) drives Grinding-machine drives Small electric armatures with special requirements |
| G 0.4 | 0.4 | Spindles, discs and armatures of precision grinders Gyroscopes |

Figure 18: Balance quality grades for various groups of representative rigid rotors [8][9]

Quality grade relates max service speed to the permissible specific unbalance. For a specific grade, as rotor service speed increases, the unbalance specification gets tighter. This means that the unbalance amount allowed decreases as rotor service speed increases.

Balance quality grades are separated from each other by a factor of 2.5. However, sometimes grades between these lines are used.

One important and fundamental aspects of balancing is the direct relationship between the displacement of center of gravity of a component from its rotation axis, and the resulting unbalance. The conversion of CG displacement to unbalance is explained as follows. Assume a perfectly balanced anode, as shown in Figure 19, rotating about its shaft axis and with a weight of 11kg. The anode in Figure 19 is balanced to specification of $2.5\text{g}\cdot\text{mm}$. This remaining unbalance causes the CG of the disc to be displaced by a distance “e” in the direction of the unbalance mass. [6]

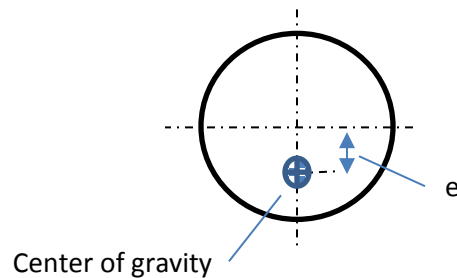


Figure 19: Disk shaped rotor with displaced CG due to unbalance

Table 1: Displacement or eccentricity of rotor CG in mm and microns

| | |
|------------|---------|
| $e=U/W$ | |
| U (g*mm) | 2.5 |
| W (g) | 11000 |
| e (mm) | 0.00023 |
| e (um) | 0.23 |

The anode mentioned in Figure 19 would have an “e” of 0.23 microns of displacement from its CG at the 2.5 g*mm spec limit. These data are presented in Table 1. Figure 20 shows the 0.23 micron center of gravity displacement along with the 8400rpm max service speed. Connecting the lines associated with G0.4 quality grade on the graph reveals just how tight the balance specification is for the required service speed. The balance specification of 2.5 g*mm is below the G0.4 balance quality level.

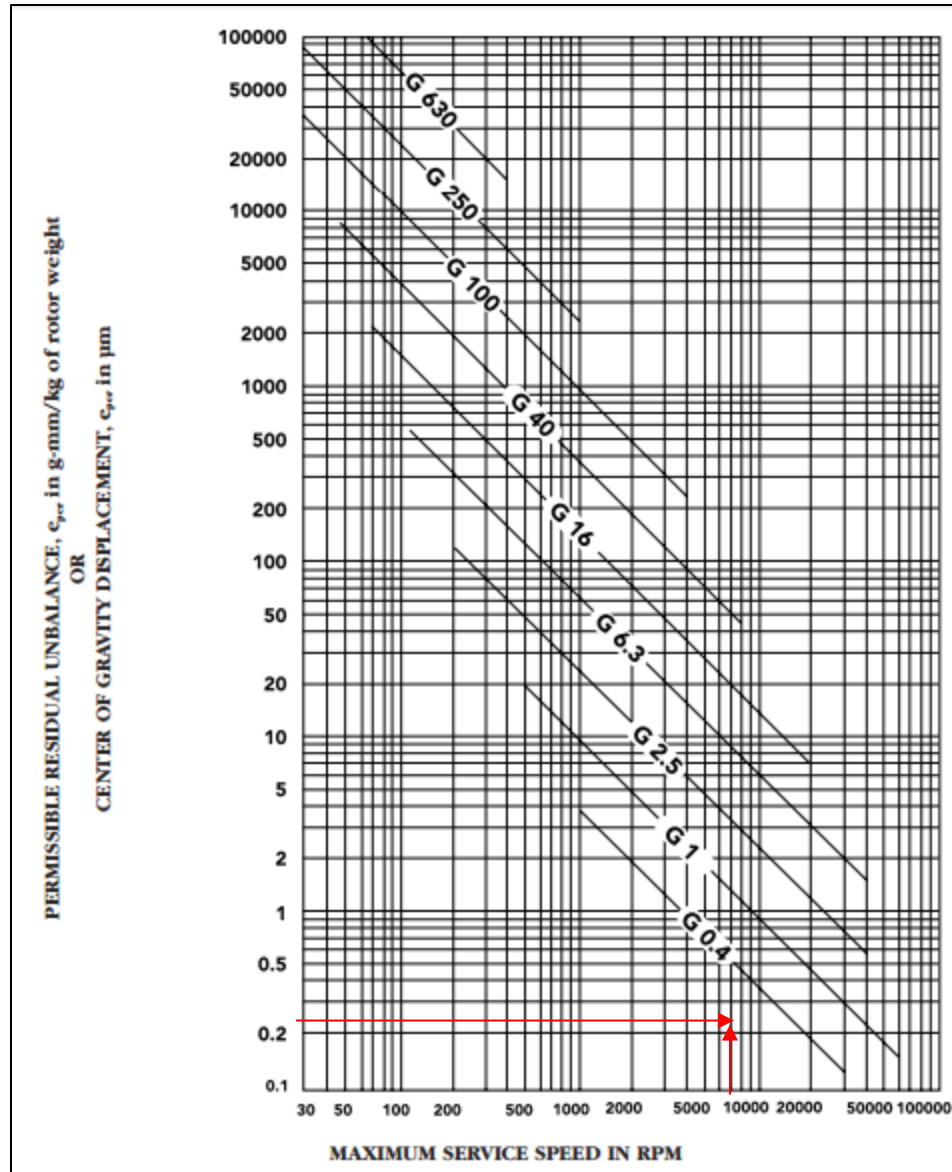


Figure 20: Maximum permissible residual unbalance [8] [9]. The red lines show where the anode balance would lie on this chart using the 0.23 micron center of gravity displacement along with the 8400rpm max service speed.

A comparison with API, ISO, and MIL-STD-167-1 shows that the current anode unbalance process is very tight controlled and the specification limit is off the chart

shown in Figure 21. A comparison with calculations is presented in Equations 2.5.2.5 through 2.5.2.9.

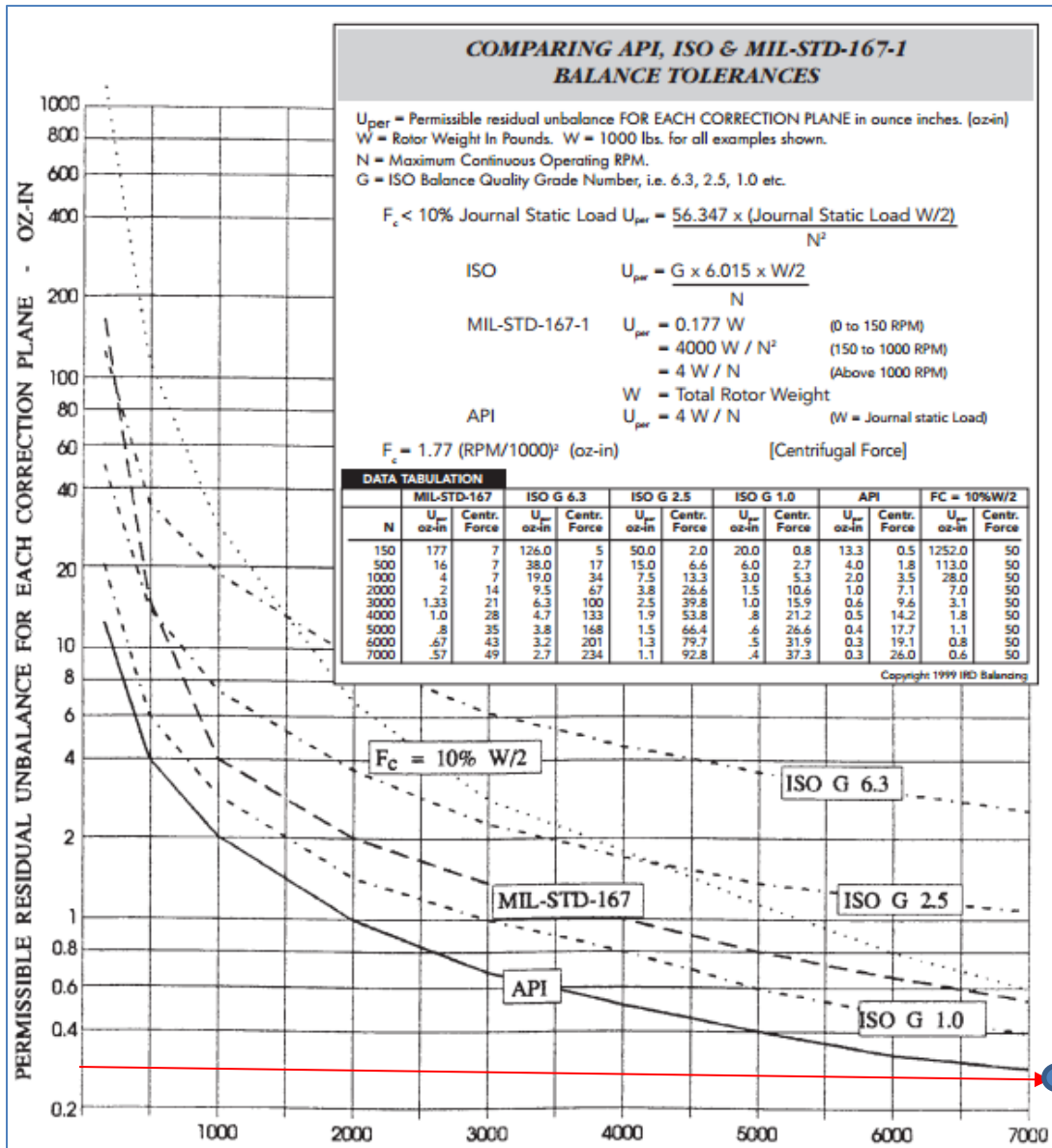


Figure 21: Comparison of API, ISO & MIL-STD-167-1 balance tolerances. Calculations show that the current balance spec is off the chart using the ISO 1940 Standard calculation of 0.0034 oz*in (which is 0.25g*cm) and 8400rpm. [19]

Using the ISO 1940 Standard with a G=0.4: [19]

$$U_{per} = 0.4 * 6.015 * (24.2 \text{ lbs} / 2) / 8400 = 0.0034 \text{ oz-in} = 0.25 \text{ g*cm} \quad 2.5.2.5$$

Using MIL-STD-167-1 Standard: [19]

$$U_{per} = 4 \text{ W/ N} \quad (\text{above } 1000 \text{ rpm}) \quad 2.5.2.6$$

$$U_{per} = 4 * 24.2 \text{ lbs} / 8400 = 0.0115 \text{ oz-in} = 0.828 \text{ g*cm} \quad 2.5.2.7$$

Using API Standard: [19]

$$U_{per} = 4 \text{ W/ N} \quad 2.5.2.8$$

$$U_{per} = 4 * 24.2 \text{ lbs} / 8400 = 0.0115 \text{ oz-in} = 0.828 \text{ g*cm} \quad 2.5.2.9$$

Because these calculations consider different rpm's, the results are different. The ISO 1940 Standard is the tightest because it uses the actual 8400 rpm's that the anode encounter. MIL-STD-167-1 and API both use the generic equation for a work piece above 1000 rpm. These are used as examples to demonstrate and reinforce how tight the balance specification of 0.25g*cm for the x-ray tube anode is.

CHAPTER 3

DATA COLLECTION

3.1 Statement of Procedure and Methodology

The newly installed vacuum balance machine was used to perform all tests. Liquid metal bearing process anodes have been used to test the unbalance of the current x-ray tube configuration. A ball bearing anode has been developed to replicate the geometry and mass distribution of the liquid metal SGB. This setup will have the capability to use the same mass components as the SGB, and will eliminate part to part variation. Large scale testing has been conducted to understand the current effects of unbalance on the liquid metal SGB. Bias checks and data collection runs have been performed to fully capture the liquid metal SGB characteristics. Gage R&R studies have been performed to understand the effects of the measurement system and operator interactions. These tests have been performed to help identify the critical variables.

3.2 Overview of Manufacturing Facility's Balance Machine

The balance process follows the diagram in Figure 4. After the rotor and target have been attached to the x-ray tube bearing, the assembly becomes known as the ROSS or anode shown in Figure 1. This anode is then placed into the Schenck HMS10/CAB920H balancing machine shown in Figure 3. The anode is rotated up to 1350rpm using an Allen Bradley Powerflex 753 stator drive, held for 5 seconds, and then let to coast down

to a measurement speed of 950rpm. During the coast down through 950-850rpm, the amount of material that needs to be removed is calculated based off the unbalance magnitude and angular location, as calculated using Equation 2.5.2.3. The balance machine will then report to the operator what angle and depth for material removal from the target and rotor planes depicted in Figure 17. After this material is removed from both the rotor and the target correction planes, the anode is spun up to speed again to find the new unbalance. This process is repeated until the rotor and target plains both reach the unbalance specification requirement.

3.2.1 Detailed Process of Balancing

This section will describe the process of performing a balance run the manufacturing facility's balance machine.



Figure 22: Balancer system comprised of Schenck Measurement Cabinet, HMI or Human Machine Interface, and balancer table.

To perform a balance run, the collets will be fastened to the anode. The anode will then be placed in the balance chamber.

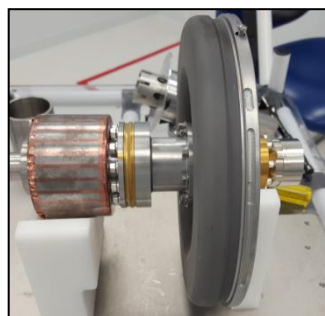


Figure 23: An anode that is ready for balance.

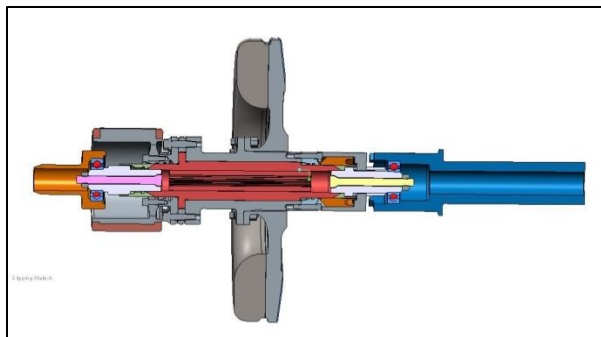


Figure 24: An anode which has the collets attached and is ready for placement into the machine.

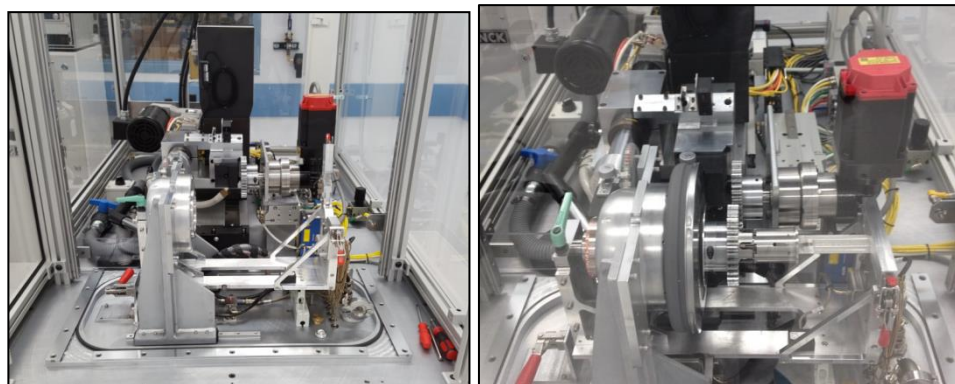


Figure 25: The balance table before and after anode installation.

The vacuum chamber will close and pull vacuum on the anode. Once the set vacuum level of 100mTorr has been reached, the anode will spin up to a speed of 1350rpm by a stator drive, hold for 5 seconds, and then begin to coast down until it stops rotating.



Figure 26: Balance machine with vacuum chamber closed with the anode inside.

While the anode coasts down between 950rpm and 850rpm, the unbalance will be captured. This unbalance is reported for the target and for the rotor. A correction algorithm that considers the size of the rotor and target and their respective densities will then output where the material removal correction will take place, shown in Figure 27.

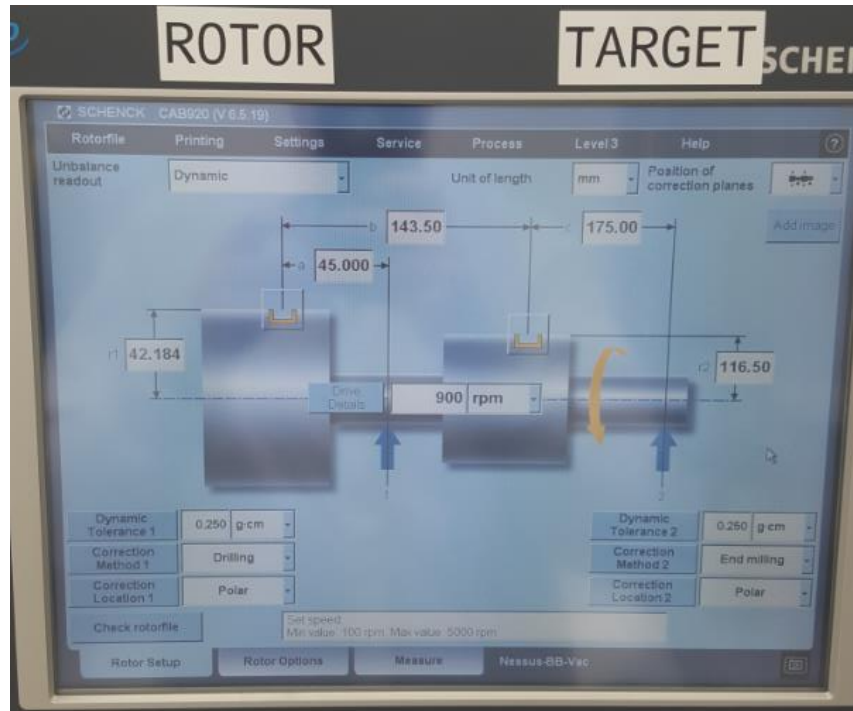


Figure 27: Schenck set up screen where the diameters and distances of the rotor and target planes are configured.

Centrifugal forces, generated by unbalance in the rotating anode, are measured by built in pickups, shown in Figure 28 and

Figure 29, which put out voltage signals. The machines electronic unit processes these signals, and the results are displayed to the operator.

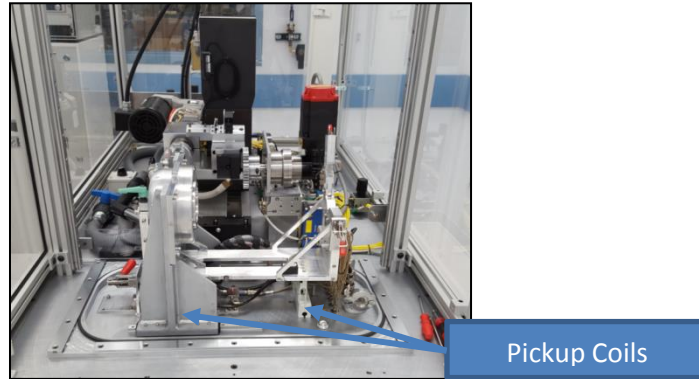


Figure 28: Two sets of pickup coils which measure the unbalance.

Most “hard-bearing” balancing machines are permanently calibrated for the entire range of rotors that fall within the capacity range of the machine. However, rotor geometry specific calibrations have been performed on this machine and anode will be detailed later. The Balancing machine used is a Schenck HMS10/CAB920H. The HMS10 balancing machine has a 19.8 inch (500mm) bed, Twin Roller Carriages, Photocell Reference, and can accommodate up to a 36 pound (16.3kg) symmetrically loaded rotor. It can achieve a balancing accuracy within 5 millionths of an inch (0.000127mm) offset from the rotor’s principle axis of inertia [20].

Table 2: Machine designation

| | |
|---------|---|
| HMS | Hard-Bearing Machine with Permanent Calibration |
| 10 | Size of Machine |
| CAB920H | Instrumentation Designation Configured for Horizontal Balancing |

All communications between the operator and the instrumentation unit take place through the touch screen monitor. The CAB920H Instrumentation can be set up to measure dynamic unbalance, couple/static unbalance, static/couple unbalance, and static unbalance. The CAB920H incorporates an automatic sensitivity selection feature that will select the proper internal sensitivity level so the instrumentation will always display the correct amount of unbalance, with proper decimal position, for any unbalance magnitude without the operator entering any additional file parameters. This is true regardless if the values are large initial unbalances, or ultra-precise, low-level, tolerance values [20].

The machine has a plane separation network to measure unbalance in two selectable planes of correction. This feature eliminates correction plane interference, making it possible to measure and correct unbalance on the rotor without affecting the target. Separate readouts are provided in grams for the left (rotor) and right (target) correction planes because the radii are different. The amount of angular position on unbalance is indicated simultaneously for both correction planes [20].

One SF-14/SF-15 vibration pickup is mounted at the rear of each support pedestal. The vibration pickup senses the movement of the support pedestal and provides an electrical signal to the instrument unit. This specific vibration pickup is designed for small balancing machines up to size 10, which is the size of the machine being used in this experiment. [20]

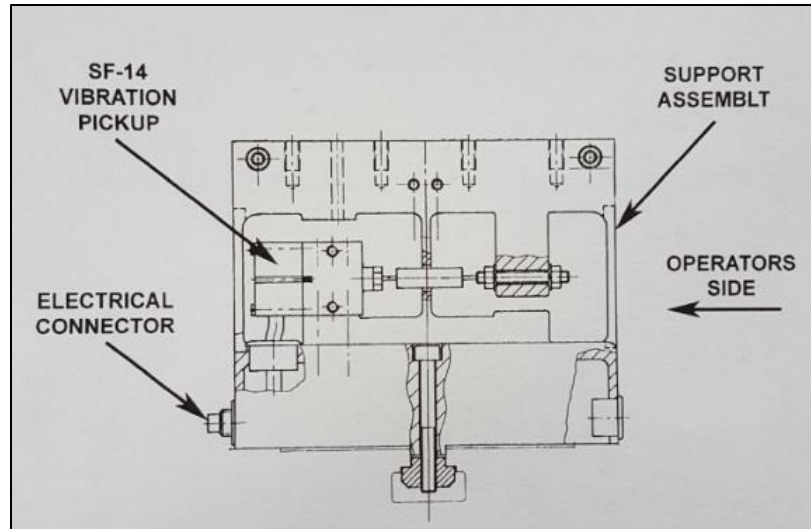


Figure 29: SF-14/SF-15 Vibration Pickup Installation [20].

Figure 30 shows that for this given run, the rotor has a 2.1 g*cm unbalance at 316 degrees and the target has an unbalance of 57 g*cm at 8 degrees.



Figure 30: Example of the Schenck output that tells where and what the unbalance is after a balance measurement run.

The chamber will vent to atmosphere and open so that the rotor can be drilled and the target can be milled to the specified correction limits. Based on the unbalance calculated in Figure 30, Figure 31 shows where the correction should take place. The target plane unbalance of 57 g*cm at 8 degrees is translated into a correction on the target of removing material 2.0mm deep at an arc from 351 to 25 degrees. The measurement and correction cycles will repeat until the anode has reached the unbalance specification limit.



Figure 31: This screen outputs where and how the correction will take place based on the unbalance. This information is sent to the HMI, Figure 32, so that the operator can begin the material removal process.



Figure 32: HMI screen showing the depths and degree of the cuts to be made for the rotor and target planes.

Currently, the average number of cycles to achieve the balance specification is 8. Figure 33 shows 15 different balance operations to illustrate what the balance process looks like. Figure 34 shows a zoomed in view of Figure 33 to give a glimpse into the area around the specification limit. Each MAN### corresponds to a unique anode which the balance operation was performed on. The starting target unbalance varies dramatically; the average starting target unbalance is 60 g*cm with a 20 g*cm standard deviation shown in Figure 35. If you take that 61g*cm average and divide that by the 0.25g*cm specification, then the average target is starting 240 times the 0.25g*cm tolerance.

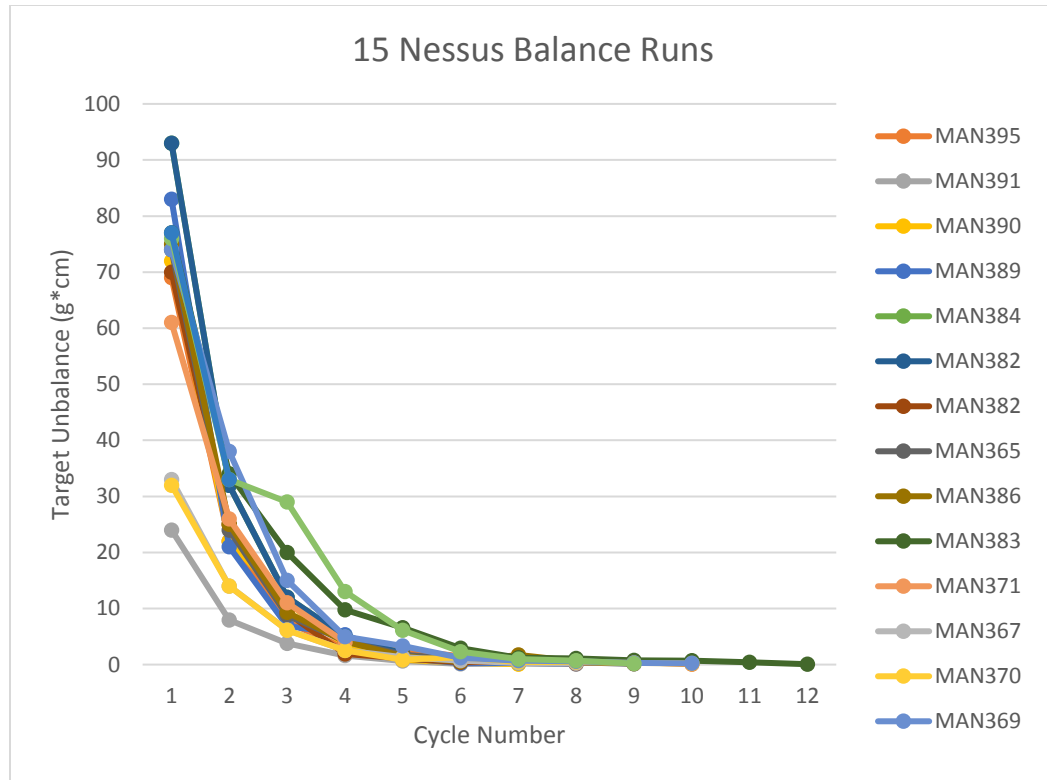


Figure 33: Run chart of the Target Unbalance vs the number of cycles for 15 different balance runs.

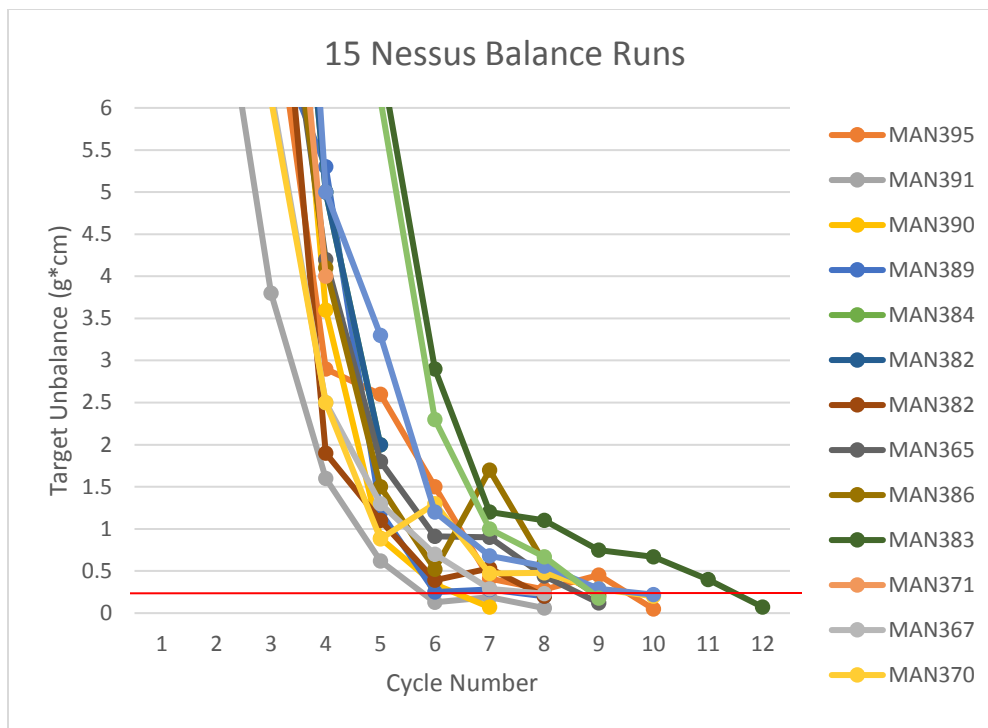


Figure 34: Zoomed in view of Figure 33 run chart showing the 0.25g*cm specification shown in red.

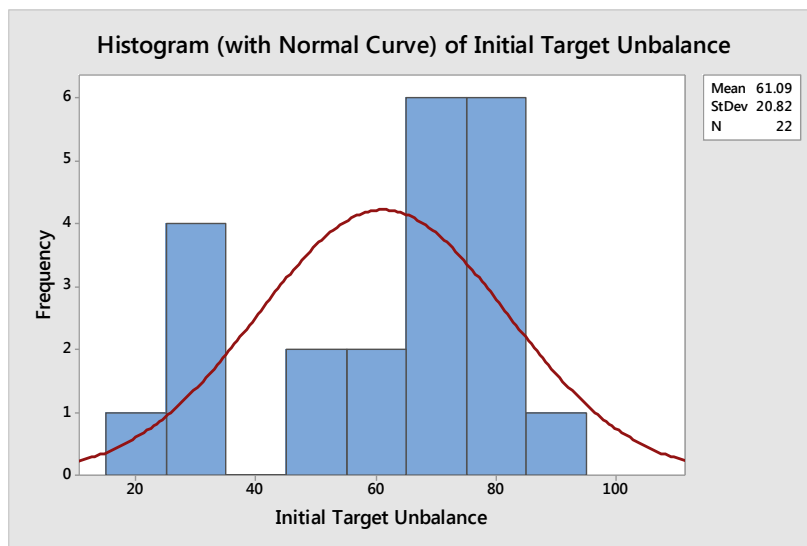


Figure 35: Initial Target Unbalance.

Throughout most this document, the focus will be on the target unbalance. The target is made of a special Tungsten alloy which is made using a hot isostatic pressing process so that it can withstand the tremendous thermals it experiences during x-ray tube operation. Thus, the targets have non-uniform density. Because the target is larger in diameter and has a much greater mass than the rotor, its initial unbalance is severely greater than the rotor. The rotor has uniform density, has an average initial unbalance of 6 g*cm, and only takes on average 3 cycles to balance. Therefore, of the average 8 cycles it takes to balance the anode, 5 of the cycles are spent just balancing the target.

3.3 Data Collection Overview

The problem with the balance operation is that running consecutive measurement cycles on the same liquid metal SGB has shown very large standard deviation. In other words, if the vacuum chamber is left closed and the bearing is spun multiple times to take a measurement, different unbalance results are displayed. Figure 36 shows an example of this phenomenon. The standard deviation is 0.05g*cm or 20% of the 0.25g*cm unbalance specification.

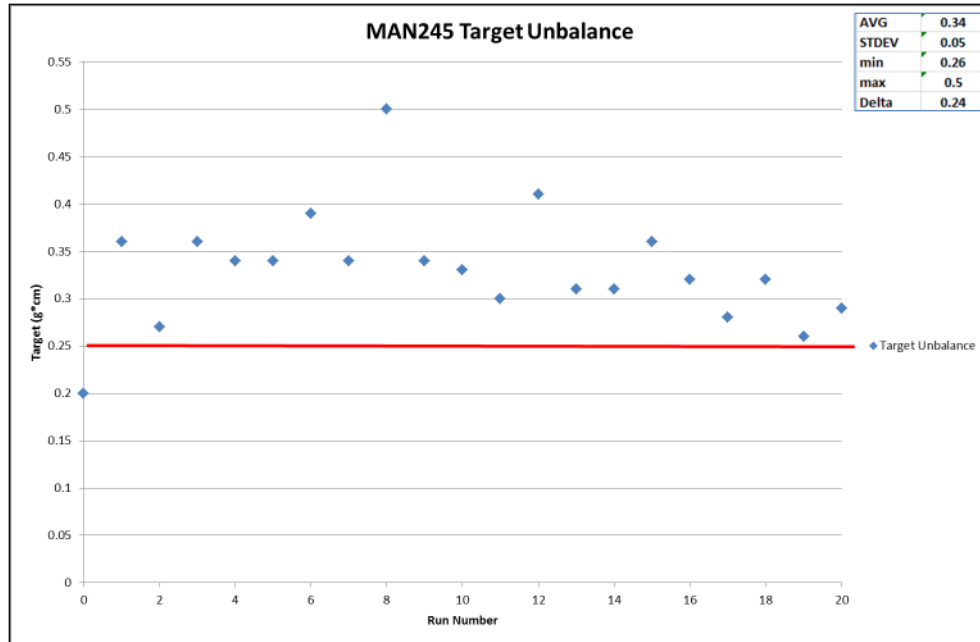


Figure 36: Example of a specific bearing being spun multiple times producing different unbalance results. The target unbalance is plotted on the y axis and the run number is plotted on the x axis.

This phenomenon will be investigated thoroughly. First a deeper look needs to be taken at the setup of the machine running it with different parts and operators to see what the baseline is. Then, determine if the liquid metal SGB is producing the large variation or if the measurement system plays a larger contribution. The same tests will be performed with a ball bearing ROSS of the same geometry to isolate the measurement system. The average unbalance and standard deviation between consecutive runs will be analyzed as the main outputs from the balance machine. This is critical because the material removal process is based on where the unbalance is located. If material is removed from an unbalance location that is not accurate, the operator could create more unbalance in the system by removing material in the improper location. The current

liquid metal SGB manufacturing balancing process needs to be more thoroughly understood to better capture the cycle variation that will be seen in production. Every additional cycle requires 15 extra minutes and can lead to process bottlenecks throughout the rest of the x-ray tube manufacturing process.

The following figure is a high-level overview of the testing performed in this section. The section numbers are on the left of the flow chart. The purpose of each test is described in the block along with how the testing was performed. A quick snap shot of the results is given with positive and negative remarks. Finally, the takeaway is the overall lesson learned from that section of testing. As the testing progressed, more questions arose which needed to be answered. Each section builds off the testing and conclusions from the previous section.

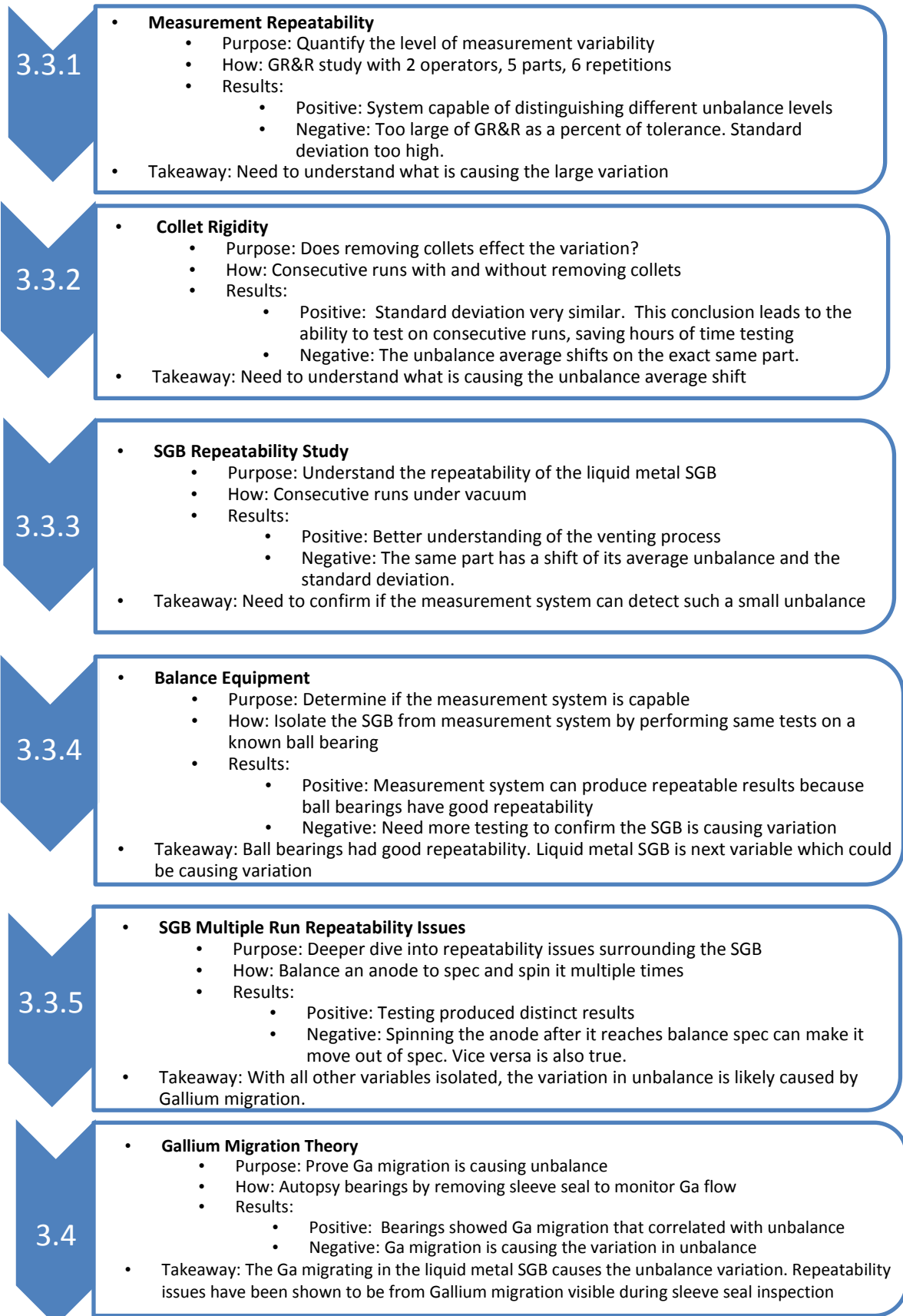


Figure 37: Overview of Data Collection and Results

The machine has a quarterly calibration requirement which is called a bias check. The bias check makes sure that the machine can detect a National Institute of Standards and Technology calibrated weight at the proper angular location. A known value weight is threaded into the target and the rotor at a known angular location. The ROSS is spun under vacuum to receive an unbalance measurement. The requirements for passing are listed in Table 3.

Table 3: Bias Check Requirements

| Bias Weight Range | Weight Tol | Angle Tol |
|--------------------------|------------------------|--------------------|
| 0.030g – 0.300g | +/- 12% Of Bias Weight | +/- 5 ⁰ |
| 0.300g – 1.000g | +/- 10% Of Bias Weight | +/- 5 ⁰ |
| 1.000g – 2.000g | +/- 8% Of Bias Weight | +/- 5 ⁰ |
| 2.000g – 2.500g | +/- 5% Of Bias Weight | +/- 5 ⁰ |

The balancer passes this test as shown in Table 4 and Table 5. The weight used was 1.118g, so the weight tolerances were all within plus or minus 8% of the bias weight and plus or minus 5% of the angle tolerance listed in the requirements. This means the machine can accurately detect the correct amount of weight at the correct angular location. This is critical in determining the machines health.

Table 4: Bias Check Results for Target Plane

| Target Plane | | | | | | |
|---------------------|--------------------|------------------------|------------------------|--------------------|-----------------------|------------------|
| Known Values | | Measured Values | | | | |
| Weight (g) | Angle (deg) | Weight (g) | % of Weight Tol | Angle (deg) | % of Angel Tol | Pass/Fail |
| 1.118 | 0 | 1.15 | 2.8% | 0 | 0.0% | PASS |
| 1.118 | 0 | 1.11 | 0.7% | 1 | 0.3% | PASS |
| 1.118 | 0 | 1.12 | 0.2% | 0 | 0.0% | PASS |
| 1.118 | 0 | 1.1 | 1.6% | 359 | 0.3% | PASS |
| 1.118 | 0 | 1.12 | 0.2% | 0 | 0.0% | PASS |
| 1.118 | 0 | 1.13 | 1.1% | 359 | 0.3% | PASS |
| 1.118 | 0 | 1.13 | 1.1% | 0 | 0.0% | PASS |

Table 5: Bias Check Results for the Rotor Plane

| Rotor Plane | | | | | | |
|---------------------|--------------------|------------------------|------------------------|--------------------|-----------------------|------------------|
| Known Values | | Measured Values | | | | |
| Weight (g) | Angle (deg) | Weight (g) | % of Weight Tol | Angle (deg) | % of Angel Tol | Pass/Fail |
| 1.118 | 0 | 1.12 | 0.2% | 1 | 0.3% | PASS |
| 1.118 | 0 | 1.11 | 0.7% | 0 | 0.0% | PASS |
| 1.118 | 0 | 1.12 | 0.2% | 1 | 0.3% | PASS |
| 1.118 | 0 | 1.1 | 1.6% | 359 | 0.3% | PASS |
| 1.118 | 0 | 1.12 | 0.2% | 0 | 0.0% | PASS |
| 1.118 | 0 | 1.11 | 0.7% | 0 | 0.3% | PASS |
| 1.118 | 0 | 1.13 | 1.1% | 0 | 0.0% | PASS |

Since the balancer passes the bias check, a closer look must be taken to see what else is effecting the large variation shown back in Figure 36. The physical installation setup of the ROSS in the balancer is important. Likewise, multiple different ROSS's should be tested at difference unbalance levels. A study

will be performed to see if the machine can pass a GR&R where different operators are involved with the setup of different parts.

3.3.1 Measurement Repeatability

The objective of this test was to quantify the level of unbalance measurement variability by determine the Gage R&R performance for the balance measuring system used in production. The study was performed with 2 operators, 5 parts, 6 repetitions and vented the chamber to remove collets between each run. The Gage R&R is the Reproducibility and Repeatability of the measurement system. The primary objective of a Gage R&R study is to quantify the level of measurement variability. A secondary objective of the Gage R&R study is to separate the contributions of variability from different sources. The gage study represents the total variation in the measurement system [69]. Threaded holes were added to a target and a rotor to perform measurements at different unbalance ranges using calibrated weights. Figure 38 shows a picture of the ROSS and the adjustable set screws. The set screws will be adjusted to simulate 5 different levels of unbalance on the ROSS simulating different points during the balance process. Recall, the ROSS usually starts with an average target unbalance of $60\text{g}\cdot\text{cm}$ and a rotor unbalance of $6\text{g}\cdot\text{cm}$ but most of the cycles take place near the specification limit.

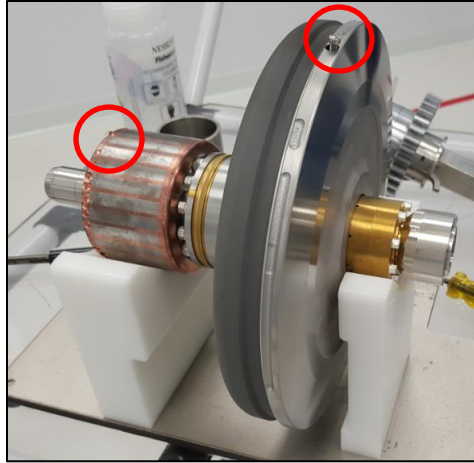


Figure 38: Set screw, which is a calibrated weight, placement in the modified target and the rotor.

Table 6 shows the unbalance range goal for each of the 5 assemblies or “parts”. Two “parts” in the lower end of the unbalance range are chosen to have enough samples to analyze the variance near the $0.25\text{g}\cdot\text{cm}$ tolerance specification. This was chosen because it is more critical to have repeatability at the specification limit.

Table 6: The unbalance range for the target and rotor, along with the tolerance allocation. Notice 'parts' 1 and 5 are in the lower range near the $0.25\text{g}\cdot\text{cm}$ specification limit.

| ROSS Part # | Rotor Unbalance (g*cm) | Target Unbalance (g*cm) | X Times Tolerance |
|--------------------|-------------------------------|--------------------------------|--------------------------|
| 1 | 0 – 0.5 | 0 – 0.5 | 1 - 2 |
| 2 | 0.6 – 2.5 | 0.6 – 2.5 | 2 - 10 |
| 3 | 2.6 – 5.5 | 2.6 – 5.5 | 10 - 20 |
| 4 | 5.6 – 7.0 | 5.6 – 7.0 | 20 – 30 |
| 5 | 0 – 0.5 | 0 – 0.5 | 1 - 2 |

Once a balance level has been set with the weighted screw, it should not be adjusted until each operator and test replication has been completed for that unbalance level.

Minitab v17 was used to create a Gage R&R run list for the 5 ROSS unbalance levels, 2 operators, and 3 replicates, shown in Table 7.

Between each run for a ROSS unbalance level, the chamber was vented so the target and rotor collet adapters could be completely removed and reinstalled prior to the next run. This was done to test the operator collet installation repeatability. Hence, after each run the anode was taken out of the vacuum chamber, collets uninstalled, then reinstalled, then placed back in the vacuum chamber. The vacuum pump would then turn on to pump down the chamber to reach 100mTorr or less for the ROSS to spin, collect the unbalance data, and then coast down. Each run would take about 10 minutes to complete.

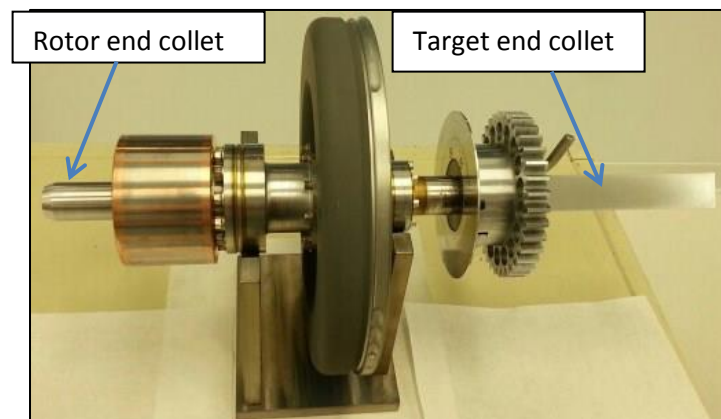


Figure 39: RoSS attached to collets.

The raw test data is shown Appendix A. The mean and standard deviation for the 6 runs for each of the 5 “parts” is shown in Table 7.

Table 7: Mean and Standard Deviation for the 6 runs with each 'part'.

| RunOrder | Parts | Operators | Rotor Imbalance (g*cm) | Rotor Imbalance (deg) | Delta from 0 deg | Target Imbalance (g*cm) | Target Imbalance (deg) | Delta from 0 deg |
|----------|-------|-----------|------------------------------|-----------------------------|---------------------|-------------------------------|------------------------------|---------------------|
| 3 | 1 | 1 | 0.12 | 213 | 147 | 0.16 | 162 | 162 |
| 8 | 1 | 2 | 0.17 | 259 | 101 | 0.49 | 137 | 137 |
| 10 | 1 | 1 | 0.11 | 165 | 165 | 0.32 | 221 | 139 |
| 14 | 1 | 2 | 0.062 | 206 | 154 | 0.35 | 181 | 179 |
| 20 | 1 | 1 | 0.15 | 202 | 158 | 0.24 | 163 | 163 |
| 21 | 1 | 2 | 0.17 | 217 | 143 | 0.093 | 100 | 100 |
| | | mean | 0.130 | | 144.667 | 0.276 | | 146.667 |
| | | stdev | 0.042 | | 22.774 | 0.142 | | 27.847 |
| 4 | 2 | 1 | 0.91 | 0 | 0 | 2.4 | 208 | 152 |
| 7 | 2 | 2 | 0.87 | 5 | 5 | 2.3 | 215 | 145 |
| 9 | 2 | 1 | 0.86 | 0 | 0 | 2.2 | 210 | 150 |
| 15 | 2 | 2 | 0.88 | 358 | 2 | 2.2 | 211 | 149 |
| 19 | 2 | 1 | 0.86 | 359 | 1 | 2.2 | 211 | 149 |
| 23 | 2 | 2 | 0.94 | 359 | 1 | 2.5 | 205 | 155 |
| | | mean | 0.890 | | 1.500 | 2.300 | | 150.000 |
| | | stdev | 0.035 | | 1.871 | 0.141 | | 3.347 |
| 1 | 3 | 1 | 4.3 | 4 | 4 | 4.3 | 18 | 18 |
| 6 | 3 | 2 | 4.4 | 2 | 2 | 4.4 | 25 | 25 |
| 11 | 3 | 1 | 4.4 | 4 | 4 | 4.2 | 24 | 24 |
| 13 | 3 | 2 | 4.4 | 3 | 3 | 4.5 | 24 | 24 |
| 17 | 3 | 1 | 4.4 | 4 | 4 | 4 | 26 | 26 |
| 22 | 3 | 2 | 4.3 | 1 | 1 | 4.9 | 25 | 25 |
| | | mean | 4.367 | | 3.000 | 4.383 | | 23.667 |
| | | stdev | 0.052 | | 1.265 | 0.306 | | 2.875 |
| 2 | 4 | 1 | 6.1 | 1 | 1 | 6.2 | 355 | 5 |
| 5 | 4 | 2 | 6 | 3 | 3 | 6.6 | 348 | 12 |
| 12 | 4 | 1 | 6.2 | 4 | 4 | 6.3 | 347 | 13 |
| 16 | 4 | 2 | 6.1 | 3 | 3 | 6.7 | 351 | 9 |
| 18 | 4 | 1 | 6 | 1 | 1 | 6.8 | 351 | 9 |
| 24 | 4 | 2 | 6 | 1 | 1 | 7 | 353 | 7 |
| | | mean | 6.067 | | 2.167 | 6.600 | | 9.167 |
| | | stdev | 0.082 | | 1.329 | 0.303 | | 2.994 |
| 25 | 5 | 1 | 0.11 | 351 | 9 | 0.15 | 173 | 173 |
| 26 | 5 | 1 | 0.1 | 275 | 85 | 0.21 | 27 | 27 |
| 27 | 5 | 1 | 0.19 | 240 | 120 | 0.57 | 34 | 34 |
| 28 | 5 | 2 | 0.13 | 223 | 137 | 0.53 | 13 | 13 |
| 29 | 5 | 2 | 0.19 | 327 | 33 | 0.3 | 120 | 120 |
| 30 | 5 | 2 | 0.13 | 243 | 117 | 0.47 | 18 | 18 |
| | | mean | 0.142 | | 83.500 | 0.372 | | 64.167 |
| | | stdev | 0.039 | | 51.806 | 0.176 | | 66.337 |

As shown in Figure 40 from the plotted data of Table 7, the unbalance standard deviation generally decreases with decrease in balance mean. For the target, the plateau is about $0.15\text{g}\cdot\text{cm}$ and for the rotor it's about $0.04\text{g}\cdot\text{cm}$. This makes sense because a piece part with a larger starting unbalance would likely have a higher standard deviation.

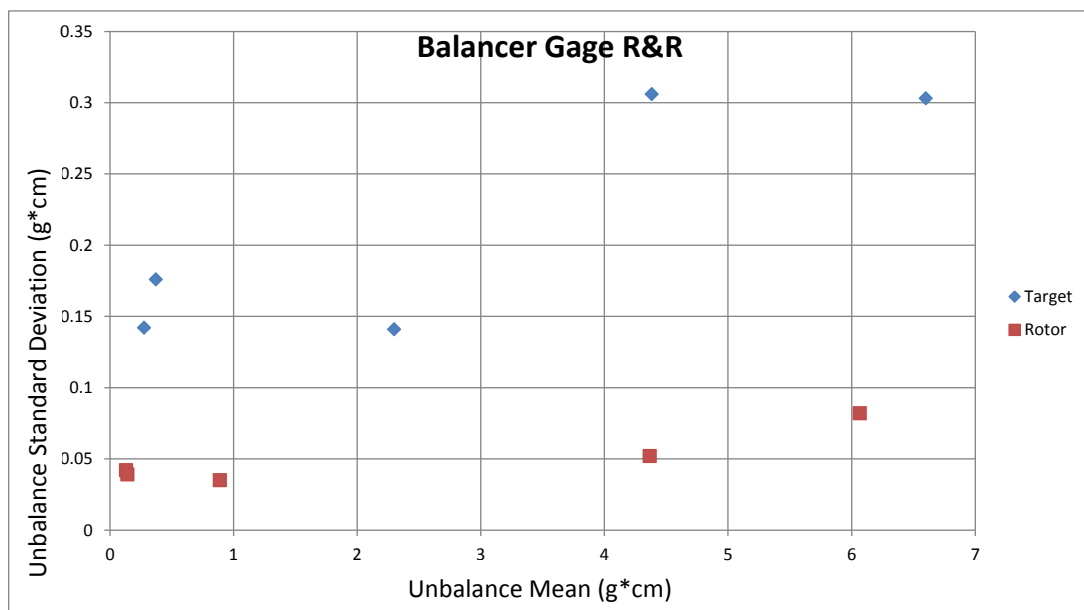


Figure 40: Unbalance average vs the unbalance standard deviation

Not surprisingly, Minitab analysis shows the ability of the balancer to accurately differentiate between ROSS parts that have significant differences in unbalance.

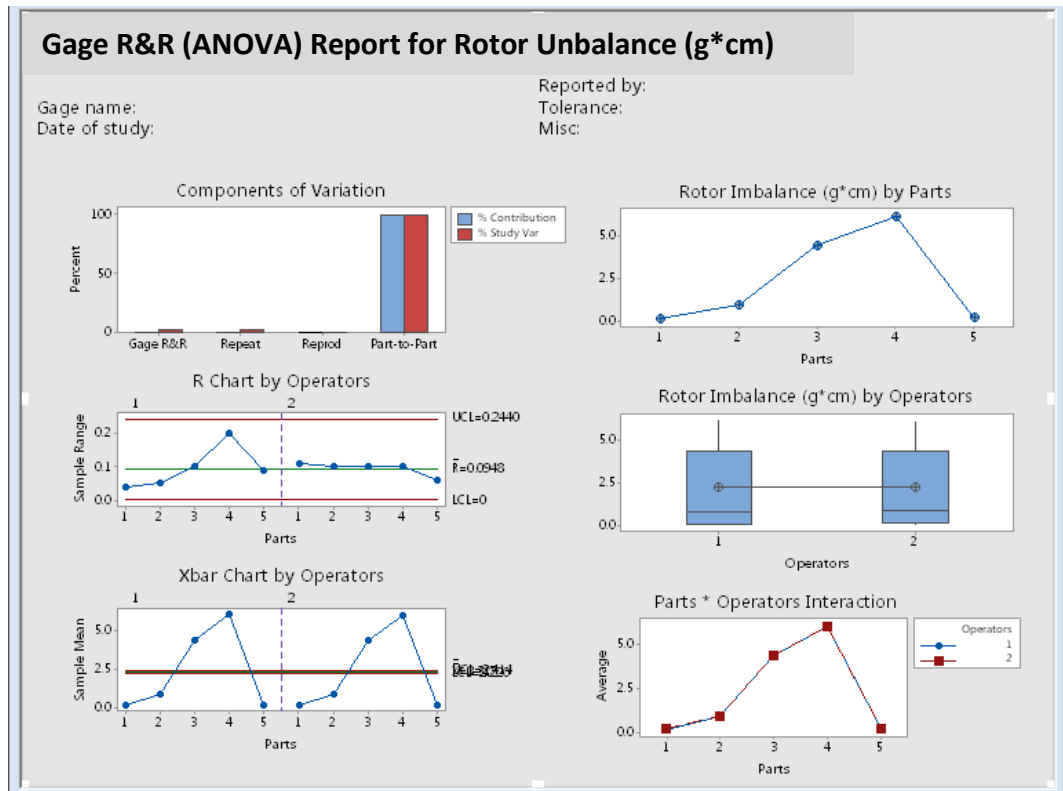


Figure 41: Gage R&R report for rotor unbalance showing part to part variation can be detected.

These results were starting points that confirm the measurement system can indeed determine the difference in part to part variation for the rotor.

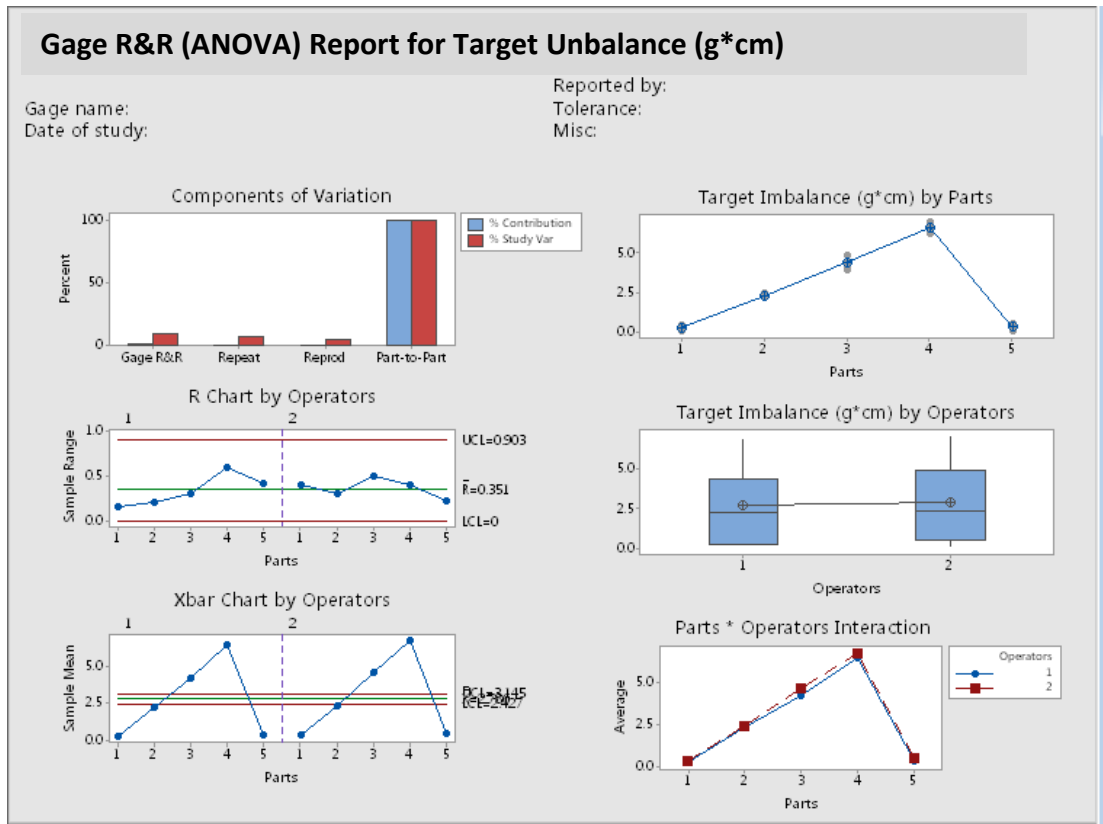


Figure 42: Gage R&R for target unbalance.

Again, the target plane results confirm the measurement system can indeed determine the difference in part to part variation for the target. This part to part variation identification is critical, because the data says that the measurement system can distinguishing between different levels of rotor and target unbalance. The system needs to identify the unbalance level so that the proper correction can be performed on the rotor and target.

Now focus on the 2 samples that were initially balanced to the 0.25g*cm specification on both the target and rotor plane, “parts 1 and 5”. The following run chart of the data shows significant variation with respect to the 0.25g*cm unbalance

specification, especially in the target plane. Recall, the same ROSS was being used during this entire study, and 'parts 1 and 5' were at the same unbalance weight.

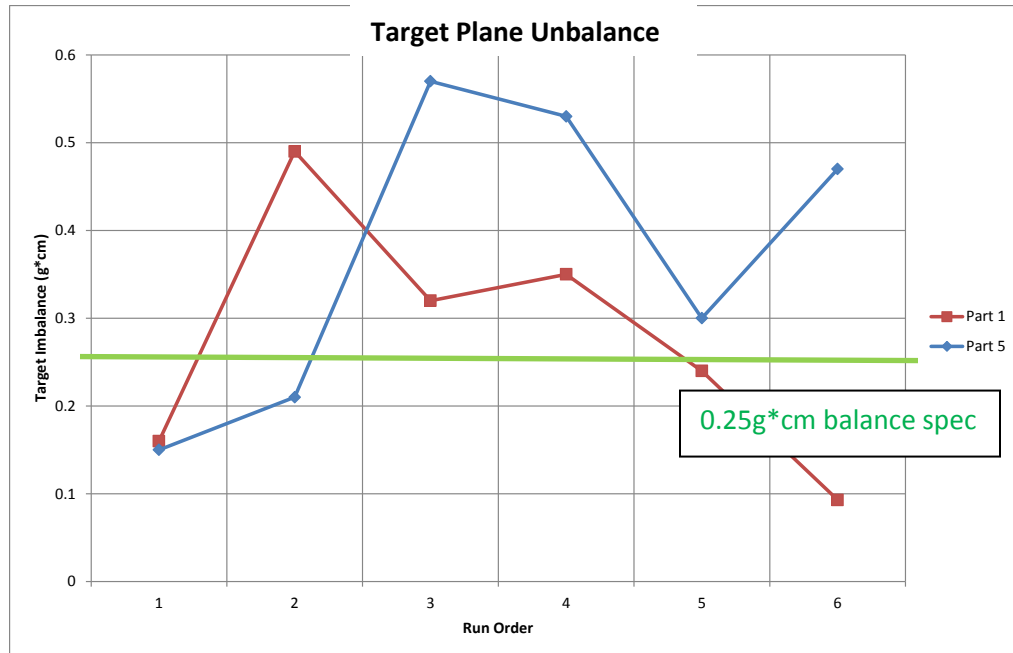


Figure 43: Run chart of Target 'parts' 1 and 5 which were balanced near the specification limit.

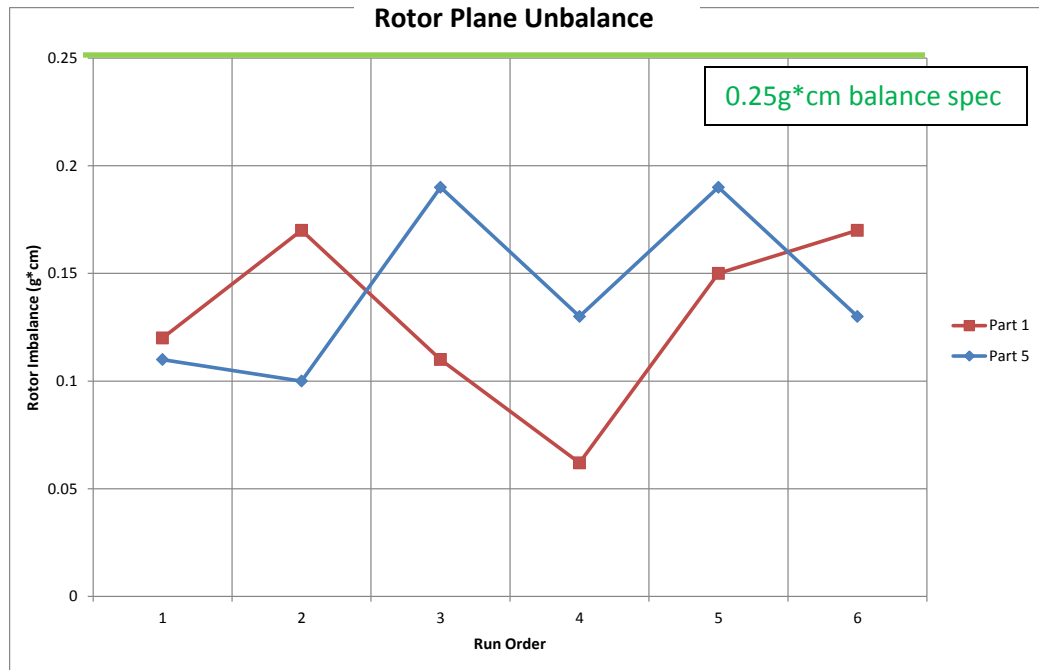


Figure 44: Run chart of Rotor 'parts' 1 and 5 which were balanced near the specification limit.

The MiniTab analysis on the parts 1 and 5 (the “in tolerance” samples) shows that neither the rotor nor target planes meet the general rule that the standard deviation due to Gage R&R be 10% of tolerance [69]. The tolerance or specification limit is 0 – 0.25g*cm, which means that 10% would be 0.025g*cm. For the rotor, the standard deviation due to Gage R&R was 0.042 g*cm and the study variation (5.15 sigma * standard deviation of 0.042g*cm) was 0.216g*cm. For the target, the standard deviation due to Gage R&R was 0.161g*cm and the study variation (5.15 sigma* standard deviation of 0.161g*cm) was 0.829 g*cm.

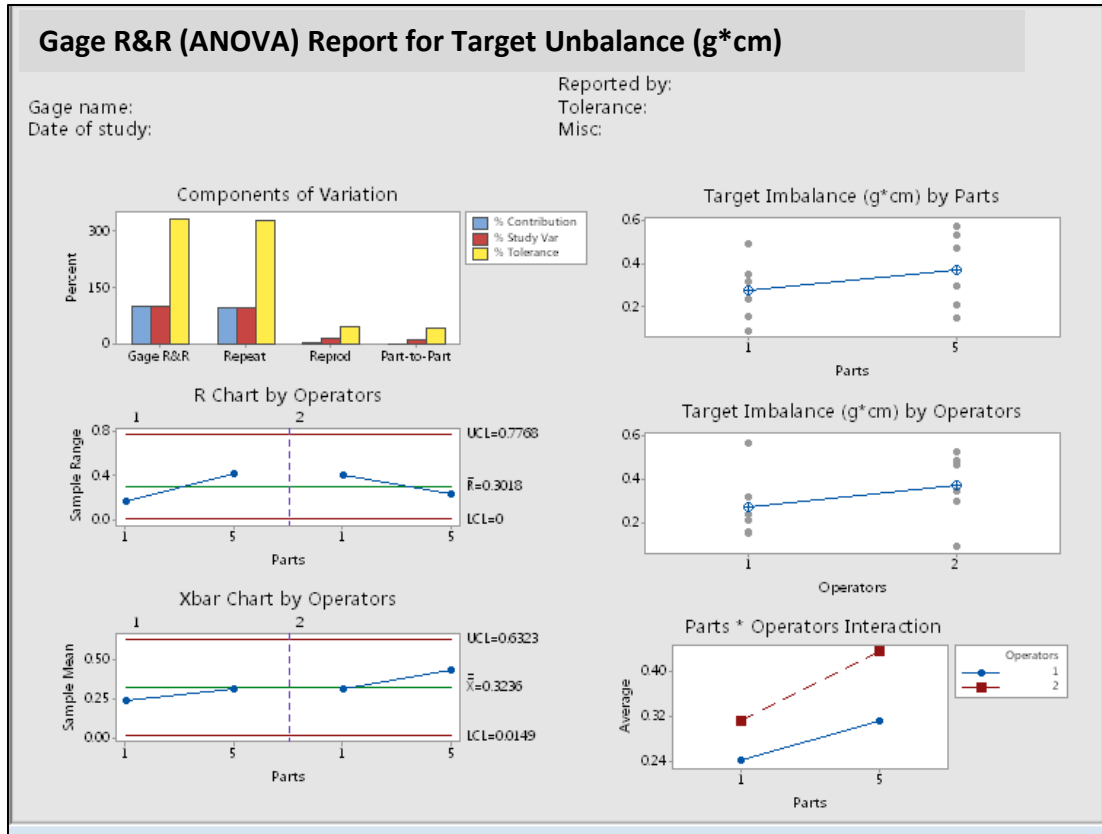


Figure 45: Gage R&R report for Target which shows very high percent contribution. The gage R&R as a percent of tolerance is over 300%.

Minitab results of the Target Imbalance shown in Appendix B. Similarly, the rotor plane results for ‘parts’ 1 and 5 were also put into Minitab.

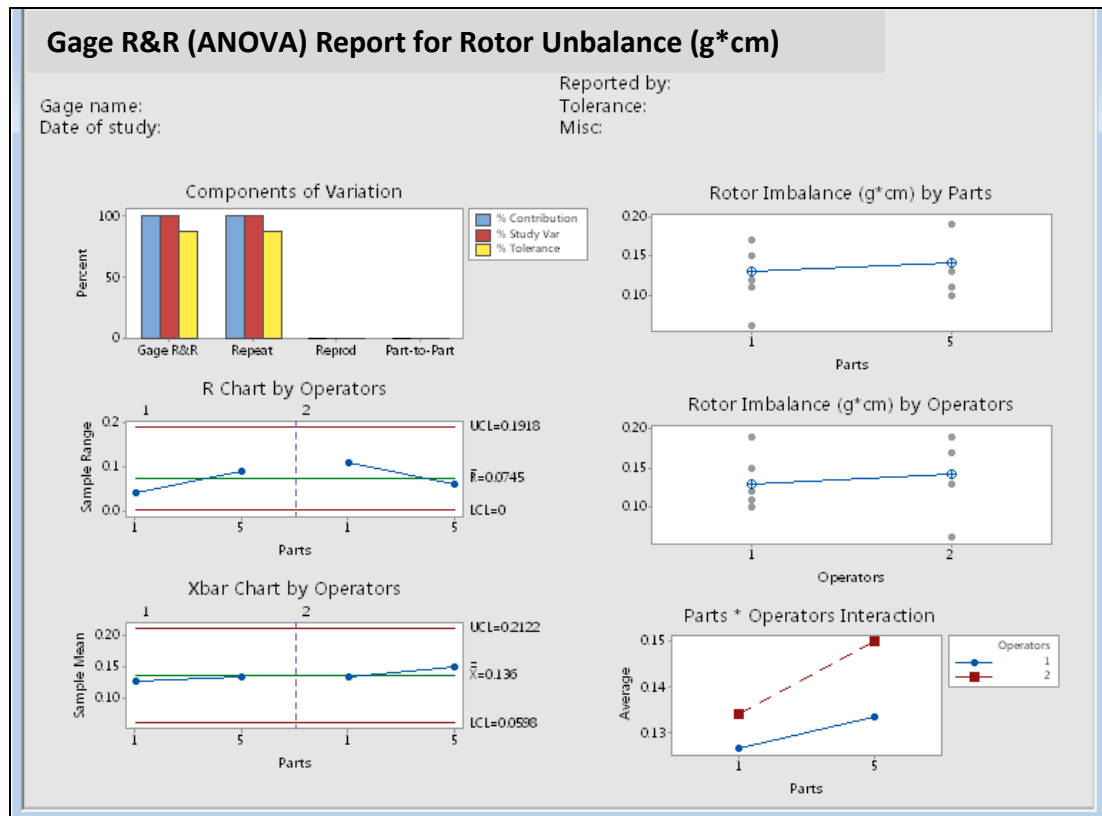


Figure 46: Gage R&R report for the Rotor shows very high percent contribution. The Gage R&R as a percent of tolerance is 86%.

If no changes are made to improve the measurement system, to meet the 10% rule of thumb requirement, the rotor tolerance would have to increase to 2 g*cm and the target tolerance to 8g*cm.

3.3.2 Collet Rigidity

In addition to the above Gage R&R study, an investigation was done to determine other possible variation causes. An investigation was done to see if keeping the collets on between runs would differ from removing the collets on run to run, such as the

previous study showed. Using the same ROSS as “part 1 and 5” from the study, it was measured 6 times without removing it from the balancer each time (Part 6). This means that the vacuum chamber remained closed the entire test. After the anode finished coasting down, it was spun up again to get a measurement reading. Each run showed the same trend in variation as the Gage R&R procedure.

Table 8: Investigation to determine variation by keeping the collets on shown as Part 6.

| RunOrder | Parts | Operators | Rotor Imbalance (g*cm) | Rotor Imbalance (deg) | Target Imbalance (g*cm) | Target Imbalance (deg) |
|-------------------------------------|-------|-----------|------------------------|-----------------------|-------------------------|------------------------|
| Did not remove collets between runs | | | | | | |
| 31 | 6 | 1 | 0.165 | 287 | 0.36 | 11 |
| 32 | 6 | 1 | 0.29 | 301 | 0.44 | 87 |
| 33 | 6 | 1 | 0.39 | 280 | 0.2 | 74 |
| 34 | 6 | 2 | 0.15 | 261 | 0.59 | 7 |
| 35 | 6 | 2 | 0.16 | 231 | 0.61 | 4 |
| 36 | 6 | 2 | 0.3 | 294 | 0.62 | 90 |

Table 9: The average of the runs for Target Unbalance for Part 1, 5, 6. Collets were removed between each run for Parts 1 and 5. The collets were kept on during Part 6.

| | Target Unbalance (g*cm) | | |
|--------------|-------------------------|--------|--------|
| | Part 1 | Part 5 | Part 6 |
| AVG | 0.28 | 0.37 | 0.47 |
| STDEV | 0.14 | 0.18 | 0.15 |

The averages were different even though the same ROSS was used at the same unbalance level. The standard deviation was very similar however.

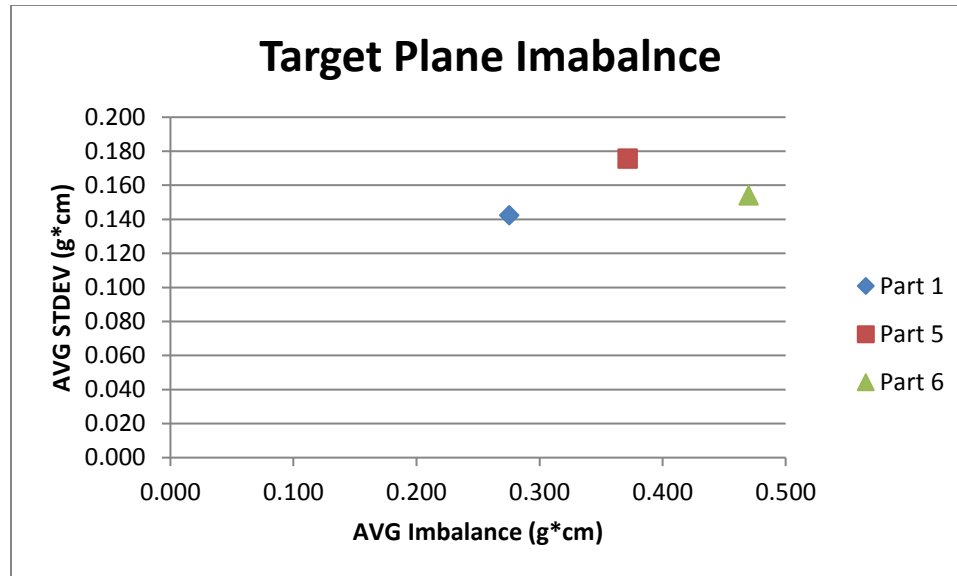


Figure 47: Plot of Table 9 showing the Avg Unbalance vs Avg STDEV of Parts 1 and 5 (removal of collets between each run) and Part 6 (consecutive runs without collet removal). The standard deviation was similar.

The balancer can differentiate unbalance levels magnitudes apart, but does not meet the 10% Gage R&R rule for imbalance levels near the current 0.25g*cm balance requirement. Taking a measurement on the same ROSS at the same unbalance level is not repeatable. However, this additional testing showed installing the collets or leaving them on each run does not appear to be a significant cause of variation due to the standard deviation being very similar. These collets are securely fastened to the ROSS and have undergone substantial tolerance stack up analysis, ensuring that their variation is negligible. By removing collets before each run, or by leaving the collets on run to run, there was very little unbalance standard deviation. Yet, the difference in the average unbalance between part 1 and 6 was 0.19 g*cm which is 76% of the tolerance, shown in

Table 9 above. This finding proves that further testing is needed to understand why there was an average unbalance shift.

3.3.3 SGB Repeatability Study

The purpose of this testing was to understand the repeatability of the liquid metal SGB and the chamber venting process by performing consecutive runs under vacuum. The same ROSS with the threaded rotor and target was used again in this study to try to gather information on consecutive measurements. A weight of 0.3798g was added to the target and then 5 consecutive measurement runs were performed under vacuum. The chamber was vented after the 5th run (which appears as run number 6 in Table 10). Then, the chamber closed and vacuum was pulled again. 5 more runs were made with the 0.3798g weight attached to the target. Then, after venting the chamber, a 0.7638g weight was attached to the target and run 5 more times to see the results at a higher unbalance level. This study was performed this way in hopes of gaining some understanding if the venting process between runs has any effect on the unbalance measurement. Table 10 displays the results.

Table 10: Every 5 runs, the chamber was vented.

| | | Rotor | | Target | | | |
|-------------------------------|---|-------|------|--------|------|-------|------------|
| | | Run | g*cm | Angle | g*cm | Angle | Mass added |
| Vented chamber | → | 1 | 0.18 | 232 | 0.75 | 140 | No weight |
| | → | 2 | 0.28 | 253 | 3.8 | 19 | 0.3798 g |
| Consecutive runs under vacuum | } | 3 | 0.14 | 231 | 4.1 | 9 | 0.3798 g |
| | | 4 | 0.25 | 248 | 3.9 | 17 | 0.3798 g |
| | | 5 | 0.21 | 280 | 3.8 | 115 | 0.3798 g |
| | | 6 | 0.32 | 256 | 3.9 | 20 | 0.3798 g |
| | | AVG | 0.24 | 253.60 | 3.90 | 36.00 | |
| | | STD | 0.06 | 14.41 | 0.10 | 36.23 | |
| Vented chamber | → | 7 | 0.16 | 336 | 3.2 | 16 | 0.3798 g |
| Consecutive runs under vacuum | } | 8 | 0.35 | 338 | 2.9 | 16 | 0.3798 g |
| | | 9 | 0.29 | 330 | 2.9 | 25 | 0.3798 g |
| | | 10 | 0.26 | 342 | 3 | 12 | 0.3798 g |
| | | 11 | 0.36 | 208 | 4.2 | 14 | 0.3798 g |
| | | AVG | 0.28 | 310.80 | 3.24 | 16.60 | |
| | | STD | 0.07 | 47.05 | 0.45 | 4.07 | |
| Vented chamber | → | 12 | 0.28 | 245 | 7.2 | 12 | .7638g |
| Consecutive runs under vacuum | } | 13 | 0.22 | 355 | 6.7 | 5 | .7638g |
| | | 14 | 0.14 | 245 | 7.3 | 12 | .7638g |
| | | 15 | 0.17 | 223 | 7.5 | 10 | .7638g |
| | | 16 | 0.24 | 201 | 8 | 9 | .7638g |
| | | AVG | 0.21 | 253.80 | 7.34 | 9.60 | |
| | | STD | 0.05 | 48.53 | 0.39 | 2.35 | |

Baseline run without weight

0.3798g weight on Target

0.3798g weight on Target

0.7638g weight on Target

Table 11: The average and standard deviation of the 5 separate runs from Table 9. Runs 2-11 had a 0.3798g weight attached while runs 12-16 had a 0.7638g weight attached.

| | Rotor Unbalance (g*cm) | | Target Unbalance (g*cm) | | | Rotor Unbalance (Angle) | | Target Unbalance (Angle) | |
|------------|------------------------|------|-------------------------|------|--|-------------------------|-------|--------------------------|-------|
| | AVG | STD | AVG | STD | | AVG | STD | AVG | STD |
| Runs 2-6 | 0.24 | 0.06 | 3.9 | 0.10 | | 253.6 | 14.41 | 36 | 36.23 |
| Runs 7-11 | 0.28 | 0.07 | 3.24 | 0.45 | | 310.80 | 47.05 | 16.60 | 4.07 |
| Runs 12-16 | 0.21 | 0.05 | 7.34 | 0.39 | | 253.80 | 48.53 | 9.60 | 2.35 |

There is a $0.66\text{g}\cdot\text{cm}$ difference in the average target unbalance between runs 2-6 ($3.9\text{g}\cdot\text{cm}$) and runs 7-11 ($3.24\text{g}\cdot\text{cm}$). As seen in Figure 48, the rotor has a much smaller standard deviation in regards to unbalance in $\text{g}\cdot\text{cm}$ which is why we will continue to focus on the target.

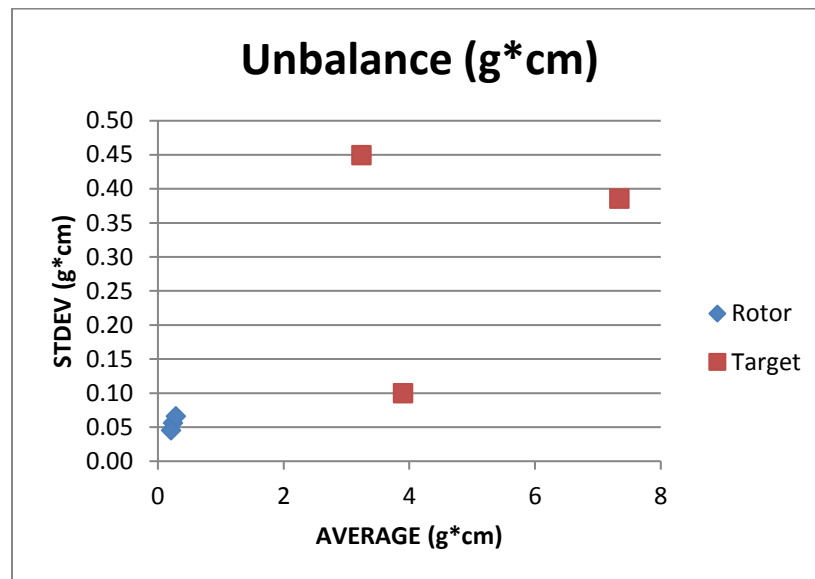


Figure 48: The rotor and target unbalance are graphed as the standard deviation vs the average. Each dot represents the 5 run average and standard deviation from the Table 11.

The introduction of variability in the angle at which the unbalance takes place will now be considered. If the angle is incorrect, the material removal will take place in the improper location, possibly creating unbalance in the part instead of removing it. Both the target and the rotor have too large variation in angle shown in Figure 49. Runs 2-6

had an average angle of 36 degrees but runs 7-11 had an average of 16.6 degrees. These two identical ROSS's would have had a cut 20 degrees apart solely based off which run average was used.



Figure 49: Each dot represents the 5 run average and standard deviation from the table above. The rotor and target angle are graphed.

Similarly, there was a discrepancy between the average and standard deviation unbalance in runs 2-6 and runs 7-11 seen in Table 11. The same 0.3798g weight was attached to the target. The only difference between these runs was that the chamber was vented between the 6th and 7th run. The results show that runs 2-6 had an average target plane unbalance of 3.9g*cm and a standard deviation of 0.10g*cm. Runs 7-11 had an

average target plane unbalance of 3.24g*cm and a standard deviation of 0.45 g*cm. This is a huge discrepancy for a test under the same conditions using the same parts. With the 0.3798g weight attached, these two different run sections had a difference in standard deviation of 0.30g*cm. This is over 120% of the 0.25g*cm balance specification limit.

This result is very similar to the Section 3.2.1 Measurement Repeatability results. Recall that in this test both 'parts' 1 and 5 were the same ROSS under the same conditions. This ROSS also had a large variation in the average of the runs, but the standard deviation was closer. It seems that the large variation between ROSS runs must do with something other than venting the chamber, running consecutively, or installing the collets. These results lead to questioning the measurement system's capability of measuring such a small tolerance. To determine if the measurement system can consistently distinguish between parts at such a low tolerance, the measurement system must be isolated from the SGB.

3.3.4 Balance Equipment

The results presented in earlier sections suggested to the possibility that the balancer might not actually be able to detect such a small unbalance. The variation seen in earlier plot might just be system noise. A way to determine if the balance equipment is capable or not is to isolate the measurement system from the SGB. By isolating the SGB, it leaves the liquid metal bearing out of the questions. A ball bearing ROSS was used to see what effect the measurement system had on its unbalance. This ROSS had large precision ball bearings used for high speed burst testing that were class 4 using ISO 492, which is the tolerances for rolling bearings.

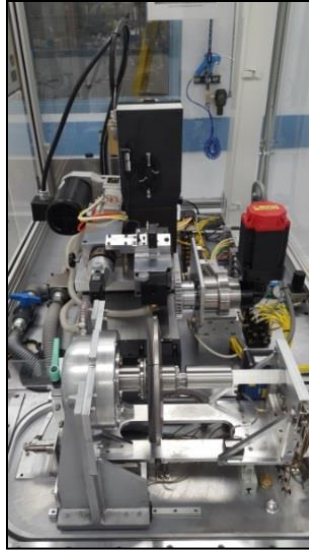


Figure 50: Ball Bearing ROSS in balancer.

Two of the exact same revision ball bearing anodes were used for this test: 100001, which will be known as BB1, and 100002, which will be known as BB2. The results are shown in Table 12. The ball bearings were coated in grease and would not work under vacuum due to contamination, so the vacuum pump was turned off to allow the process to take place in air. Each 'run' represents the 5 run average. For example, Run 1 in the 100001 chart was spun 5 times at that unbalance level. Then, the correction was made to the rotor and to the target by drilling and milling. The process was repeated multiple times.

Table 12: Data from the ball bearing testing. Highlighted sections are graphed in Figure 51. Each ‘Run’ represents the average of 5 consecutive runs under vacuum.

| 12-Jan-16 | | | | | | | | | |
|--|-------------------------------|-------------|--------------------------------|-------------|--------------------------|-------------|---------------------------|-------------|--|
| Ball Bearing slotted target run 100001 | | | | | | | | | |
| | <u>Rotor Unbalance (g*cm)</u> | | <u>Target Unbalance (g*cm)</u> | | <u>Rotor Angle (deg)</u> | | <u>Target Angle (deg)</u> | | |
| Run | g*cm | std | g*cm | std | deg | std | deg | std | |
| 1 | 13 | 0.000 | 5.43 | 0.047 | 333.00 | 0.00 | 346.00 | 0.82 | |
| 2 | 3.8 | 0.000 | 5.9 | 0.047 | 30.3 | 0.47 | 343.7 | 0.47 | |
| 3 | 0.26 | 0.009 | 2.13 | 0.047 | 137.67 | 4.11 | 0.33 | 0.47 | |
| 4 | 0.16 | 0.005 | 1.03 | 0.050 | 131.67 | 2.62 | 4.00 | 0.82 | |
| 5 | 0.11 | 0.005 | 0.49 | 0.005 | 117.33 | 0.5 | 6.00 | 0.82 | |
| 6 | 0.07 | 0.007 | 0.13 | 0.005 | 90.67 | 5.73 | 152.00 | 3.27 | |
| | AVG | 0.00 | AVG | 0.03 | AVG | 2.24 | AVG | 1.34 | |

| 18-Feb-16 | | | | | | | | | |
|--|-------------------------------|-------------|--------------------------------|-------------|--------------------------|-------------|---------------------------|-------------|--|
| Ball Bearing slotted target run 100002 | | | | | | | | | |
| | <u>Rotor Unbalance (g*cm)</u> | | <u>Target Unbalance (g*cm)</u> | | <u>Rotor Angle (deg)</u> | | <u>Target Angle (deg)</u> | | |
| Run | avg | std | avg | std | avg | std | avg | std | |
| 1 | 2.80 | 0.000 | 12.00 | 0.000 | 80.33 | 0.47 | 129.67 | 0.47 | |
| 2 | 1.5 | 0.047 | 9.9 | 0.000 | 242.0 | 0.8 | 129.0 | 0.00 | |
| 3 | 0.14 | 0.012 | 9.30 | 0.000 | 190.33 | 8.58 | 129.00 | 0.00 | |
| 4 | 0.28 | 0.012 | 5.60 | 0.000 | 109.33 | 4.50 | 132.67 | 0.47 | |
| | AVG | 0.02 | AVG | 0.00 | AVG | 3.59 | AVG | 0.24 | |

These results have a much better repeatability than the SGB testing that was performed. The target and rotor have a much smaller standard deviation between consecutive runs. The target especially performs much better than previous SGB results seen in Table 11. The average of standard deviation is much smaller as well. There also does not appear to be a higher deviation at a higher unbalance limit either.

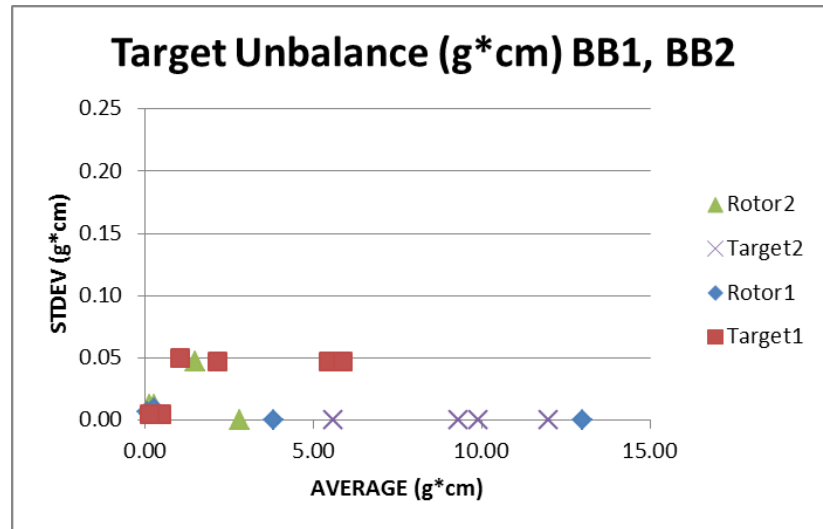


Figure 51: The results of performing similar repeatability tests on a ball bearing anode.

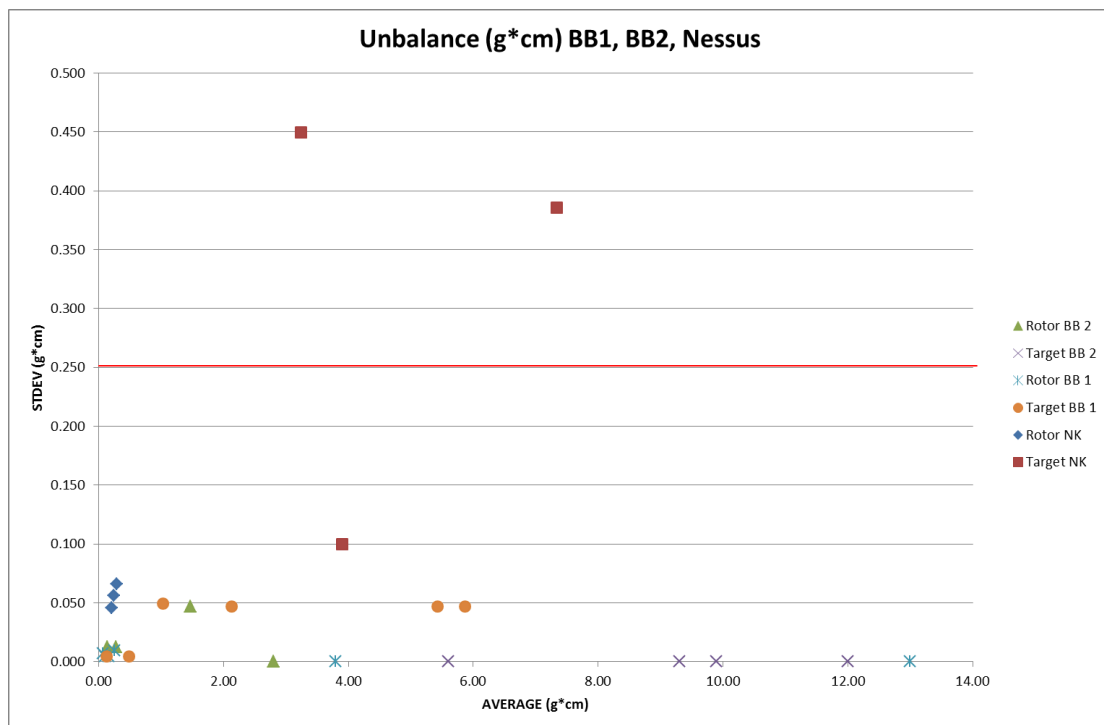


Figure 52: Ball Bearing Testing (BB1 and BB2) from Figure 51 combined with the SGB results from Figure 48, appearing in the legend as Rotor NK and Target NK. The specification limit is highlighted in red at 0.25g*cm.

Figure 52 proves that the measurement system is very capable since the ball bearing testing had a very low standard deviation for the target plane unbalance: 0.0 g*cm for BB2 and 0.03g*cm for BB1 which is 0% of tolerance and 12% of tolerance respectfully. In fact, if only the data below 1g*cm is accounted for on the ball bearing, there is standard deviation that is only 2% of the balance specification. Therefore, this rules out the measurement system as a caused of variation and can be eliminated from the variables suspected of causing repeatability issues. The measurement system was able to accurately measure with repeatable results on a known quality ball bearing. Since the SGB was isolated form this test, this indicates that the SGB is one of the main factors left to be looked at in detail which could be causing the variation in unbalance measurements. More testing is needed to understand the SGB variation.

3.3.5 SGB Multiple Run Repeatability Issues

To better understand what kind of repeatability issues are present on production parts, more testing of consecutive runs was performed on the SGB. This testing was developed to take a deeper dive into repeatability issues surrounding the SGB by balancing an anode to 0.25g*cm spec and then spinning it multiple times to see the variability.

The next two trials were done on production bearings that went through the balance process. Instead of venting the chamber after the 0.25g*cm specification limit was reached, the ROSS was spun 4 more times to see what the repeatability looked like on a balanced assembly. Note, this was a balanced assembly that was ready to move on to its next manufacturing operation. Shockingly, 3 out of the 5 rotor unbalances jumped

above the specification. Similarly, 4 out of the 5 target unbalances jumped up above the 0.25g*cm specification limit as well. Figure 53 and Figure 54 show the details of this testing.

Trial 1:

| | Test Set-up | MAN280 | | | | |
|-------------|--------------|------------------|---------------|------------------|---------------|------------------|
| | | Rotor | | Target | | |
| | Run # | Unbalance (g*cm) | Angle (deg) | Unbalance (g*cm) | Angle (deg) | Coast down (sec) |
| | 1 | 11 | 287 | 22 | 210 | 77 |
| | 2 | 1.2 | 60 | 2 | 226 | 76 |
| | 3 | 0.2 | 151 | 0.71 | 88 | 81 |
| | 4 | 0.28 | 199 | 0.82 | 249 | 93 |
| | 5 | 0.26 | 198 | 0.34 | 44 | 82 |
| Repeat Runs | 6 | 0.27 | 187 | 0.36 | 65 | 98 |
| 1 | 7 | 0.17 | 11 | 0.25 | 265 | 113 |
| 2 | | 0.27 | 28 | 0.28 | 300 | 146 |
| 3 | | 0.14 | 314 | 0.43 | 252 | 136 |
| 4 | | 0.22 | 312 | 0.43 | 263 | 150 |
| 5 | | 0.23 | 325 | 0.54 | 259 | 127 |
| | AVG | 0.21 | 198.00 | 0.39 | 267.80 | 134.40 |
| | STDEV | 0.05 | 145.91 | 0.11 | 16.70 | 13.37 |

Figure 53: A balance was performed on bearing MAN280 to specification. Before venting the chamber the anode was spun 4 more times. The target unbalance increased on subsequent runs.

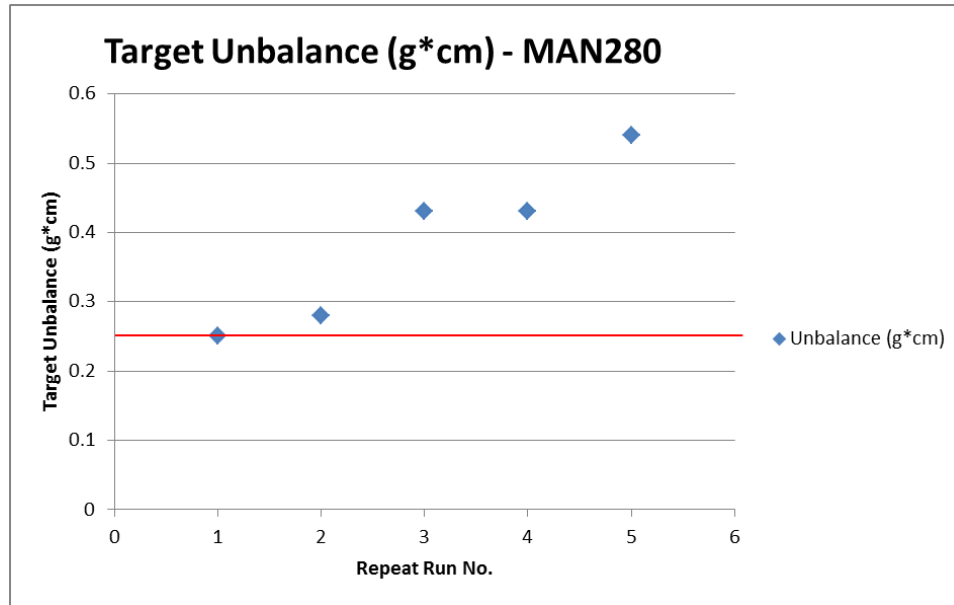


Figure 54: Plot showing Figure 53's data. The target unbalance trended upward after the ROSS MAN280 was balanced to specification.

At first glance, the results of this study do not bode well for the repeatability of this machine. If the ROSS is balanced on one run, the next run might indicate that it is not within specification, even though no material has been removed. Serious questions surround the confidence of reaching such a tight tolerance on a liquid metal SGB. This study was replicated with another unique ROSS since it proved so valuable.

Trial 2:

| | Test Set-up | MAN304 | | | | |
|-------------|--------------|------------------|---------------|------------------|---------------|------------------|
| | | Rotor | | Target | | |
| | Run # | Unbalance (g*cm) | Angle (deg) | Unbalance (g*cm) | Angle (deg) | Coast down (sec) |
| | 1 | 3.6 | 232 | 16 | 105 | |
| | 2 | 3.4 | | 4.5 | | |
| | 3 | 0.69 | | 0.66 | | |
| | 4 | 0.62 | | 0.82 | | |
| Repeat Runs | 5 | 0.27 | | 0.14 | | |
| 1 | 6 | 0.21 | 111 | 0.25 | 356 | |
| 2 | | 0.27 | 115 | 0.25 | 357 | |
| 3 | | 0.22 | 129 | 0.075 | 324 | |
| 4 | | 0.17 | 124 | 0.12 | 346 | |
| 5 | | 0.21 | 118 | 0.23 | 301 | |
| | AVG | 0.22 | 119.40 | 0.19 | 336.80 | |
| | STDEV | 0.03 | 6.41 | 0.07 | 21.48 | |

Figure 55: ROSS MAN304 was balanced to specification and then spun 4 more times while it remained under vacuum. The target unbalance lowered on subsequent runs.

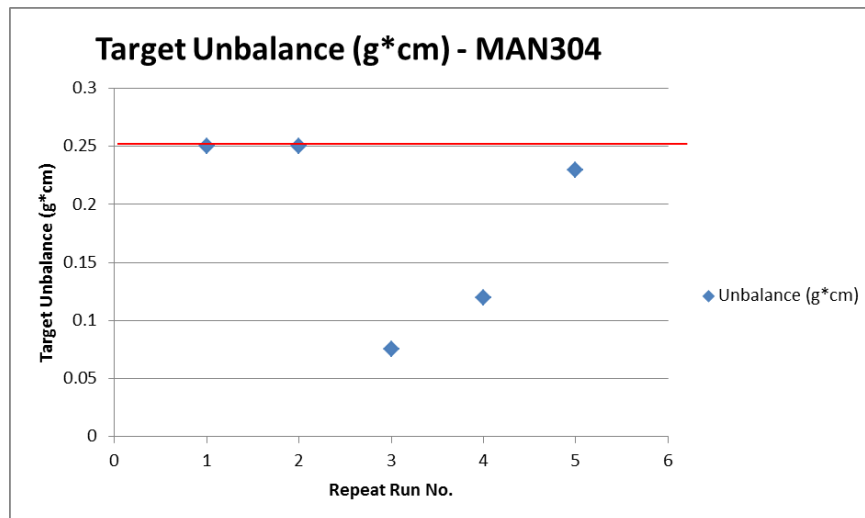


Figure 56: Plot showing Figure 55's data. The target unbalance lowered on subsequent runs after ROSS MAN280 was balanced to specification.

The results of the second trial trend in the opposite direction of the first trial. If an anode is balanced, spinning the anode again might make the unbalance lower. However, trial 1 proved that spinning the assembly again might make the unbalance higher. This phenomenon did not happen on the ball bearing trial which proved out the measurement system capability. The results from the previous trials indicate that an operator could just keep spinning the bearing if it was close to the limit in hopes of reaching the specification limit. With the unbalance of the target having such a high standard deviation, it is possible to spin the bearing again and get the result of a passing balance without making any correction cuts. This is not a robust manufacturing process. The variable that needs to be understood is the Gallium inside of the SGB.

3.4 Gallium Movement

The liquid metal SGB is a fixed design. Its life testing capability has been proven out over thousands of exams at high G-load, tremendous thermals, and constant operation. However, effects that the liquid metal have on the balance of the anode have never been fully understood. This section will describe and demonstrate how the Gallium can shift around in the bearing and cause unbalance in the anode during the balance operation.

3.4.1 Gallium Migration Theory

The liquid metal SGB is a complicated and intricate mechanical design. The purpose of the Gallium migration theory is not to fully explain how the bearing is

processed or manufactured. It is also not meant to fully explain all the elaborate wear patterns, intermetallic layers, or hydrodynamic effects. The purpose of this is to prove the liquid metal SGB is causing the difficulties in the manufacturing facilities balance operation. Below is a schematic of the liquid metal SGB.

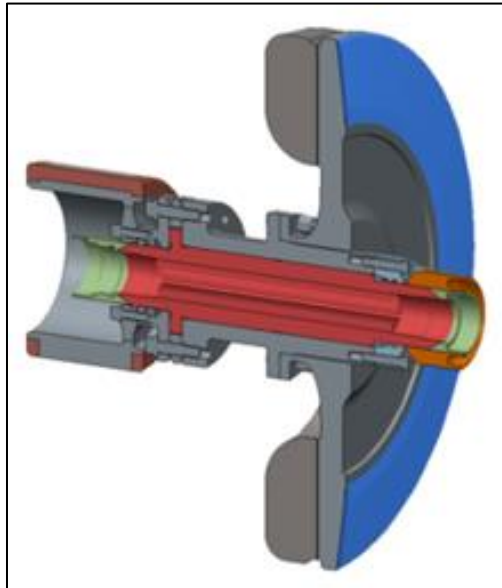


Figure 57: Cross section of a ROSS.

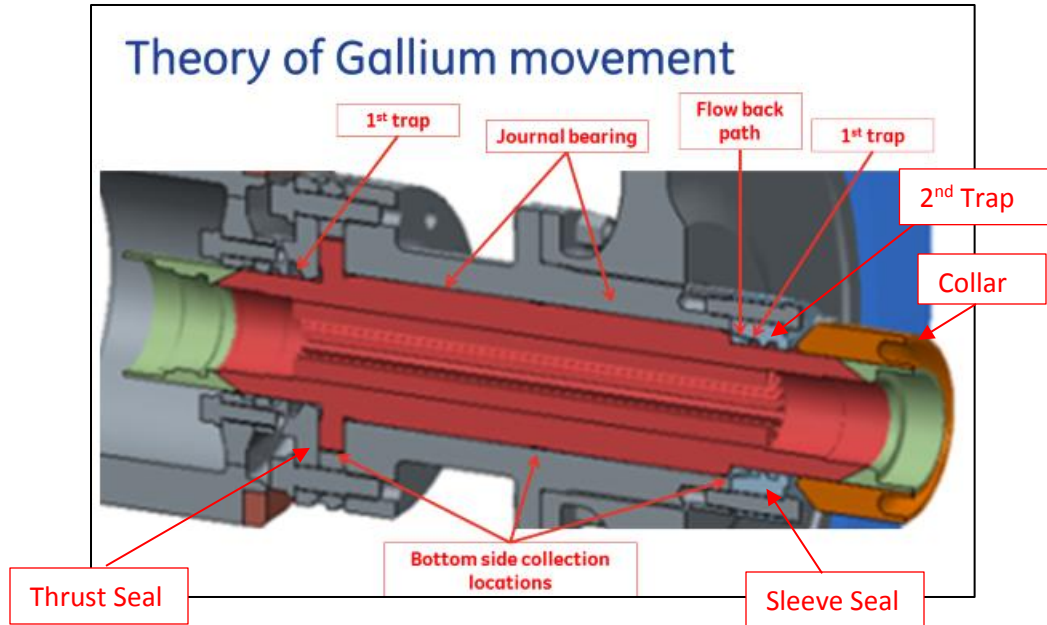


Figure 58: Cross section of the liquid metal SGB.

Figure 58 shows a cross section of the SGB. During operation, the Gallium is pumped by the bearing to the center of the shaft. However, while the bearing is stationary the Gallium collects on the bottom side. During the balance measurement and vacuum pump downs, the Gallium migrates within the bearing. Some of the that Gallium moves into the first traps on both the rotor and target side, as shown in Figure 58. The pressure generated from rotation pushes the Gallium from the first trap back into the journal bearings. The design calls for this kind of Gallium movement at operational speed of 140Hz. However, this movement had never been suspected at lower speeds such as 15Hz balance and was never considered detrimental to the process. In contrast, the repeatability testing in previous sections showed how un-repeatable the balance process

is. With all other variables having been investigated, the Gallium is the lone factor driving the large standard deviations that is not yet fully understood.

There is no way to tell the position that the Gallium has while inside the bearing. However, bearing autopsies can show where the Gallium is in the traps when the bearing is disassembled. This evidence will lead to proving that the Gallium indeed is causing the repeatability issues.

3.4.2 Ga Movement Proved in Bearing Autopsy

Historically, SGB bearing assemblies, like shown in Figure 1, have been spun by locking the shaft to the sleeve and rotating at 2500rpm for 5 minutes to redistribute the Gallium in the bearing. This centrifugal spin was thought to move all the Ga out of the traps to reset the Ga position. A test was performed by balancing a ROSS to 0.25g*cm specification. At this point it is now safe to lock the shaft and sleeve together to do the centrifugal ROSS spin. See Figure 58 for the part location and nomenclature. It is very time intensive and expensive to get bearings which are made just for this balance testing which will allow for the sleeve seal to be removed. The sleeve seal removal is a highly skilled job that is very risky. The danger of removing the sleeve seal is getting the sleeve seal back on the bearing in the exact orientation as it was built. There can be no contamination on any parts. There must not be any lost Gallium in the removal process either, to ensure an accurate weight measurement. To remove the sleeve seal, the bolts are backed out and the sleeve seal is carefully lifted off. The sleeve seal was removed, weighed, then re-assembled with great care using special fixturing shown in Figure 59. The ROSS Spin process removed about 0.5g of Gallium from the traps.



Figure 59: Sleeve seal was removed and weighed on the scale to determine the amount of Ga in the traps.

This ROSS was then placed in the balance chamber and run 4 times consecutively under vacuum to get a balance measurement. The chamber was vented and then closed again to see if the venting influenced the unbalance. Then the ROSS was left in the balancer chamber overnight and then spun 4 more times consecutively the next morning. The rotor and target average and standard deviation of the 4 runs are shown in Figure 60.

| closed chamber and ran consecutively | | Rotor | Rotor Deg | Target | Target Deg | Coast Down |
|--|-------------------------|-------|-----------|--------|------------|------------|
| closed chamber and ran consecutively | Avg | 0.063 | 35 | 0.228 | 327 | 151 |
| closed chamber and ran consecutively | stdev | 0.074 | 8 | 0.032 | 6 | 12 |
| closed chamber and ran consecutively | Avg= 25% of tolerance | | | | | |
| 12 oct 2016 vented chamber | | | | | | |
| 13 oct 2016 overnight in balancer - 16 hrs | | | | | | |
| 13 oct 2016 post collar fit | | Rotor | Rotor Deg | Target | Target Deg | Coast Down |
| closed chamber and ran consecutively | Avg | 0.303 | 15 | 0.260 | 333 | 144 |
| closed chamber and ran consecutively | stdev | 0.055 | 5 | 0.018 | 12 | 13 |
| closed chamber and ran consecutively | Avg = 121% of tolerance | | | | | |

Figure 60: Consecutive runs under vacuum. The chamber was vented in-between runs, denoted by the color change. Rotor average shifted drastically.

This trial gave more evidence of Gallium movement. However, this time the thrust seal on the rotor side of the bearing had the large discrepancy. The first 4 runs shown in blue had an average of 0.063g*cm which is 25% of the tolerance. The red is showing when the ROSS was left in the chamber overnight and then vented. The green runs show the 4 runs after the chamber vented jumped up to an average of 0.303g*cm on the rotor plane which is over 121% of the tolerance. This massive jump in rotor unbalance is likely caused by Gallium migrating into the thrust seal side traps during the venting process, just as Gallium had been observed to migrate into the first trap of the sleeve seal, both shown in Figure 58.

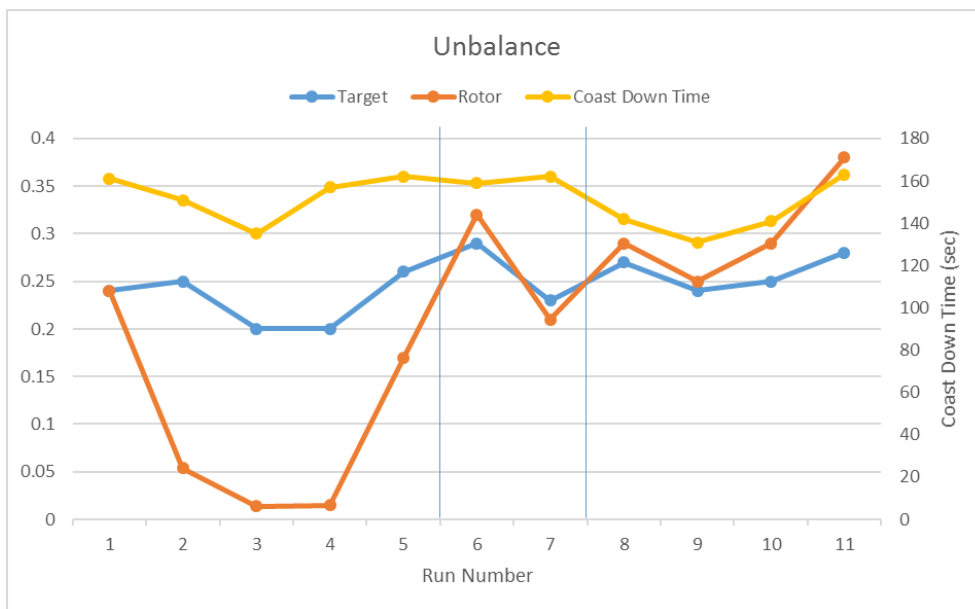


Figure 61: Run chart of Figure 60.

This test was like previous tests in showing that keeping all variables constant, the bearing appears to be causing the unbalance shift. Over a dozen sleeve seal inspections were performed. Anywhere between 0.0g to 2.0g of Gallium was found to migrate into the traps after a balance run. More sleeve seal inspections need to be performed to find a bearing where the Gallium migration can be visually detected before and after balance.

3.4.3 Smoking Gun bearing

To prove that the Gallium migration physically causes a shift in the unbalance, a bearing was needed to prove this. Sleeve seals were inspected on many bearings. They were weighed before and after balance to gain an understanding of the movement of Gallium. However, it was difficult and laborious to inspect after each run and correlate

the Gallium with an unbalance. With much perseverance, a bearing was inspected that proved the migration theory.

3.4.3.1 The Migration Bearing

A bearing was inspected before it went into the balance process. The sleeve seal was removed and revealed absolutely no Gallium in either the first or second trap. This bearing candidate was unique and perfect for monitoring the balance level because the traps had never seen any Gallium. The bearing went through 5 balance cycles to bring its target unbalance down from $66\text{g}\cdot\text{cm}$ to $3.7\text{ g}\cdot\text{cm}$. At this point the sleeve seal was again removed with confirmation that the bearing traps were still dry. It was spun 5 times consecutively with perfect repeatability of $0.0\text{g}\cdot\text{cm}$ standard deviation. The chamber was vented, and then closed again. During the subsequent 5 runs, the unbalance average stayed the same $3.7\text{g}\cdot\text{cm}$ but the standard deviation increased to $0.268\text{g}\cdot\text{cm}$. The coast down time increased as well, an indication that Ga had moved. Gallium should have migrated into the first trap on the sleeve seal side to prove the theory. When the sleeve seal was removed, it was found to contain a substantial amount of Gallium weighing in at 1.0g . Figure 62 walks through the entire process.

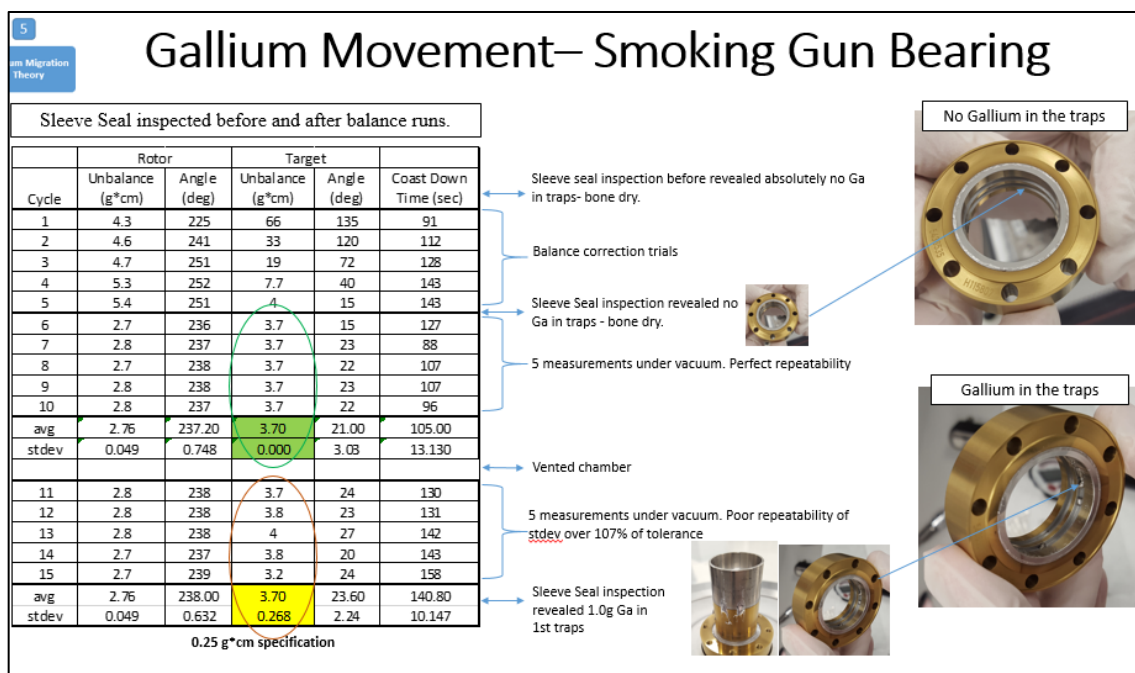


Figure 62: Chart laying out the test parameters showing no Gallium in the traps on the repeatable runs, while there was 1.0g of Gallium in the traps during the less repeatable runs for the Target unbalance.

The coast down time is also a great indicator of the bearing health and Gallium movement. As Gallium migrates into the traps, there is less fluid friction between the shaft and the sleeve. Less friction means a longer coast down time. Figure 63 shows a clear distinction of where the Gallium migrated. The target average started to rise, then lowered. The coast down time increased by an average of 35 seconds or 75%.

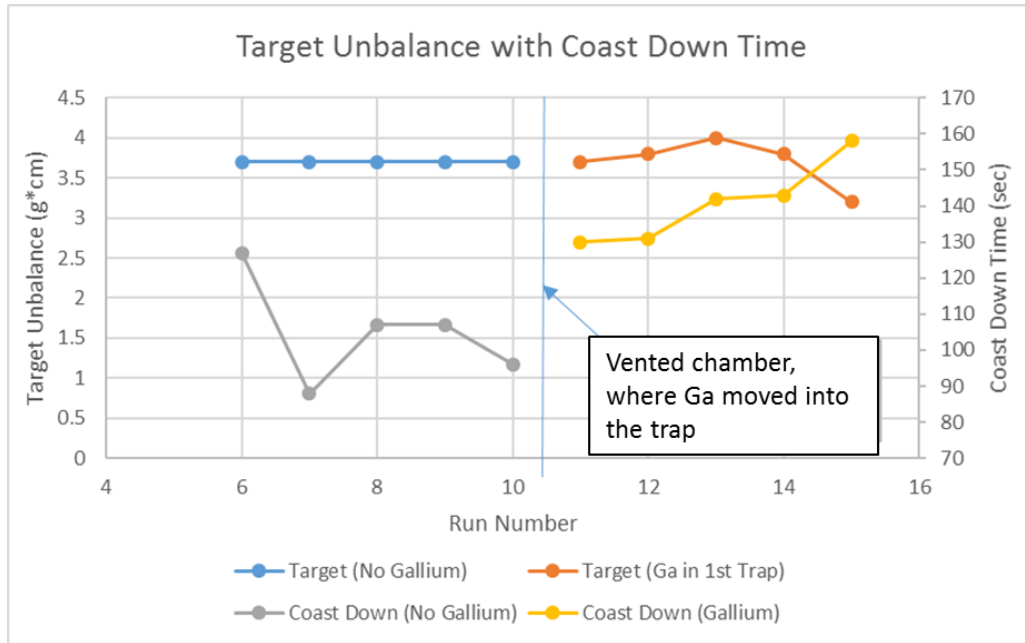


Figure 63: Plot showing where on the run chart the Gallium shifted into the first trap.

This finding proves that the Gallium migration affects unbalance. If the unbalance indicated by the machine is picking up Gallium in the traps, it will incorrectly suggest to remove material to correct for perceived piece part unbalance. On the subsequent spin, the Gallium could possibly move to a different location within the bearing traps. The correction done could cause an unbalance to the system making it worse and creating a balance chasing scenario. Herein lies the root problem of the balancing operation. The Gallium shifts giving different unbalance results depending on where it moved to. This bearing proved once again that the machine is capable of measuring repeatedly if it is measuring a consistent SGB, such as the first 5 runs when the Gallium had not entered the traps.

The calculations match this as well. 1.0g of Gallium at a 10mm radius out from the center of the shaft, acting as a point mass in the first trap, can produce an unbalance of $0.1\text{g}\cdot\text{cm}$, which is 40% of the balance specification.

3.4.3.2 Statistical Evaluation of Bearing Components

The following example will help explain the tight manufacturing processes used to build the current x-ray tube anode. There is a 20 micron slip fit between the target and the bearing sleeve. There is a 10 micron clearance between the shaft and sleeve of the liquid metal SGB.

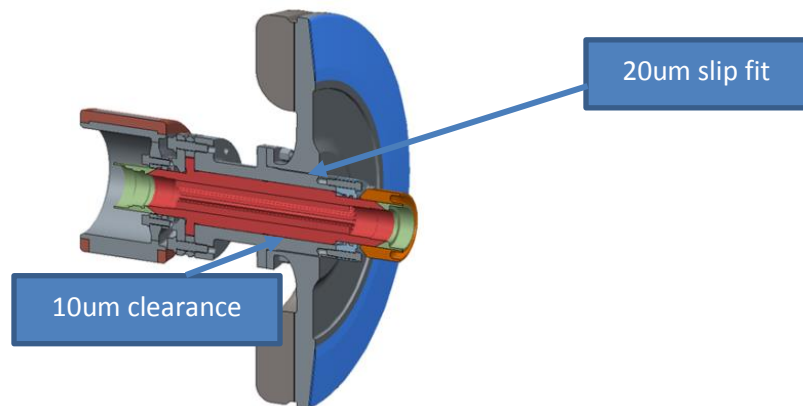


Figure 64: Cross section of the anode showing the target to sleeve fit and the shaft to sleeve gap.

The tighter the balance tolerance, the more important it is to keep all working surfaces as square and concentric as possible. Any eccentricity of the rotor mounting surface or looseness in the fit of the rotor causes balance errors. To determine the balance error U caused by eccentricity “ e ” of the rotor mounting surface and by the rotor clearance, use the following formula [6]:

$$U \text{ (g*cm)} = W \text{ (g)} * e \text{ (cm)} \quad 3.4.3.1$$

U = Unbalance (g*cm) caused by eccentric rotor mounting surface or rotor clearance

W = weight of rotor (g)

e = eccentricity (cm) = $\frac{1}{2}$ TIR (Total indicated runout) of the rotor mounting surface relative to the arbor axis, times $\frac{1}{2}$ its clearance

Example:

$$W = 11000\text{g}$$

$$E = U1) \quad \frac{1}{2} \text{ TIR target mounting to sleeve} = (1/2 * 0.002\text{cm}) = 0.001\text{cm} \quad 3.4.3.2$$

$$11000\text{g} * 0.001\text{cm} = 11\text{g*cm} \quad 3.4.3.3$$

$$U2) \quad \frac{1}{2} \text{ TIR bearing to sleeve} = (1/2 * 0.001\text{cm}) = 0.0005\text{cm} \quad 3.4.3.4$$

$$11000\text{g} * 0.0005\text{cm} = 5.5\text{g*cm} \quad 3.4.3.5$$

Table 13: Total Error and Error Squared

| Error (g*cm) | Error Squared |
|---------------------------------------|--------------------------------|
| $U1 = 11 \text{ g*cm}$ | 121 |
| $U2 = 5.5\text{g*cm}$ | 30.25 |
| $U \text{ Total} = 16.5 \text{ g*cm}$ | $U \text{ Total}^2 = 22,876.5$ |

$$U \text{ Total (RSS)} = \text{sqrt}(22,876.5) = 151.25 \text{ g*cm} \quad 3.4.3.6$$

This means that looking at worst case target fit and bearing run out, the anode could be 151.25g*cm unbalanced. This example does not include a target piece part unbalance that is present during the assembly of unbalanced parts. Specifically, even if the target and rotor are balanced to less than 2.5g*mm and attached perfectly concentric to the bearing, a 5.5g*cm unbalance could be due just to the shaft moving about the sleeve. This is the inherent challenges with a floating sleeve/target in liquid metal bearing. Theoretical balance relies on the shaft remaining impeccably centered during its orbital rotation if a 0.25g*cm spec is to be achieved. The shaft moving inside of the sleeve, even ever so slightly, combined with Gallium migrating in and out of the traps, is what is causing the unbalance uncertainty.

CHAPTER 4

CONCLUSIONS, OBSERVATIONS, and RECOMMENDATIONS**4.1 Conclusions:**

- The vacuum balance machine passes the bias checks
- Isolating the measurement system with a ball bearing proved that the measurement system does not have large variation. The average standard deviation between both ball bearing trials was 0.015g*cm, which corresponds to only 6% of the specification limit.
- SGB anodes can have a variation of up to 0.50g*cm of unbalance, which is twice the 0.25g*cm specification limit.
- The average number of balance cycles was reduced from 8 to 6 by identifying and fixing issues related to the balance process

The bias check proved that the machine can detect a known value weight at the proper angular location. This was critical in determining machine health. The balance machine also proved that it was capable of producing results that were very repeatable when the ball bearing anode was tested. Two different ball bearing anodes were tested where the average standard deviation between both trials was 0.015g*cm, which corresponds to only 6% of the specification limit. On the contrary, SGB anodes can have a variation of up to 0.50g*cm of unbalance, which is 200% of the 0.25g*cm specification limit. The ball bearing testing was critical because up until this trial, it was thought that the variation seen on the SGB anode could be attributed to the measurement system and not the variation in the bearing.

The increased scrutiny on the machine helped fix issues that would decrease cycle time as shown in Figure 65. Stronger operator training made the users of the machine more aware of the details in the balance process. Having the operators follow standard work ensured that the process was consistent. The collet set up on the ROSS was made more robust by adding in poke-yoke fixturing. The target material removal was also looked at very closely. Fine tuning the drill bit speeds and feeds, as well as using a better cutting bit, has allowed for more reliable cuts on the tungsten targets. Adding rigidity to the cutting system also allowed for increased cut accuracy. Better zeroing of the cutter also improved the cut depth into the target and rotor. This was accomplished by creating a fixture to give a permanent drill and mill bit height setting. Upstream processing also improved to give a better initial target unbalance. Starting with a ROSS closer to specification helps decrease cycles and minimize the amount of material that is needed to be removed. After these changes were made, the average number of balance cycles dropped from 8 to 6. This cycle reduction lead to the machine meeting its takt time of balancing 2 ROSS's a shift.

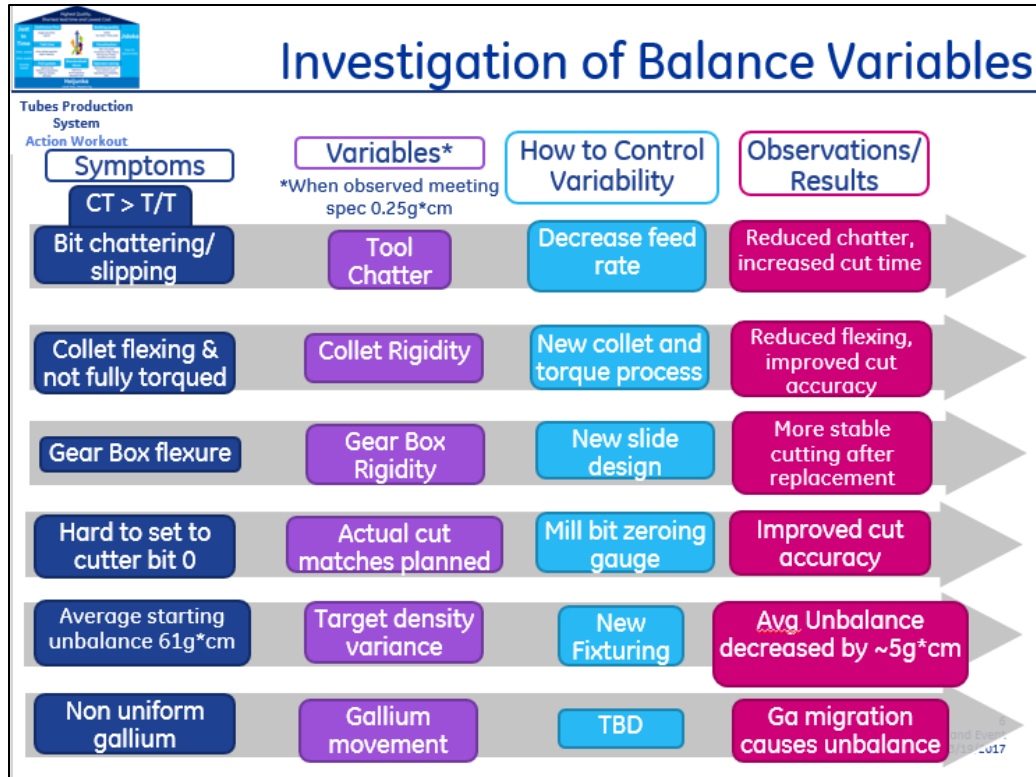


Figure 65: Investigation of balance variables reduced the average number of balance cycles by two.

4.2 Observations:

- A SGB, which was visually identified to have no Gallium in the first trap of the sleeve seal, was found to have perfect repeatability. When Gallium migrated into the first sleeve seal trap of the same bearing, it produced a standard deviation of 0.27 g*cm, which is 108% of the 0.25g*cm specification. The coast down time also increased by 75% after the Gallium migrated into the first trap, which was a result of less fluid friction in the bearing.
- The Gallium was found to shift during the balance process and cause the poor repeatability. This can result in the possibility that the last material removal process incorrectly removed material from the rotor and target, creating unbalance in the system.

After isolating variables, the factor causing the repeatability issues with the balancer was determined to be the shifting Gallium inside of the bearing. It is a known and accepted design feature of the liquid metal SGB that the Gallium can migrate in and out of the first traps of the bearing during its life in an x-ray tube. The novel conclusion of this thesis is that the Gallium was found to shift during the balance process and cause the poor repeatability. The shifting Gallium can cause up to a $0.5\text{g}\cdot\text{cm}$ unbalance variation depending on where the Gallium has migrated to in the traps of the bearing. This enormous amount of variation is twice the specification limit of $0.25\text{g}\cdot\text{cm}$. The machine picks up the Gallium in the trap and reports this as an actual unbalance in the rotor or the target. This artificial unbalance is then removed from either the target or rotor by a drilling and milling operation. When the bearing is spun again to check the unbalance, the Gallium will have shifted, resulting in the possibility that the last material removal process incorrectly removed material from the rotor and target, creating unbalance in the system. This can cause extra balance cycles and pump downs. It is very difficult to balance this SGB to such a tight specification. Recall that due to the weight and speed of this operation, the balance quality grade is a G0.4 which is the equivalent balance grade as gyroscopes.

4.3 Recommendations:

- Investigate an air balance process that locks the shaft and sleeve together and spins the entire anode on roller bearings. This process will take place in air, removing the vacuum pump down variability in the current process.
- Increase the specification limit to $1.0\text{g}\cdot\text{cm}$. Prove that there is no impact to quality by autopsying current x-ray tubes and measuring the balance shift.

- Balance a fixed number population of engineering tubes to the higher specification to monitor and test the impact on quality

It is recommended in future work to investigate a balance process that locks the shaft and sleeve together, allowing the entire anode to be spun on roller bearings. This process will take place in air, removing the vacuum pump down variability in the current process. However, there are many details such as fixturing and handling that will need to be worked out. Early trials of air balance have indicated success.

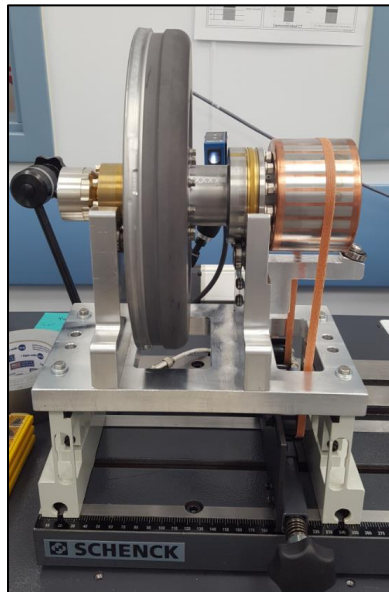


Figure 66: Air Balance setup.

These details pale in comparison to the larger problem of unreliable vacuum balance though. The vacuum balance pump downs cause the Gallium to shift, migrating into the traps, which leads to an unpredictable balance operation. Added pump downs also increase the risk of bearing leaks, due to pressure differentials on the anti-wetting bearing seals.

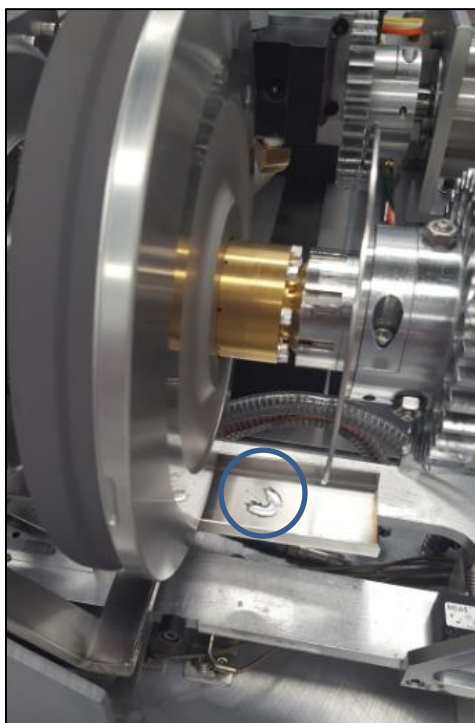


Figure 67: A bearing which leaked in the balancer resulting in a pool of Gallium.

It is also recommended to consider increasing the balance specification from 0.25g*cm to 1.0 g*cm. The 0.25g*cm legacy specification limit was originally the threshold thought to keep a ball bearing glass x-ray tube from breaking due to high vibration. Now, the stronger metal frame x-ray tubes can withstand much greater vibration forces. Increasing the specification limit is no small task and requires the monitoring and autopsy of many x-ray tubes. These tubes have seen tremendous thermal loads, causing the unbalance to shift during its operation. For comparison, other product lines have a field return balance that is anywhere between 3 to 4 times the specification limit of 0.25g*cm, which equates to 0.75g*cm to 1.0g*cm. With this SGB product being so new, there are not enough field returns available for testing. However, a SGB ROSS was cut out of an x-ray tube that went through all its back operation and final acceptance testing. When it was placed back on the balancer, the balance was 4.1g*cm on the target and 1.2g*cm on the rotor. This is 16.4 times the starting tolerance on the target and 4.8 times the starting tolerance on the rotor. It is widely accepted that the unbalance will shift during use, but the transfer function is not well established. It is recommended to autopsy tubes after their HALT testing at 20,000 x-ray exams to understand what effect this has on its unbalance. It is also recommended to balance a fixed number population of tubes to 1.0 g*cm and compare this with similar tubes at 0.25g*cm.

4.4 Explicit Contributions:

- The researcher assembled all anodes used for testing and performed every test.

- The researcher is the manufacturing engineer responsible for the balance process and all equipment used. All anode builds and balances followed the company's documented quality requirements.
- The researcher has autopsied over a two dozen bearings, performing the challenging sleeve seal inspection for Gallium. The researcher balanced these, gathering much more data than is presented in this document.
- The researcher was instrumental in driving for next generation anodes to be balanced to 1.0g*cm for engineering trials.
- The researcher has balanced field returns for different products, collecting data on the unbalance shift seen in the field. The researcher placed the first SGB ROSS back on the balancer to measure unbalance after back operational testing.
- The researcher is helping lead a team to set up the air balance system.

Because of the work of this thesis, the next generation of SGB x-ray tubes are being balanced to 1.0g*cm. Early engineering tests have indicated that the 1.0g*cm specification does not have an impact on the product quality. If the quality is proved out, increasing the specification has a very positive impact on the balance process too. The engineering units that have been balanced to 1.0g*cm have an average of 4 cycles, which is 2 cycles less. This also cuts the original cycle time in half.

In conclusion, the hypothesis was determined to be correct. The shifting Gallium within the bearing was causing the unbalance variability. The statistical evaluation of bearing components could not account for the level of balance variability. The intense work surrounding the machine to identify problems also helped reduce cycle time by lowering the average number of cycles which it takes to balance an anode.

BIBLIOGRAPHY

- [1] Grave, Brian. "Method for Balancing Rotatable Anodes for X-ray Tubes." Patent 5,689,543. 18 Nov 1997.
- [2] Feese, Troy. "Balance This!" *Engineering Dynamics Incorporated*. September 2004. Web. 31 January 2016.
- [3] Grim, Gary. "The Basics of Balancing 202." *Balancetechnology*. 2014. Web. 31 January 2016.
- [4] Behling, Rolf. "Balancing of Rotary Anode of an X-ray Tube." Patent WO2011039662A1. 7 April 2011.
- [5] Rogers, Lindsay Louise, "Method of Tolerance Allocation to Maintain Rotary Balance of Multi-Component Bodies" (2011). Master's Theses (2009 -). Paper 87.
- [6] Stadelbauer, Douglas. "Fundamentals of Balancing", Schenck Trebel, Third Edition, April 1990.
- [7] ISO 1925:2001. Mechanical Vibration – Balancing – Vocabulary. Geneva, Switzerland.
- [8] ISO 1940/1:2003. Balance Quality of Rigid Rotors Geneva, Switzerland.
- [9] "Balance Quality Requirements of Rigid Rotors", *IRD Balancing*. Louisville, KY. REV 2: March 2009.
- [10] Behling, Rolf. Modern Diagnostic X-Ray Sources : *Technology, Manufacturing, Reliability*. Boca Raton, FL, USA: CRC Press, 2015. ProQuest ebrary. Web. 3 April 2016.
- [11] Tiarney, Thomas. *New Tubes Technology for Edison's*. Milwaukee, WI: General Electric Company. December 2013. Electronic.
- [12] Sherman, Max. *Medical Device Packaging Handbook*. New York: Marcel Dekker, 1998. Print.
- [13] Farncombe, Troy, and Krzysztof Iniewski. *Medical Imaging: Technology and Applications*. CRC Press. 2014. Print.
- [14] Dowsett, David, and Kenny, Patrick, and Johnston, Eugene. *The Physics of Diagnostic Imaging*. Hodder Arnold. 2nd Edition. 2006. Print

- [15] Schultz, Christopher. "SOLID LUBRICATION BEARING DESIGN THROUGH ANALYTICAL AND EMPIRICAL VIBRATION ANALYSIS OF CHARACTERISTIC FREQUENCIES". Thesis. Marquette University. 2015. Print.
- [16] "100 YEARS OF BALANCING TECHNOLOGY." *Schenck USA*. N.p., n.d. Web. 9 Feb 2017. <<http://www.schenck-usa.com/company/information/history.php>>.
- [17] Rolf Behling. "HISTORY AND FUTURE OF X-RAY TUBES." N.p., n.d. Web. 10 Nov 2016. <<http://amos3.aapm.org/abstracts/pdf/113-31203-379492-117965-107716066.pdf>>.
- [18] "X-RAY TUBES". *Toshiba Electron Tubes and Devices*. N.p., n.d. Web. 15 Oct 2016. <<http://www.toshiba-tetd.co.jp/eng/tech/xray.htm>>.
- [19] "QUALITY REQUIREMENTS". *IRD Balancing*. N.p., n.d. Web. 18 Sept 2016. <<http://www.irdbalancing.com/downloads/techpaper1balqualityreqmts.pdf>>.
- [20] "HMS10/CAB920H Balancing Machine Manual". Schenck Trebel, Serial Number SQAHC1204. Deer Park, NY. May 2013.
- [21] Harris, Tedric A. *Rolling Bearing Analysis*. New York: John Wiley, 2001. Print.
- [22] Hattori, Hitoshi, Harunobu Fukushima, Yasuo Yoshii, Hironori Nakamuta, Mitsuo Iwase, and Koichi Kitade. "Proposal of a High Rigidity and High Speed Rotating Mechanism Using a New Concept Hydrodynamic Bearing in X-Ray Tube for High Speed Computed Tomography." *Journal of Advanced Mechanical Design, Systems, and Manufacturing* 3.1 (2009): 105-14. Web.
- [23] Triscari, Andrew T. "Effects of Gallium-Molybdenum Intermetallic on Wear Mechanisms in Herringbone-Spiral Groove Bearing Systems". Thesis. Milwaukee School of Engineering, 2014. N.p.: n.p., n.d. Print.
- [24] "X-Ray Bearings." *Barden UK Super Precision Ball Bearings*. N.p., n.d. Web. 06 September 2014. <http://www.bardenbearings.co.uk/x_ray_bearings.html>.
- [25] X-ray Tube. Digital image. *X-Alliance*. N.p., n.d. Web. 5 Sept. 2014. <http://www.x-alliance.com/public/images/components_xraytube.png>.
- [26] X-ray Tube Schematic. Digital image. *Radiopaedia*. Web. 5 Sept. 2014. <http://images.radiopaedia.org/images/3165401/7ef2c07bd518defc594a4328dbfd2b_big_gallery.jpg>.

- [27] Qiu, Liangheng, Carey S. Rogers, Michael J. Danyluk, and Dennis M. Gray. Titanium Carbide plus Silver Coated Balls for X-ray Tube Bearings. General Electric Company, assignee. Patent US7492869 B1. 17 Feb. 2009. Print.
- [28] Hattori, Hitoshi, Harunobu Fukushima, Yasuo Yoshii, Hironori Nakamuta, Mitsuo Iwase, and Koichi Kitade. "Proposal of a High Rigidity and High Speed Rotating Mechanism Using a New Concept Hydrodynamic Bearing in X-Ray Tube for High Speed Computed Tomography." *Journal of Advanced Mechanical Design, Systems, and Manufacturing* 3.1 (2009): 105-14. Web.
- [29] Szeri, A Z. *Fluid Film Lubrication: Theory and Design*. Cambridge: Cambridge University Press, 2005.

APPENDIX

Appendix A

Table 14: Data from Gage R&R Trials with SGB

| RunOrder | Parts | Operators | Rotor Imbalance (g*cm) | Rotor Imbalance (deg) | Target Imbalance (g*cm) | Target Imbalance (deg) |
|----------|-------|-----------|------------------------|-----------------------|-------------------------|------------------------|
| 1 | 3 | 1 | 4.3 | 4 | 4.3 | 18 |
| 2 | 4 | 1 | 6.1 | 1 | 6.2 | 355 |
| 3 | 1 | 1 | 0.12 | 213 | 0.16 | 162 |
| 4 | 2 | 1 | 0.91 | 0 | 2.4 | 208 |
| 5 | 4 | 2 | 6 | 3 | 6.6 | 348 |
| 6 | 3 | 2 | 4.4 | 2 | 4.4 | 25 |
| 7 | 2 | 2 | 0.84 | 5 | 2.3 | 215 |
| 8 | 1 | 2 | 0.17 | 259 | 0.49 | 137 |
| 9 | 2 | 1 | 0.86 | 0 | 2.2 | 210 |
| 10 | 1 | 1 | 0.11 | 165 | 0.32 | 221 |
| 11 | 3 | 1 | 4.4 | 4 | 4.2 | 24 |
| 12 | 4 | 1 | 6.2 | 4 | 6.3 | 347 |
| 13 | 3 | 2 | 4.4 | 3 | 4.5 | 24 |
| 14 | 1 | 2 | 0.062 | 206 | 0.35 | 181 |
| 15 | 2 | 2 | 0.88 | 358 | 2.2 | 211 |
| 16 | 4 | 2 | 6.1 | 3 | 6.7 | 351 |
| 17 | 3 | 1 | 4.4 | 4 | 4 | 26 |
| 18 | 4 | 1 | 6 | 1 | 6.8 | 351 |
| 19 | 2 | 1 | 0.86 | 359 | 2.2 | 211 |
| 20 | 1 | 1 | 0.15 | 202 | 0.24 | 163 |
| 21 | 1 | 2 | 0.17 | 217 | 0.093 | 100 |
| 22 | 3 | 2 | 4.3 | 1 | 4.9 | 25 |
| 23 | 2 | 2 | 0.94 | 359 | 2.5 | 205 |
| 24 | 4 | 2 | 6 | 1 | 7 | 353 |
| 25 | 5 | 1 | 0.11 | 351 | 0.15 | 173 |
| 26 | 5 | 1 | 0.1 | 275 | 0.21 | 27 |
| 27 | 5 | 1 | 0.19 | 240 | 0.57 | 34 |
| 28 | 5 | 2 | 0.13 | 223 | 0.53 | 13 |
| 29 | 5 | 2 | 0.19 | 327 | 0.3 | 120 |
| 30 | 5 | 2 | 0.13 | 243 | 0.47 | 18 |

Appendix B

Minitab results of the Target Imbalance shown below:

Gage R&R Study - XBar/R Method

Gage R&R for Target Imbalance (g*cm)

Gage name: Target Imbalance

Date of study:

Reported by:

Tolerance: .25 g*cm

Misc:

| Source | VarComp | % Contribution (of VarComp) |
|-----------------|-----------|--------------------------------|
| Total Gage R&R | 0.0297316 | 86.47 |
| Repeatability | 0.0297316 | 86.47 |
| Reproducibility | 0.0000000 | 0.00 |
| Part-To-Part | 0.0046517 | 13.53 |
| Total Variation | 0.0343833 | 100.00 |

Process tolerance = 0.25

| Source | StdDev (SD) | Study Var (5.15 * SD) | %Study Var (%SV) | %Tolerance (SV/Toler) |
|-----------------|-------------|--------------------------|---------------------|--------------------------|
| Total Gage R&R | 0.172429 | 0.888007 | 92.99 | 355.20 |
| Repeatability | 0.172429 | 0.888007 | 92.99 | 355.20 |
| Reproducibility | 0.000000 | 0.000000 | 0.00 | 0.00 |
| Part-To-Part | 0.068203 | 0.351247 | 36.78 | 140.50 |
| Total Variation | 0.185427 | 0.954951 | 100.00 | 381.98 |

Number of Distinct Categories = 1

Gage R&R for Target Imbalance (g*cm)

Appendix C

6.1 Future Work: Ga High Speed Wear Tests and Theory Behind Higher Balance Speed

Previous tests have identified ROSS stability at the operation speed of 8400rpm. However, the balance equipment is not capable of spinning that fast. Likewise, it would harm the bearing spinning this fast if the ROSS was unbalanced. The Schenck balance table recommends not to exceed the limit set forth in the table below. The percentage of the max limit has been calculated for the normal 1350rpm boost speed and for the highest and safest possible run speed. As shown, 2100rpm would be on the verge of breaking the equipment. However, 2000rpm would give safe enough margin to perform a balance test a higher speed than what is used currently.

Table 15: Schenck System Limitations

| Speed Limitation Ranges | Rotor Weight x Speed (Wn^2) | % of Max Limit |
|-----------------------------|---------------------------------|----------------|
| The Max Limit Not to Exceed | 1.1E+08 | 100% |
| At 1350 RPM | 4.4E+07 | 40% |
| At 2000 RPM | 9.7E+07 | 88% |
| At 2100 RPM | 1.1E+08 | 97% |

Therefore, a trial will be performed when spinning to a maximum of 2000rpm and measuring at 1500rpm. This is a speed increase over the currently used 1350rpm max

spin speed and 900rpm measuring speed. The goal is to evaluate changes in bearing stability resulting from the increased speed.

6.1.1.1 Design of Test

The first portion of the test is to create a new Rotorfile for the higher speed measurements named “Janus – BB- Vac” and complete a rotor specific calibration on the Schenck equipment. The Allen Bradley Powerflex753 drive controls the rotor speed. As shown, the run speed (Parameter 571) was changed from 45 Hz to 67 Hz. The 3 phase drive means that the frequency input into the drive will be cut in half. The original 45Hz is actually 1350 rpm. The new 67 Hz is actually 2010 rpm.



Figure 68: PowerFlex Drive showing the parameter changes to increase the speed

On the Schenck screen the “Janus-BB-Vac” rotor file was selected. The measurement speed was changed to 1500rpm and saved as “Nessus-Vac-1500”.

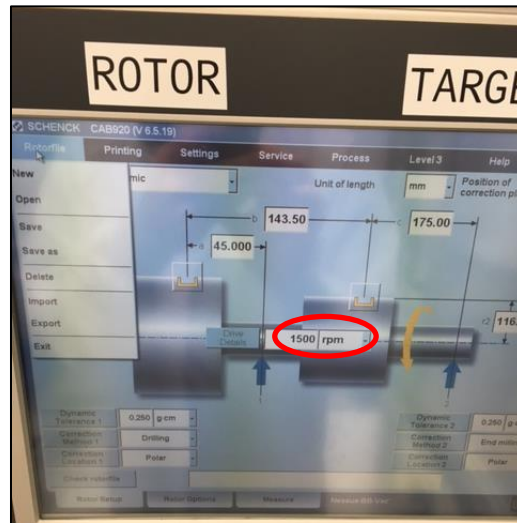


Figure 69: Changing the measurement speed to 1500rpm

A rotor specific calibration was performed on the new rotor file at the increased speed should be used to create the rotor specific calibration.

6.1.2 High Speed Consecutive Run Study based on Chamber Venting

Bearing MAN 245 was balanced to specification. The final unbalance was performed at the normal 1350rpm run speed while averaging over 900rpm using the

Nessus-BB-Vac. The program called JANUS-BB-VAC was used to test out the capabilities of this ROSS at a higher ramp speed of 2000rpm.

Table 16: Vented chamber after 5 consecutive runs for two different rotor specific calibration programs

| Run # | Rotor Unbalance (g*cm) | Rotor Angle (Deg) | Target Unbalance (g*cm) | Target Angle (deg) | Program |
|--------------|------------------------|-------------------|-------------------------|--------------------|---------------|
| 0 | 0.13 | | 0.2 | | |
| 1 | 0.25 | 352 | 0.36 | 249 | Janus-BB-vac |
| 2 | 0.25 | 349 | 0.27 | 245 | Janus-BB-vac |
| 3 | 0.26 | 348 | 0.36 | 248 | Janus-BB-vac |
| 4 | 0.26 | 346 | 0.34 | 257 | Janus-BB-vac |
| 5 | 0.25 | 346 | 0.34 | 257 | Janus-BB-vac |
| 6 | 0.26 | 351 | 0.39 | 258 | Janus-BB-vac |
| 7 | 0.26 | 354 | 0.34 | 246 | Janus-BB-vac |
| 8 | 0.23 | 349 | 0.5 | 252 | Janus-BB-vac |
| 9 | 0.24 | 349 | 0.34 | 261 | Janus-BB-vac |
| 10 | 0.23 | 348 | 0.33 | 258 | Janus-BB-vac |
| AVG | 0.25 | 349.20 | 0.36 | 253.10 | |
| STDEV | 0.011 | 2.40 | 0.056 | 5.49 | |
| | | | | | |
| 11 | 0.24 | 352 | 0.3 | 281 | Nessus-BB-vac |
| 12 | 0.23 | 350 | 0.41 | 272 | Nessus-BB-vac |
| 13 | 0.24 | 346 | 0.31 | 258 | Nessus-BB-vac |
| 14 | 0.25 | 349 | 0.31 | 266 | Nessus-BB-vac |
| 15 | 0.24 | 353 | 0.36 | 268 | Nessus-BB-vac |
| 16 | 0.24 | 350 | 0.32 | 265 | Nessus-BB-vac |
| 17 | 0.24 | 352 | 0.28 | 267 | Nessus-BB-vac |
| 18 | 0.25 | 353 | 0.32 | 263 | Nessus-BB-vac |
| 19 | 0.2 | 346 | 0.26 | 239 | Nessus-BB-vac |
| 20 | 0.24 | 347 | 0.29 | 257 | Nessus-BB-vac |
| AVG | 0.24 | 349.80 | 0.32 | 263.60 | |
| STDEV | 0.013 | 2.60 | 0.040 | 10.45 | |

Recall this is the same bearing under the same testing conditions, except that boost and measure speeds. As the data shows, the average unbalance in both the rotor and target planes was very close. The standard deviation of the low speed "Nessus-BB-Vac" program was lower (0.04g*cm vs 0.056g*cm) than the high speed. This could be due to the Gallium position in the bearing as previously mentioned. However, this discrepancy means that the bearing was not spun up to a high enough speed to redistribute the Gallium and move it back into the center of the shaft.

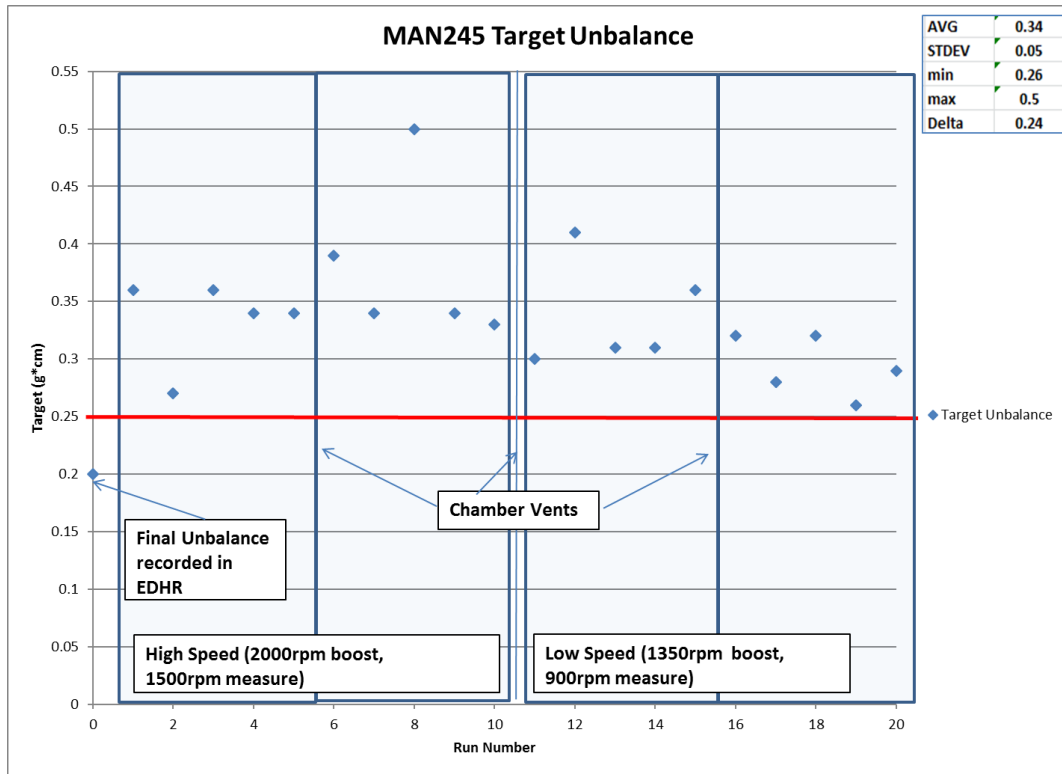


Figure 70: MAN245 Target Unbalance run chart showing the high speed "Janus-BB-Vac Program" and the normal "Nessus-BB-Vac"Program

6.1.3 More High Speed Trials

To consider bearing variability, another ROSS was used to test the high and low speed theory. A ROSS with a threaded hole in the target was used to shift the unbalance easily for testing.

| | | Rotor | | Target | |
|-------------------------------|--------------|------------------|---------------|------------------|---------------|
| | | Unbalance (g*cm) | Angle (deg) | Unbalance (g*cm) | Angle (deg) |
| 1350rpm no wieght (1) | avg | 0.199 | 124.40 | 0.427 | 309.40 |
| | stdev | 0.016 | 4.13 | 0.022 | 6.37 |
| 1350rpm no wieght (2) | avg | 0.247 | 123.60 | 0.355 | 318.20 |
| | stdev | 0.009 | 3.26 | 0.045 | 8.70 |
| 2000rpm no weight (1) | avg | 0.207 | 114.00 | 0.329 | 299.60 |
| | stdev | 0.024 | 1.79 | 0.016 | 6.47 |
| 2000rpm no weight (2) | avg | 0.196 | 120.20 | 0.373 | 311.60 |
| | stdev | 0.008 | 2.99 | 0.021 | 1.85 |
| | | Rotor | | Target | |
| | | Unbalance (g*cm) | Angle (deg) | Unbalance (g*cm) | Angle (deg) |
| 1350rpm 0.4592g weight | avg | 0.215 | 142.00 | 5.803 | 17.80 |
| | stdev | 0.005 | 1.41 | 0.028 | 0.40 |
| 2000rpm 0.4592g weight | avg | 0.296 | 115.00 | 5.889 | 359.00 |
| | stdev | 0.005 | 0.89 | 0.028 | 0.00 |
| | | Rotor | | Target | |
| | | Unbalance (g*cm) | Angle (deg) | Unbalance (g*cm) | Angle (deg) |
| 1350rpm 0.6531g weight | avg | 0.201 | 130.40 | 7.684 | 17.40 |
| | stdev | 0.015 | 1.02 | 0.034 | 0.49 |
| 2000rpm 0.6531g weight | avg | 0.292 | 130.40 | 7.917 | 1.00 |
| | stdev | 0.006 | 1.02 | 0.042 | 0.00 |

Figure 71: High and Low speed comparisons of the same ROSS. The best run was highlighted in green for each vertical column/category. Note that there some tied. The avg is of 5 consecutive runs.

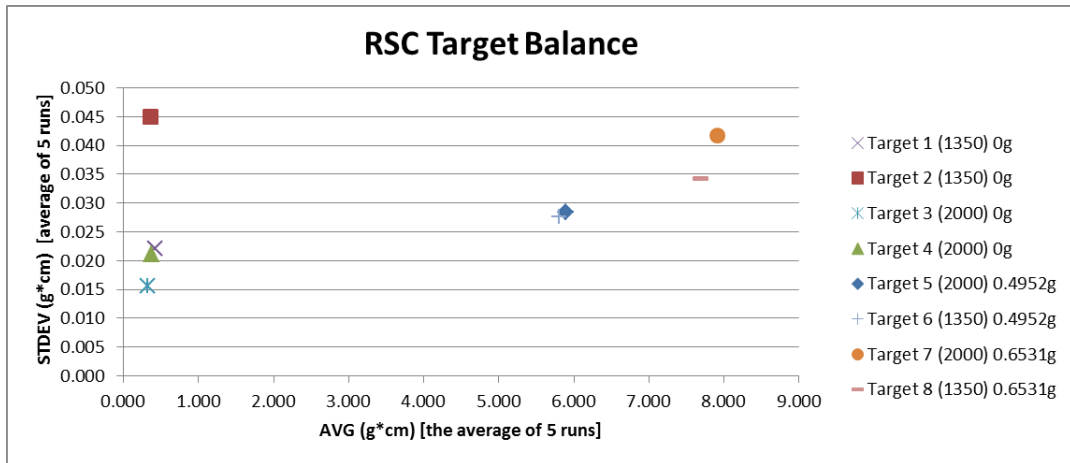


Figure 72: Target Unbalance comparison at high and low speeds.

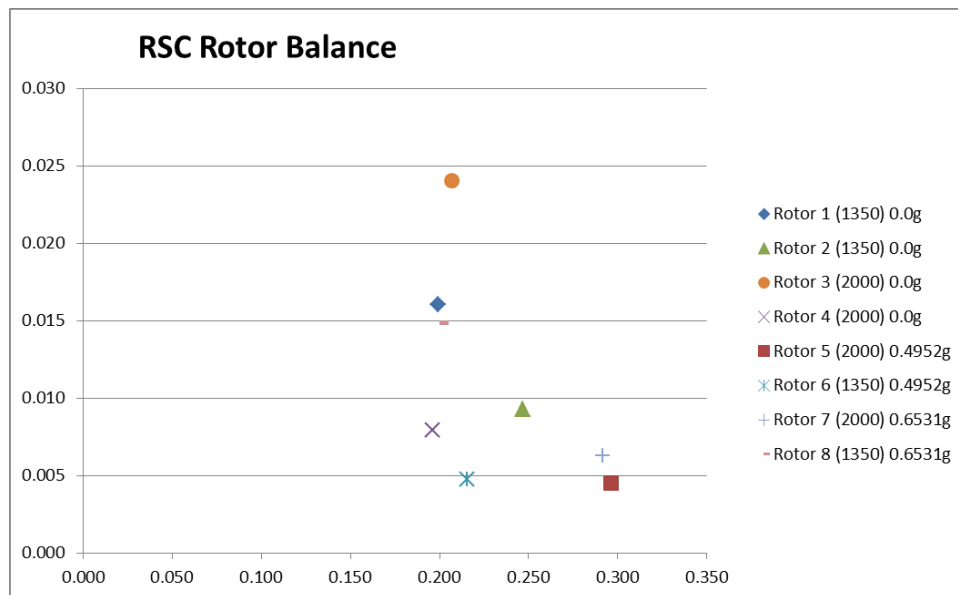


Figure 73: Rotor Unbalance comparison at high and low speeds

There does not appear to be a significant difference in the high and low speed runs. Both the target and the rotor sometimes have a better standard deviation at low and at the high speeds. This testing is inconclusive and shows that the bearing speed will need to be drastically increased to have any significant effect on the repeatability of the unbalance measurement.